SANDIA REPORT
SAND2002-0005
Unlimited Release
Printed January 2002

Microscale Shock Wave Physics Using Photonic Driver Techniques

R. E. Setchell, W. M. Trott, A. V. Farnsworth, Jr., J. N. Casteneda, and D. M. Berry

Prepared by
Sandia National Laboratories
Albuquerque, New Mexico 87185 and Livermore, California 94550

Sandia is a multiprogram laboratory operated by Sandia Corporation, a Lockheed Martin Company, for the United States Department of Energy under Contract DE-AC04-94AL85000.

Issued by Sandia National Laboratories, operated for the United States Department of Energy by Sandia Corporation.

Available to DOE and DOE contractors from
U.S. Department of Energy
Office of Scientific and Technical Information
P.O. Box 62
Oak Ridge, TN 37831

Telephone: (865)576-8401
Facsimile: (865)576-5728
E-Mail: reports@adonis.osti.gov
Online ordering: http://www.doe.gov/bridge

Available to the public from
U.S. Department of Commerce
National Technical Information Service
5285 Port Royal Rd
Springfield, VA 22161

Telephone: (800)553-6847
Facsimile: (703)605-6900
E-Mail: orders@ntis.fedworld.gov
Online order: http://www.ntis.gov/ordering.htm

SAND2002-0005
Unlimited Release
Printed January 2002

Microscale Shock Wave Physics Using Photonic Driver Techniques

Robert E. Setchell
Nanostructures and Advanced Materials Chemistry Department

Wayne M. Trott and Jaime N. Castaneda
Thermal/Fluid Experimental Sciences Department

Archie V. Farnsworth Jr.
Computational Physics and Simulation Frameworks Department

Dante M. Berry
Firing Set and Optical Engineering Department

Sandia National Laboratories
P.O. Box 5800
Albuquerque, NM 87185-2356

Abstract

This report summarizes a multiyear effort to establish a new capability for determining dynamic material properties. By utilizing a significant reduction in experimental length and time scales, this new capability addresses both the high per-experiment costs of current methods and the inability of these methods to characterize materials having very small dimensions. Possible applications include bulk-processed materials with minimal dimensions, very scarce or hazardous materials, and materials that can only be made with microscale dimensions. Based on earlier work to develop laser-based techniques for detonating explosives, the current study examined the laser acceleration, or *photonic* driving, of small metal discs ("flyers") that can generate controlled, planar shock waves in test materials upon impact. Sub-nanosecond interferometric diagnostics were developed previously to examine the motion and impact of laser-driven flyers. To address a broad range of materials and stress states, photonic driving levels must be scaled up considerably from the levels used in earlier studies. Higher driving

levels, however, increase concerns over laser-induced damage in optics and excessive heating of laser-accelerated materials. Sufficiently high levels require custom beam-shaping optics to ensure planar acceleration of flyers.

The present study involved the development and evaluation of photonic driving systems at two driving levels, numerical simulations of flyer acceleration and impact using the CTH hydrodynamics code, design and fabrication of launch assemblies, improvements in diagnostic instrumentation, and validation experiments on both bulk and thin-film materials having well-established shock properties. The primary conclusion is that photonic driving techniques are viable additions to the methods currently used to obtain dynamic material properties. Improvements in launch conditions and diagnostics can certainly be made, but the main challenge to future applications will be the successful design and fabrication of test assemblies for materials of interest.

Acknowledgment

The authors would like to thank Juan Romero and Cathy Sifford of Sandia's Thin Film, Vacuum, and Packaging Department for their many contributions to this study. This work was supported by Laboratory Directed Research and Development funding.

Contents

Figures

Microscale Shock Wave Physics Using Photonic Driver Techniques

1. Introduction

The dynamic behavior of a material must be characterized if the material is to be incorporated into a designed structure that can experience significant transient stresses before or during its intended use. Such a characterization typically involves a description of the thermodynamic behavior (equation of state) as well as a constitutive model for the dynamic stress-strain behavior over the anticipated range of strain rates. Determining these properties involves a variety of well-established static and dynamic techniques. In dynamic testing, Hopkinson bar techniques and shock-wave loading techniques are used to generate intermediate and high strain rates, respectively. Shock waves are typically generated in material samples using planar loading methods involving either the detonation of explosives or the impact of flat-faced projectiles accelerated in compressed-gas or powder guns. Available diagnostic methods and corresponding interpretations of material behavior are predominantly based on the assumption of one-dimensional, uniaxial strain conditions for a sufficient test time. To ensure such conditions are achieved experimentally and to facilitate most diagnostic methods, minimum sample dimensions need to be from a few millimeters to a few centimeters, resulting in test times from a few tenths of a microsecond to several microseconds. Projectile diameters need to be a few centimeters or more in high-precision gas gun experiments, and projectile accelerations require many meters of evacuated, tight-tolerance barrel sections. Consequently, experimental systems for generating precisely controlled shock loading conditions can be relatively large and expensive facilities. Initial construction and necessary instrumentation can cost well over a million dollars, annual maintenance can cost many tens of thousands of dollars, and per-experiment costs can range from a few thousand to more than ten thousand dollars. Because defense technologies encompass many materials for which dynamic properties must be determined, several dozen shock-physics facilities were constructed in this country at Department of Defense and Department of Energy sites. Reduced defense budgets and high operational costs have forced a significant reduction in the number of these facilities in recent years.

The dynamic behavior of many materials must still be characterized at Sandia National Laboratories and elsewhere. Increased emphasis on numerical simulations both for design and for assessing reliability and safety is amplifying the need for improved material models based on

sufficient, well-characterized experimental data. In addition, there is growing interest in materials that can only be fabricated with dimensions that are too small for conventional testing techniques. An important example is polycrystalline silicon, the basic structural material in surface micromachines, which is typically processed as a film having a thickness of a few microns. Before miniaturized technology could replace current components in defense systems, the static and dynamic properties of any new material would need to be adequately characterized. This is particularly true for any safety-critical component, whose response under a variety of abnormal environments (including shock loading) must be predictable. Finally, because of the relatively large scale of conventional testing techniques, there has always been difficulty in characterizing the shock wave response of materials that are extremely expensive, or scarce, or hazardous to handle except in very small quantities.

This report summarizes a multiyear effort to develop a new experimental capability for characterizing the dynamic properties of materials. By utilizing a significant reduction in experimental length and time scales, the new capability seeks to address both the high per-experiment costs of current testing methods and the inability of these methods to characterize materials having very small dimensions. Planar impact conditions resulting in uniaxial strain states are achieved over much smaller dimensions, and very fast diagnostic tools are used to ensure that the smaller test times are sufficient. Test assemblies can be fabricated so that a number of impact experiments can be performed quickly and economically. The basis for this new capability is the knowledge gained during the development of laser-based techniques for detonating explosives at Sandia National Laboratories and at Los Alamos National Laboratory during the late 1980s and early 1990s. In particular, a key development was the ability to laser-accelerate small discs of metal films to very high velocities using Q-switched, solid-state lasers. Planar impact of one of these films on certain explosives results in a prompt detonation. Sub-nanosecond interferometric diagnostics were developed for examining the motion and impact of these films. Although specifically directed towards explosives, this work established the basic feasibility of using a laser-based approach to study the dynamic properties of materials over some range of conditions. This approach can be described as shock wave generation through planar impact using *photonic* driving, in contrast to explosive or compressed-gas driving.

In a basic photonic-driving configuration, a small metal disc, or "flyer," is attached to an optical substrate. A Q-switched laser pulse is directed through the substrate and delivered

uniformly over the substrate/flyer interface. At peak laser intensities of ~0.1 GW/cm^2 or greater, a plasma will be quickly generated from a thin portion of the flyer which can then absorb a significant fraction of the remaining pulse energy. The rapid energy deposition results in plasma pressures that can reach several GPa, and the flyer is accelerated away from the substrate. To observe the acceleration history, conventional laser interferometry techniques are modified so that optical interference fringes are recorded on a very fast streak camera with sub-nanosecond temporal resolution. Flyer impact into a second material will result in the generation of a shock wave whose amplitude and duration depend on the materials involved, the impact velocity, and the flyer thickness. A test material can be impacted into a well-characterized optical window in a "reverse impact" configuration, or a well-characterized material can be impacted into a stationary test material having an optical window on the back surface (a "direct impact" configuration). From these two cases, the interferometry records can be used to obtain specific equation-of-state (shock Hugoniot) data or constitutive stress-strain properties, respectively.

In order to address a useful range of materials, stress states, and test times, the laser driving conditions must be scaled up significantly from the earlier work with explosives. This introduces a number of challenges associated with laser-induced damage in optics, laser beam shaping, excessive thermal transport and instabilities in laser-accelerated materials, and fabrication techniques for photonic-driving test assemblies. Addressing these challenges was the purpose of the present study. The next section of this report provides a brief summary of the various development studies that led to photonic driving techniques. The following section reviews scaling laws, a simple analytical model, and important limitations. The next section summarizes numerical simulation activities. Subsequent sections describe two photonic driving systems that were assembled at different scale-up levels. The first system was used for evaluation of design options and for providing qualitative insights into plasma generation and flow processes. The second system had extensive interferometry diagnostics, and was used for shock-physics demonstration experiments. The demonstration experiments are described in a separate section, followed by a general summary.

2. Background

The use of lasers for generating shock waves in solids began when Q-switched, solid-state lasers became available in the 1960s. The relatively high pulse energies and very short pulse widths of these lasers can produce very high intensities (>>GW/cm^2) within a focused beam. Initial studies examined the effects of Q-switched laser pulses incident upon materials at free surfaces [1], and this remains a significant area of interest. In the 1970s, L. C. Yang and co-workers at JPL conducted extensive studies on the generation of shock waves by laser pulses incident on a thin metallic film confined between a material of interest and an optical substrate [2,3]. These studies utilized a ruby laser producing 15-ns pulses at 694.3 nm, and quartz stress transducers were used to obtain time-resolved measurements of the stress pulses generated by the laser. The mechanism for shock generation, which will be discussed shortly, required that the average laser intensity (average incident fluence divided by the pulse width) be sufficiently high ($\geq$ 0.1 GW/cm^2). Yang found that the temporal shape of a laser-generated stress pulse was similar to that of the laser pulse, but the stress pulse duration was approximately twice as long. The peak stress scaled nearly linearly with the incident laser fluence over the observed range of 2-14 J/cm^2, with maximum values near 2.0 GPa observed using glass samples. The film material and its thickness did not strongly influence the peak stress, provided the thickness was at least several hundred Angstroms. Yang's application of interest was the detonation of relatively insensitive, secondary explosives, and his work helped motivate studies at Los Alamos National Laboratory [4] and Sandia National Laboratories [5] during the late 1980s to further develop laser-based methods for the prompt detonation of these explosives. In a typical configuration for these studies, a metallic film was vapor-deposited on an optical substrate (or on the polished end of an optical fiber), and a low-density pellet of a secondary explosive (such as PETN) was pressed directly against this film. In the experiments, a pulse from a Q-switched, Nd:YAG or Nd:glass laser would be incident upon the film, and various optical and electrical diagnostics were used to assess the response of the adjacent explosive. Laser parameters and explosive properties were widely varied to examine their role in detonation mechanisms. The work at both labs led to the successful design of optical detonators that had performance characteristics comparable to exploding bridgewire (EBW) electrical detonators.

The mechanism for laser-driven shock generation at a confined metal film was well established by the time of the optical detonator work [1-3]. At the start of the laser pulse, a small

amount of absorption occurs because the incident electromagnetic field penetrates into the metal film to a depth that depends on the metal's optical properties and the laser wavelength. For example, this depth is approximately 5 nm for 1.06-micron laser light incident on aluminum. The penetrating field interacts with the metal's free electrons, whose subsequent collisions are so rapid that the absorbed optical energy can be treated as an instantaneous heat source. Thermal diffusion rapidly spreads this heat over a depth that varies as the square root of the product of the metal's thermal diffusivity and the laser pulse width. For a 20 ns pulse incident on a thick aluminum film, the thermal diffusion depth is approximately 2 microns. In the absence of phase transitions, the average temperature rise within this heated layer is proportional to the incident laser intensity and pulse width, and inversely proportional to the thermal diffusion depth. If the incident laser intensity is sufficiently high, part or all of the film can be rapidly heated through melting, vaporization, and finally ionization. As these phase transitions occur, the fraction of incident laser power that is being absorbed will increase. Once a sufficient electron number density in the ionized material is reached, the remainder of the laser pulse can be absorbed efficiently in the plasma through the inverse Bremsstrahlung process. Thus, a high-pressure, high-temperature plasma can be generated from the confined metal film on the time scale of the laser pulse. Loss mechanisms include radiative transport and thermal conduction into the confining materials. For plasma pressures reaching several GPa, Yang estimated plasma temperatures as high as 10^5 K. In the experimental configuration used by Yang, compressive stress waves were generated in both of the adjacent, confining materials by the transient pressure rise occurring at their interface with the laser-generated plasma. In the case where one of these materials is a low-density explosive, the plasma is less confined and expands into and compresses the explosive material, leading to detonation from a combination of thermal ignition and shock transition processes.

Around 1990, both the Sandia and Los Alamos laboratories became interested in developing an optical version of an exploding foil initiator (EFI), also known as a "slapper" detonator. In an electrical slapper detonator, very fast Joule heating localized in a thin metal foil results in foil explosion, which in turn accelerates an adjacent layer of dielectric material towards an explosive pellet. Impact of an area of this material layer, called the "flyer," produces a shock wave in the explosive, and a shock-to-detonation transition process follows. Compared to exploding bridgewire devices, slapper detonators can use explosive materials that are significantly less

shock sensitive. The slapper device is a miniaturized plate-impact configuration, typical of the experimental approach used in many shock-wave physics studies. Achieving an optical version of this device required finding a practical means for laser-acceleration of an equivalent "flyer." Earlier studies at Sandia had examined the laser acceleration of metal foils, both free-standing and with substrate tamping, using Q-switched Nd:YAG and Nd:glass lasers [6,7]. If a metal foil of sufficient thickness is adjacent to an optical substrate, a Q-switched laser pulse delivered through the substrate will result in the same plasma generation process described previously, with some fraction of the original foil thickness involved in the rapid phase transitions. The remainder of the foil is accelerated away from the optical substrate by the rising plasma pressure. The foil provides some degree of inertial confinement for the plasma during this process, depending on its mass per unit area. With a free-standing foil, the absence of the confining (or tamping) effect of the substrate results in much lower plasma pressures acting on the foil, leading to substantially reduced foil velocities. Foil accelerations were measured in the Sandia experiments using an optically recorded, laser interferometer system developed at Sandia known as ORVIS [8].

A period of active development of optical slapper detonators began with studies by Paisley, who used a Nd:YAG laser to accelerate metal films made by physical vapor deposition on optical substrates [9]. Laser interferometry and streak camera techniques were used to examine the launching of films that varied in composition, thickness, and diameter. Trott and Meeks introduced the use of optical fibers to deliver Q-switched Nd:glass laser pulses to aluminum foils [10,11]. In these studies, foils from 5 to 66 microns thick were held across the polished ends of fibers having diameters from 0.2 to 1.0 mm. The fiber end face performed the same tamping role as an optical substrate, and laser pulses delivered through the fiber launched a "flyer" having a diameter determined by the fiber core diameter. An ORVIS system was used to record the flyer acceleration history during each experiment. These studies provided early insights into laser breakdown and fiber damage issues that represent limitations to fiber delivery of high-intensity laser pulses. The efficiency of laser-acceleration of flyers was also examined, with laser pulse energy, laser pulse width, and foil thickness as parameters. Neglecting the loss of flyer mass during the plasma formation process, a coupling efficiency was defined as the ratio of the final flyer kinetic energy (assuming the original thickness) to the incident laser pulse energy. Values for coupling efficiency were determined to be near 25% for a broad range of conditions, with

values somewhat higher at the shortest pulse width (16 ns) and lower at the longest pulse width (48 ns).

During the next decade, many additional experimental and analytical studies were conducted on laser acceleration of small metal flyers. The role of laser pulse width on the efficiency of flyer acceleration was examined over a broader range [12]. Physical vapor deposition was introduced as a means of achieving thin metal films on the polished ends of fibers, and the determination of dynamic material properties such as spall strength was identified as an additional application for laser-accelerated flyers [13]. An "effective properties" model, based on the well-known Gurney theory for explosively driven plates, was developed and utilized very successfully to examine how final flyer velocities would vary over broad ranges of laser and flyer characteristics [14,15]. A capability for more detailed, time-dependent numerical simulations was developed, initially with the LASNEX hydrodynamics code [14] and later with the more versatile CTH hydrodynamics code [16]. An extension of these numerical simulations was a part of the present study, and will be discussed in a subsequent section of this report. Additional diagnostic techniques utilizing high-speed streak and framing cameras were developed to examine plasma motion and flyer integrity [17-20]. Finally, concern over excessive thermal transport through laser-accelerated flyers, as well as interest in optimizing coupling efficiencies, led to studies of composite flyers consisting of two or more layers of different materials. A number of studies examined the benefits of a "thermal barrier" layer of amorphous Al_2O_3 embedded within a thicker structure of pure aluminum or copper [9, 16, 18, 20-23]. These studies concluded that such a layer was advantageous in minimizing flyer heating and improving coupling efficiency, particularly at lower laser fluences. Labaste et al. [24] compared the use of titanium, hafnium, carbon, or germanium at various thicknesses instead of aluminum in the initial flyer layer that forms the accelerating plasma. In terms of final flyer velocity for a given incident fluence, they found that thin layers of germanium or carbon would give improvements up to 10% compared to the other materials.

Considering applications other than shock initiation of explosives, Paisley and co-workers at Los Alamos National Laboratory introduced the concept of conducting basic shock-wave physics experiments on a miniaturized scale using laser-accelerated flyers [13]. Initial experiments to measure spall strength in aluminum and copper were limited to flyer launch conditions that could be achieved using optical fiber delivery and flyers made through physical vapor deposition.

Subsequently, experiments were conducted using higher-energy Nd:YAG laser pulses incident on bulk-processed OFHC copper foils mounted on optical substrates [25]. The foil thickness was nominally 25 μm and flyer diameters were 1-3 mm. Laser interferometry (VISAR) was used to record both the flyer acceleration and the motion of the impact interface when the flyer impacted into an optical window. If the flyer impact velocity, the subsequent impact interface velocity, and the shock properties of the window material are known, then a fundamental shock property of the flyer material – a shock Hugoniot state – can be determined. Copper data obtained in this fashion were consistent with previous data obtained with conventional shock physics techniques. Later improvements to this system enabled 50-μm thick foils, 3-mm in diameter, to be launched at velocities up to 0.65 km/s [26]. Fiber optics were not used for beam delivery, but a diffractive optic was added to a focusing lens to flatten the laser beam profile incident on a flyer. Different optical substrate materials were evaluated, but performance differences were found to be small. A composite structure consisting of 0.5 μm of carbon, 0.5 μm of Al_2O_3, and 0.5 μm or more of aluminum was first deposited on the substrate surface. The foil flyers were then attached to this structure using an adhesive. Coupling efficiencies with this configuration were found to be near 20%. This system was used to examine spall characteristics of gold foils having different thicknesses [27].

3. Scaling Laws, a Simple Model, and Limitations

In the earlier work on detonation of explosives, either bulk-processed metal foils or films produced by physical vapor deposition were the source of laser-accelerated flyers. When beam delivery was through a step-index, multimode fiber, a fairly flat intensity profile was produced at the exit face over the diameter of the fiber core. The foil or film typically extended beyond the fiber's cladding layer to the adjacent support structure (a metal ferrule in which the fiber had been bonded prior to polishing). When significant pressures developed in the laser-generated plasma at the fiber/foil interface, an area of the foil corresponding to the fiber core would separate from the remainder of this layer by a dynamic shearing and yielding process. Neglecting the flyer material converted to plasma, the mass of this flyer could be estimated by: $m_f = \rho_f A_c \delta$, where ρ_f is the density of the flyer material, A_c is the fiber core area, and δ is the original foil or film thickness. During a typical experiment, a calibrated beam splitter was used to measure the actual laser energy E_l delivered through the fiber, and an ORVIS interferometry system was used to record flyer velocity throughout the acceleration process. An estimate of the final flyer kinetic energy is given by: $E_f = 0.5\, m_f v_f^2$, where v_f is the final (peak) flyer velocity. The incident laser fluence is $F_o = E_l / A_c$. A fairly extensive data base [10-15] was generated that showed how v_f values varied over a range of E_l, δ, A_c, ρ_f, and τ values, where τ is the laser pulse width. An important performance parameter was the coupling efficiency, defined as the ratio of flyer kinetic energy to incident laser pulse energy: $\eta = E_f / E_l$. For pure aluminum flyers, the data showed that the coupling efficiency was fairly constant and close to 25% over a broad range of conditions, provided the incident laser fluence, F_o, was above approximately 20 J/cm^2.

The expression for coupling efficiency can be rearranged in the form:

$$\rho_f \; \delta \; v_f^2 = 2 \; F_o \; \eta \qquad (1)$$

If the coupling efficiency is assumed to be a constant value, Eq. (1) provides a basic scaling law for estimating final flyer velocities as a function of incident laser fluence, flyer material, and flyer thickness. The flyer material (ρ_f) and final velocity determine the amplitude of a shocked state resulting from impact into a second material, and the flyer thickness determines how long this shocked state will be sustained. Equation (1) shows that the maximum impact velocity that can be achieved for a given flyer material is proportional to the square root of the ratio of laser

fluence to flyer thickness. Equivalently, to accelerate a given material to a desired impact velocity, the maximum thickness of impacting material that can be used is proportional to the laser fluence. Figure 1 shows final flyer velocities predicted by Eq. (1) for pure aluminum flyers assuming a constant coupling efficiency of 25%.

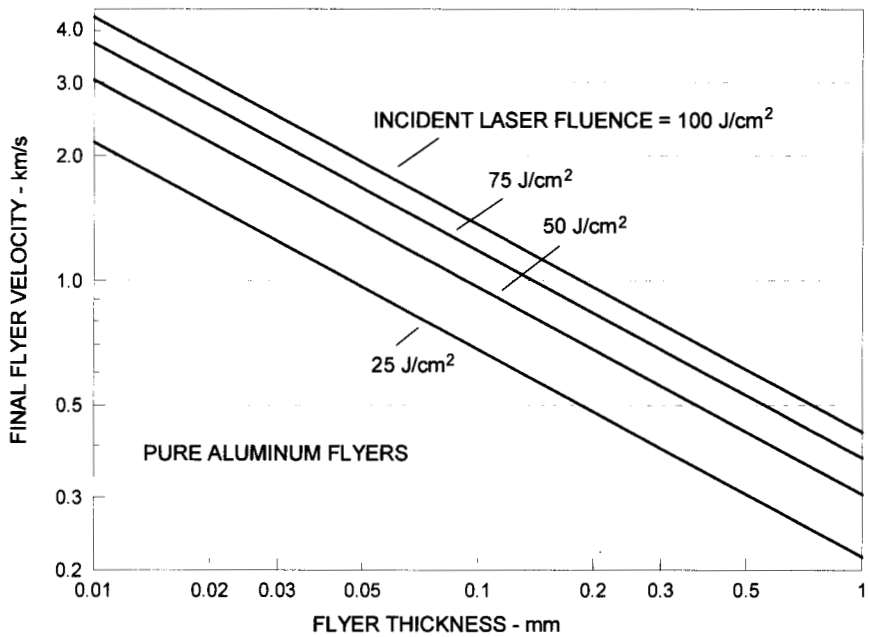

Fig. 1. Final velocity of aluminum flyers as a function of incident laser fluence and flyer thickness.

Although the simple scaling law proved useful for estimating flyer velocities, Lawrence [14,15] provided a more rigorous analysis for predicting the final velocity of a laser-accelerated flyer as a function of the various acceleration variables. His model is based on the conservation of energy formulation used in the well-known Gurney theory for explosively driven plates [28]. The analysis is one-dimensional and time-independent. At a time corresponding to the completion of the acceleration process, the kinetic energy of the flyer plus the kinetic energy of the vaporized portion of the foil are equated to an equivalent "Gurney energy" representing the laser energy deposited in the metal plasma. Assumptions include an exponential laser energy deposition within a depth much less than the foil thickness, a linear velocity profile in the expanding vapor, and a constant fraction of the incident energy lost by reflection and radiation. The derivation results in two "effective" parameters for which numerical values were obtained from a limited set of experimental measurements. The model was then applied over a broad range of initial conditions, and proved to be quite useful in predicting how final flyer velocities

would vary with incident laser fluence (including threshold conditions), laser pulse width, flyer thickness, and flyer material (e.g., magnesium and copper were compared to aluminum).

Because this model is one-dimensional, however, its applicability cannot extend to all flyer acceleration conditions of interest. As mentioned previously, many of the experiments performed in earlier studies involved laser energy delivered through a fiber to a fiber/foil interface over an area defined by the fiber core diameter. If a fiber was not used, the incident area was dependent on focusing optics and would be determined by beam profiling instrumentation. In either case, the lateral extent of the foil was typically much larger than the area experiencing laser irradiation. As rising plasma pressures resulted in foil motion within the irradiated area, the foil material around the perimeter of this area would experience strong shearing forces. This material would dynamically yield and ultimately rupture, resulting in a flyer having a distinct area. The mechanical work that must be done during material yielding and rupturing represents a loss mechanism that cannot be explicitly addressed in a one-dimensional model. For sufficiently high fluences and for thinner foils, this loss mechanism apparently is not very significant. However, when the Lawrence model was compared to data obtained with very thick (66 μm) aluminum foils, agreement could not be obtained unless an unidentified loss mechanism was addressed by increasing the assumed value for the fraction of incident laser energy lost through reflection and radiation.

Prior to rupture, the foil material around the flyer perimeter prevents free lateral expansion of the high-pressure plasma. Clearly, lateral plasma expansion will reduce plasma pressures available for accelerating the flyer, and this loss mechanism also cannot be addressed explicitly in a one-dimensional model. The fact that measured coupling efficiencies were fairly constant over some range of acceleration conditions indicates that the net effect of the two-dimensional loss mechanisms was essentially constant for these conditions. Because the goals of the present study dictated that a much broader range of conditions be addressed, an initial activity was an assessment of these loss mechanisms during the laser acceleration of thicker flyers. For this assessment, aluminum films 11-35 μm thick were vapor deposited on fused silica substrates. A length of optical fiber was used to homogenize the laser intensity distribution, and lenses were used to image the fiber output face onto the substrate/film interface. The nominal laser pulse width was 18 ns. For a 23-μm thick film, an incident fluence of approximately 20 J/cm^2 was required to have a well-defined flyer rupture cleanly from the extended film area and approach a

velocity predicted by the one-dimensional model. Below 9 J/cm^2, film material would deform but not rupture. Incident fluences less than 6 J/cm^2 would not produce visible film deformation. Acceleration experiments were also performed using films deposited on bare substrates in finite-area "islands" having a diameter slightly less than that of the incident laser beam. These experiments eliminated the loss mechanism associated with material yielding at the flyer perimeter but maximized the loss mechanism associated with lateral plasma expansion. Over the limited range of incident fluences and foil thicknesses examined, the measured flyer velocities indicated that the two loss mechanisms were quantitatively comparable in their effects on coupling efficiency. Further details of these initial experiments can be found in Appendix A.

The most important issue in any effort to increase photonic driving conditions is the limitation imposed by laser-induced damage mechanisms in the optical components that are required to deliver the laser pulse. When laser intensities approach GW/cm^2 levels, laser-induced damage can occur in high-quality optics at both optic/air interfaces (surface damage) and internally (bulk damage) [29]. A damage process during a laser pulse is typically catastrophic, with transmitted energy reduced on the damaging pulse and subsequent transmission prevented. Numerous studies on laser-induced damage in optical materials have been published during the past thirty years. In particular, interest in using optical fibers for laser delivery during the studies on laser detonation of explosives led to fairly extensive investigations of factors that govern damage thresholds in step-index, multimode, fused silica fiber [11,30,31]. For laser light incident upon a bare substrate surface, many studies at Lawrence Livermore National Laboratory have carefully examined the effects of substrate material, laser wavelength and pulse width, and surface finish [32]. Damage thresholds are typically given in terms of a limiting laser fluence, F_D, with an additional power-law scaling factor to account for variations in laser pulse width. For a laser wavelength of 1.06 μm incident upon well-polished fused silica surfaces, the Livermore studies found F_D values that averaged 35 $(\tau / \tau_o)^{0.35}$ J/cm^2, where the pulse width scaling factor, τ_o, is 3 ns over pulse widths from 0.6 to 84 ns. Because surface damage is very sensitive to surface finish and contamination, tested lots of substrates gave damage thresholds that ranged from less than half to more than twice this average value. The average threshold value becomes 65 J/cm^2 at the nominal pulse width of the lasers used in the present study (18 ns).

For flyers of a given material and thickness to be launched from the surface of a substrate, the maximum flyer velocity depends on the laser fluence incident on the substrate/foil interface. This value should be an upper bound to fluences found within the laser delivery optics. The design of the delivery optics will determine whether substantially lower fluences are actually achieved at all other locations. For example, if a laser beam is to be focused through a substrate to launch a flyer having a smaller diameter, the fluence at the initial substrate surface is reduced by using a lens with a shorter focal length and by using a thicker substrate. In practice, other factors can dominate the optics design, such as the methods used to achieve a uniform laser intensity over the flyer area. In the absence of specific laser and delivery optics characteristics, a reasonable estimate of maximum laser fluences available for accelerating flyers from a substrate is simply the laser-induced damage threshold expected for the substrate surface.

4. Numerical Simulations

A capability for numerically simulating laser acceleration of small metal flyers was one goal of the earlier studies on initiation of explosives. In particular, details of the laser energy deposition, thermal transport within the flyer throughout the acceleration process, and two-dimensional effects were issues that needed to be examined before experimental parameters could be optimized. The initial simulation work was performed by Farnsworth [14] using the Lagrangian hydrodynamics code LASNEX. The LASNEX code had been developed for applications involving much higher laser intensities, and only considered matter in a plasma state for laser energy deposition. Using an artificial means of representing the initial absorption processes leading to ionization, Farnsworth conducted one-dimensional simulations of experimental conditions used by Trott [12]. Flyer acceleration and laser reflection histories compared fairly well with experimental measurements.

In order to more realistically address laser energy deposition at a window/metal interface and the resulting phase transitions, Farnsworth switched to the CTH hydrodynamic code in his simulation work [16]. Modifications were made to provide laser energy transport and absorption features suitable for photonic driving applications. One-dimensional simulations were made to examine the role of the optical substrate material, and an important result was the surprising extent to which this material contributes to the driving plasma. This was substantiated both by examining post-test substrate surfaces and by plasma emission spectroscopy studies [21]. Farnsworth also examined the role of a "thermal barrier" layer of Al_2O_3 embedded within an aluminum flyer. The simulations showed that this layer resulted in more rapid plasma formation due to lower conduction losses early in the acceleration process, and somewhat lower temperatures throughout the flyer later in time. These effects were stronger for lower incident laser fluences. The simulation results were consistent with experimental comparisons by Trott [18] between pure-aluminum flyers and flyers containing embedded alumina layers.

The numerical simulation capabilities using the CTH hydrodynamics code were obviously desired as a component of the present study. Unfortunately, during the intervening years the CTH operating environment had been changed to take advantage of parallel processing capabilities. A substantial effort was required to adapt the specialized laser energy transport and absorption routines to the new environment. Once completed, however, this capability was used to examine important issues associated with the efforts to substantially increase photonic driving

conditions. Figure 2 shows the basic experimental configuration for CTH simulations during the current study. Elements consist of an optical substrate, a "launch layer," a metal flyer, and an optional "witness plate" window. The optical substrate and window are typically fused silica, and the launch layer consists of one or more films deposited on the substrate by physical vapor deposition. The flyer is typically assumed to be in intimate contact with the launch layer, without an adhesive layer. The incident Nd:glass laser pulse has a wavelength of 1.054 μm, a full-width-at-half-maximum pulse width of 18 ns, and normally is assumed to have a uniform intensity distribution over the flyer area.

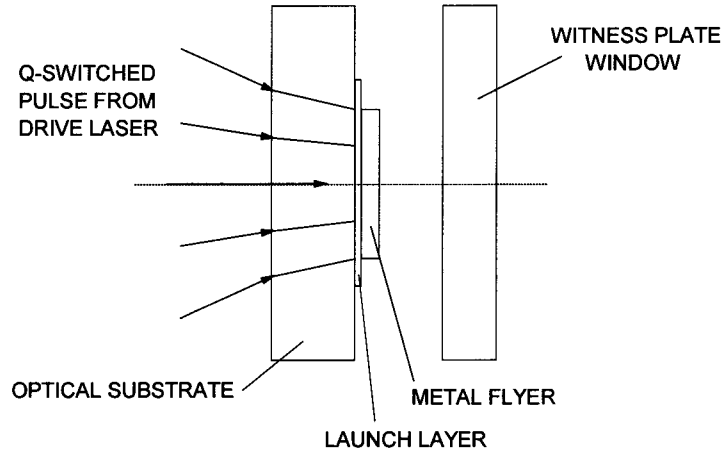

Fig. 2. Typical configuration for CTH simulations.

An important issue in photonic driving is thermal transport through the flyer thickness during the acceleration process. The thermodynamic state of the flyer when it impacts a second material will affect the shock conditions produced in that material. The composition of the launch layer can include a "thermal barrier" of low-conductivity material, such as amorphous Al_2O_3, to mitigate flyer heating. One-dimensional CTH simulations were used to assess various launch layer compositions containing such a barrier layer. Figures 3 and 4 show simulations of the launch of a 100-μm thick aluminum flyer at an incident laser fluence of 50 J/cm^2 for two different launch layer compositions. One launch layer consisted of 5 μm of pure aluminum, while the second was a composite consisting of 0.25 μm of aluminum followed by 4.75 μm of Al_2O_3. If the flyer surface originally in contact with the launch layer is designated the "front" surface, then Fig. 3 shows the velocity history of the flyer back surface (as would be measured

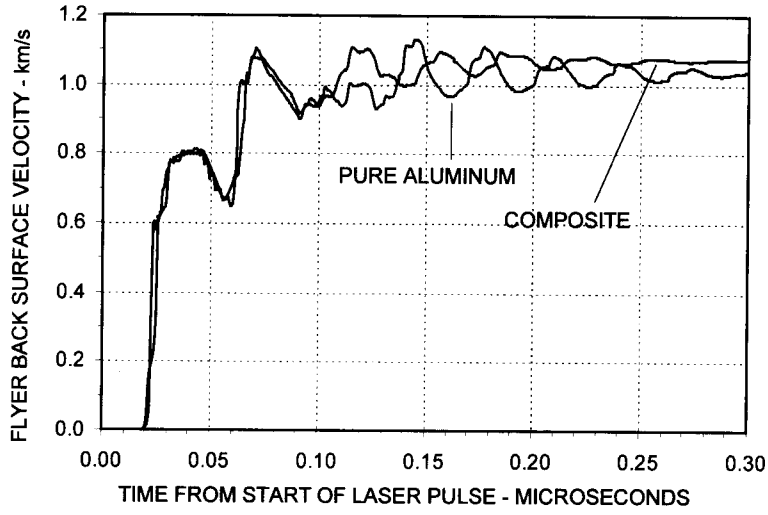

Fig. 3. Predicted velocity of the flyer back surface for two different launch layers.

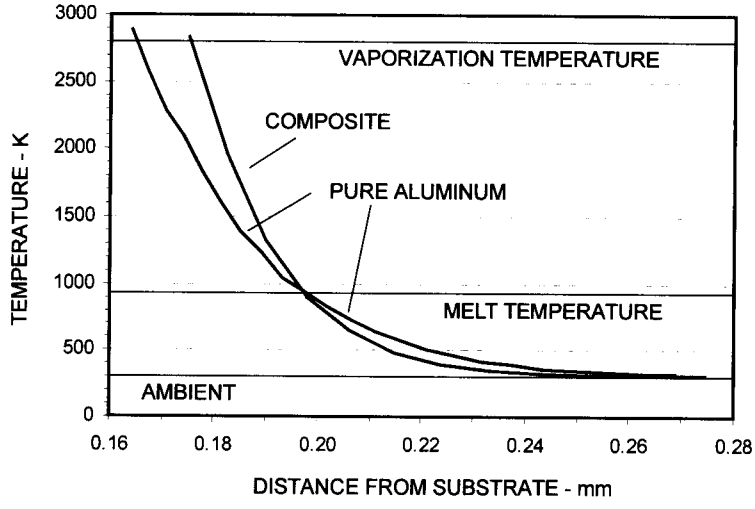

Fig. 4. Predicted temperatures in the flyer for two different launch layers, 0.20 μs after the start of the laser pulse.

experimentally using ORVIS instrumentation) for the two cases. Wave reverberations appear to damp out more quickly for the composite case, and this case shows a slightly higher final velocity. Figure 4 shows temperature profiles through the flyer for these two cases at a time 0.20 μs after the start of the laser pulse. Note that the flyer has traveled slightly farther in the composite case, consistent with the velocity profiles shown in Fig. 3. The flyer back surface is near ambient temperature in both cases, but temperatures rise past the melt temperature and

reach the aluminum vaporization temperature at the front face. Approximately 20% of the flyer has melted in the composite case, compared to 25% for the pure-aluminum case.

One-dimensional CTH simulations have been used to examine the impact of a flyer into a witness plate, including the case of a thin layer of a test material attached to the back flyer surface. This simulation case will be discussed in a subsequent section of this report. Two-dimensional CTH simulations have been conducted to examine plasma expansion at the flyer perimeter and the consequences of non-uniform incident laser intensity over the flyer area. Examples of these calculations can be found in Appendices A and B.

5. 250 mJ Photonic Driver System

Laser pulse energies of a few 10s of mJ were typical of the early studies that examined the detonation of explosives. An initial goal for the present study was to develop a functional photonic driving system that could operate at laser pulse energies up to 250 mJ. The driving fluence corresponding to this energy level depends on the flyer area, with fluence levels of 25, 50, 75, and 100 J/cm^2 corresponding to flyer diameters of 1.13, 0.80, 0.65, and 0.56 mm, respectively. A previous section discussed limitations due to laser-induced damage in optics, with 65 J/cm^2 an average fluence level expected for the onset of surface damage in well-polished substrates using the lasers available for the present study. This consideration led to the conservative choice of using flyer diameters no smaller than 0.80 mm with the 250 mJ system. The scaling relations shown previously (Fig. 1) indicate what flyer velocities can be expected for aluminum flyers at these driving conditions as a function of flyer thickness. To achieve velocities of 1 km/s, a 0.80-mm diameter aluminum flyer must have a thickness of 0.10 mm or less. Impact of an aluminum flyer with a thickness of 0.10 mm will result in a shock state sustained for approximately 30 ns at the impact interface.

Two older lasers were available for this study: a Quantel Model PG-18 Nd:glass laser with a maximum Q-switched output of 2 J, and a Lasermetrics Model 9380 Nd:glass laser with a maximum Q-switched output of 20 J. Both of these lasers have nominal pulse widths of 18 ns and multimode outputs resulting in near-field beam profiles having a partially filled "doughnut" shape with a few hot spots around the doughnut perimeter. Several options were considered for achieving a uniform laser intensity over the flyer area starting with such a challenging profile. Profile flattening using diffractive optics was a possibility, since significant development of beam-shaping optics has occurred in recent years. Since the lasers did not have simple Gaussian profiles, however, a custom design and fabrication effort would be necessary, with some risk of an inadequate outcome. Another option was to use an optical fiber for beam delivery, as in the earlier work with explosives. Assuming the laser beam can be focused into the fiber without air breakdown occurring, a length of fiber with sufficient bends in the path can produce a fairly flat intensity profile at the fiber exit face [33]. This profile will have fine-scale intensity variations ("modal noise") due to interference between propagating fiber modes, with the amplitude of these variations dependent on the temporal coherence of the laser. To launch a flyer from a substrate surface, a pair of lenses can be used to image the fiber exit face onto the flyer/substrate

interface. With commercial fibers available having 0.80-mm diameter cores, the fiber delivery option was chosen for the 250 mJ system.

The two available lasers were located in separate labs, and comparable 250 mJ systems using fiber optic delivery were assembled in both locations. For simplicity, only the Quantel laser system will be described in some detail. A sketch of the experimental configuration using this laser is shown in Fig. 5. The optical fiber is Polymicro Technologies type FVP800880930, which has an 800-μm diameter, pure fused-silica core, and a 0.22 numerical aperture. The total fiber length of 3 meters was wrapped into several loops approximately 25 cm in diameter. The

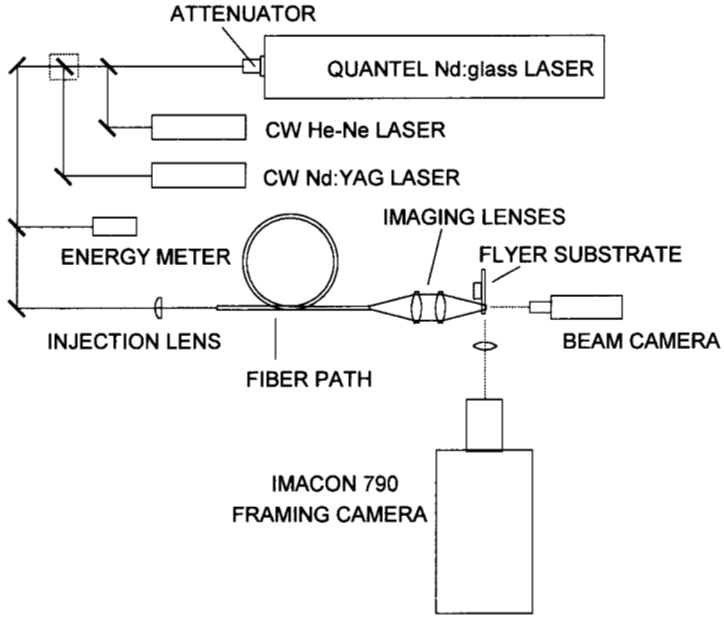

Fig. 5. 250 mJ photonic driving system using the Quantel laser.

fiber end faces were mechanically polished following a schedule that was developed to achieve high thresholds for laser-induced breakdown or damage [31]. In order to successfully transmit 250 mJ pulses, air breakdown must not occur prior to the fiber entrance face, and peak local fluences at this face must not result in local laser-induced breakdown or damage. A custom diffractive optic to mitigate these concerns was designed and fabricated at Sandia National Laboratories for the 250 mJ systems, but design or fabrication problems resulted in unacceptable performance. Fortunately, modifications to the Quantel laser cavity to significantly increase the beam divergence resulted in acceptable fiber injection using only a plano-convex lens having a 77-mm focal length and mounted backwards to increase spherical aberration. With this lens, the

measured threshold for air breakdown was approximately 450 mJ. Figure 6 shows measured beam profiles at various positions within the delivery optics. These profiles were obtained using

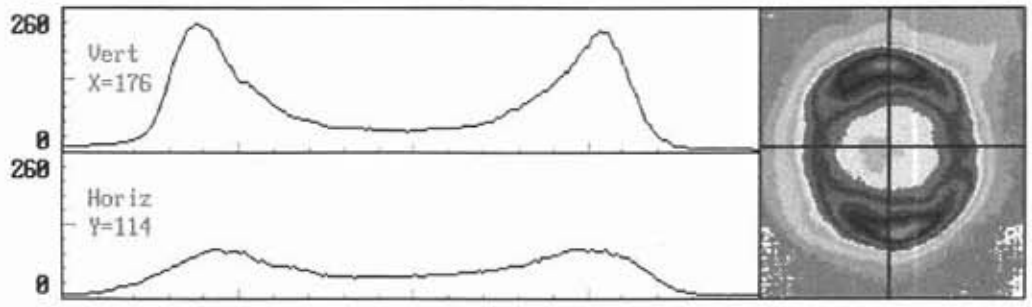

Fig. 6a. Laser near-field profile. Area shown is 12.1 mm wide by 14.2 mm high.

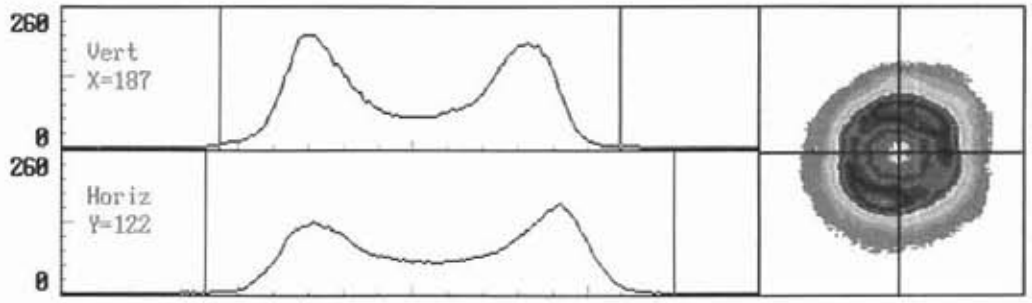

Fig. 6b. Beam profile at the fiber entrance face. Cursors show 800-μm dimensions.

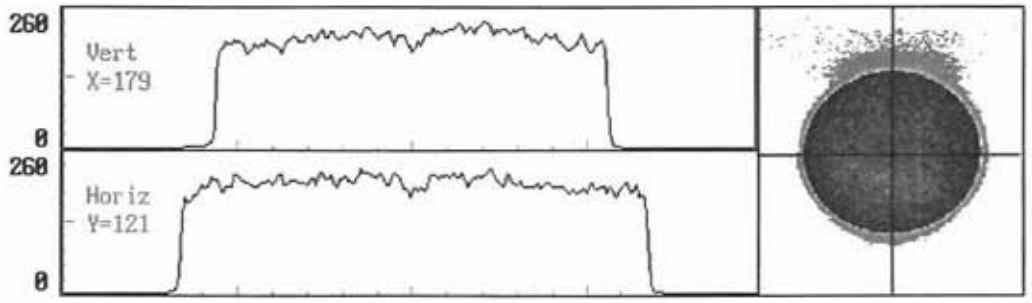

Fig. 6c. Beam profile at the exit face of the 800-μm-diameter fiber.

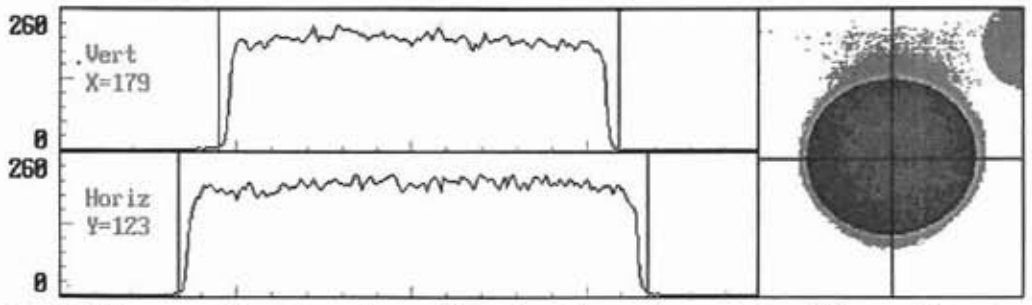

Fig. 6d. Beam profile at the substrate/flyer interface. Cursors show 800-μm dimensions.

a Cohu Model 4800 CCD camera with either demagnification (Fig. 6a) or magnification optics and commercial beam-profiling software.

A significant issue that must be addressed for photonic driving applications is the design and fabrication of launch assemblies consisting of an optical substrate, a vapor-deposited launch layer (discussed in the previous section), and the flyer discs. The objective for the Quantel laser 250 mJ system was to provide a means for assessing design and fabrication options. The Lasermetrics laser system was located in a lab with ORVIS instrumentation available for recording flyer velocity histories. As shown in Fig. 5, flyer diagnostics for the Quantel laser system consisted of a Hadland Photonics IMACON 790 framing camera. This camera produces a series of small images taken at fixed time intervals that are recorded on high-speed film. The fastest available camera electronics produced images every 100 ns having 20 ns exposure times, and up to eight full images could be recorded over the film area. Backlighting using a pulsed xenon flashlamp was chosen as the illumination method for recording images. Trigger signals from digital pulse generators were used to synchronize the laser, the xenon flashlamp, and the framing camera. Figure 7a shows a framing sequence recorded by the camera with the laser prevented from reaching the flyer. The individual images are approximately 16 mm wide and 18

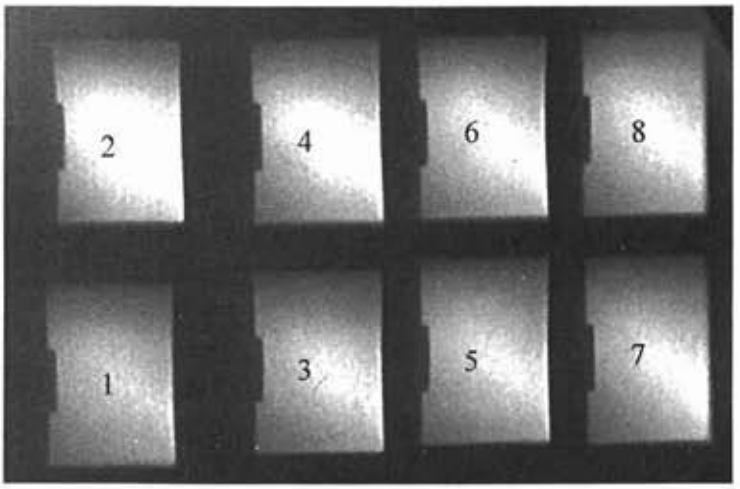

Fig. 7a. IMACON 790 image sequence showing a stationary flyer.

mm high, and show side-on views of a flyer having a thickness of 100 μm and a diameter of 800 μm resting on a substrate. The positioning of the images over the film area is not consistent, and the focus and distortion of individual images varies (much better framing cameras are currently available, but they are extremely expensive). Fig. 7b shows the corresponding timing of the

individual images relative to the start of the laser pulse. The camera generates timing signals corresponding to the individual images, and these were recorded on a digital oscilloscope along with the output from a fast phototube monitoring the laser pulse on each experiment.

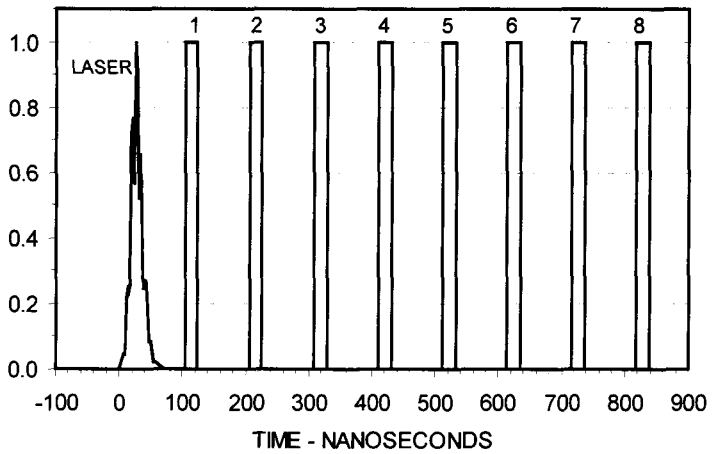

Fig. 7b. Timing of the individual camera images relative to the start of the laser pulse.

This system was used to examine plasma formation and spreading during the acceleration of flyers attached by different means to a variety of launch layers. The choice of flyer for these studies was based on a Lasermetrics system objective of conducting demonstration experiments using flyers having well-established shock properties. Consequently, an initial effort was devoted to the fabrication of aluminum flyers meeting this requirement. Two appropriate aluminum alloys are 2024 and 6061-T6 [34], which differ considerably in their ductility. This proved to be important in fabrication efforts, and 6061-T6 aluminum became the material of choice. The first challenge was achieving the intended flyer thickness of 0.1 mm. Although aluminum foil can be obtained at this thickness, 6061-T6 aluminum is only processed as sheet stock having a much larger thickness. Sheets having a thickness of 0.5 mm or 0.8 mm were obtained, and from these 5-cm by 5-cm squares were cut and carefully lapped to a thickness of approximately 0.15 mm. After some trial and error, a custom punch was designed that would consistently produce 800-μm-diameter discs from these squares with a minimum of edge distortion. These discs were then manually polished to a final thickness of 100 ± 15 microns, with a digital micrometer used to select discs within a narrower range in thickness. Once mounted on a substrate, individual flyer thickness and planarity could be carefully examined with a Wyko non-contact (laser) profilometer.

Vapor-deposited launch layers consist of various thicknesses of one or more different materials, and the composition of these layers can affect flyer performance (Figs. 3 and 4 in the previous section). A number of launch layer compositions were deposited on fused silica substrates for use with the Quantel laser system. A remaining question was how to attach the aluminum flyers to these layers. A number of adhesives and various methods for application were tried, and consistently achieving a thin, uniform bond layer proved to be challenging. One approach that worked fairly well was to use a very low-viscosity epoxy consisting of Dexter Hysol 2038 resin and 3034 hardener. A very small amount of this epoxy would be mechanically deposited on one surface of a flyer held by a miniature vacuum holder under a stereo microscope. The vacuum holder would then be positioned over the launch layer and the flyer released. A flat weight was used to hold flyers in position during a 24-hour, room-temperature cure. Excess epoxy would spread from the flyer over the substrate surface, but could be removed after curing using methanol.

To avoid the inconsistencies of adhesives, diffusion bonding techniques were also pursued. A major problem in this approach is overcoming the presence of aluminum oxide surface layers. Successful bonding required a high-temperature (460 C) vacuum environment, and a significant weight applied uniformly for a minimum time (~45 minutes). Applying weight uniformly was difficult because of small variations in flyer thicknesses, and the bonding environment appeared to slightly distort the flyer shape and change the texture of the launch layer. Figure 8 shows a complete launch assembly made using diffusion bonding. The fused silica substrate is 1.6 mm

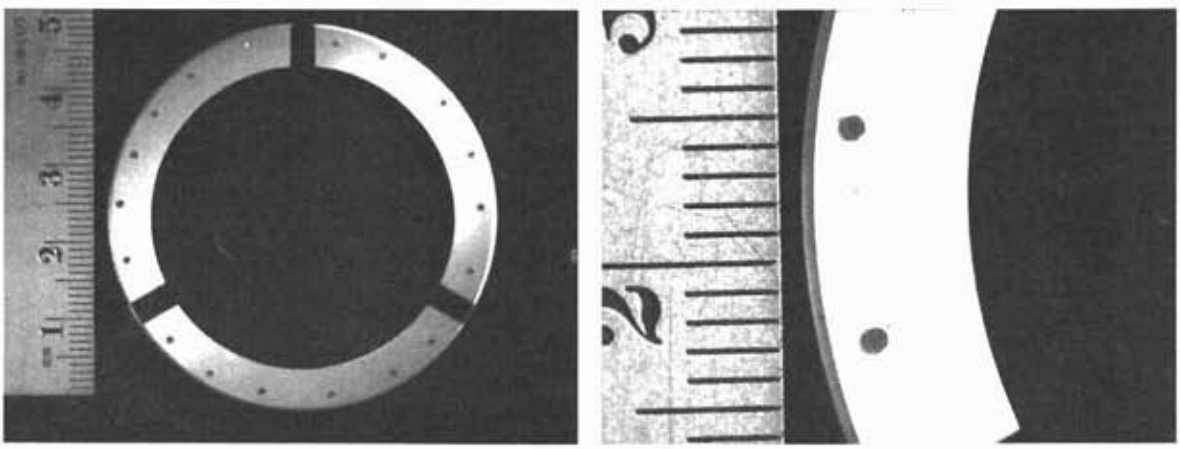

Fig. 8. A launch assembly prepared using diffusion bonding to attach aluminum flyers.

thick and has a diameter of 5 cm. The launch layer deposited around the perimeter of the substrate is 5 μm of pure aluminum, and the 18 individual flyers are 6061-T6 aluminum discs 800 μm in diameter and 100 μm thick. To hold a launch assembly in place, a small cylinder is fastened to the center of the substrate's front surface using epoxy. This cylinder fits into a standard optics mount that provides translational and rotational motion. Using a 1.06-μm CW laser passing through the beam delivery optics, the magnified beam-profiling camera can be centered on the focused image of the fiber exit face appearing at an uncoated region of the launch side of the substrate. The substrate can then be translated until a flyer is centered at the same position within the camera's field of view.

Figure 9 shows four different launch assembly configurations. The top left picture shows a flyer (not completely polished) attached to a 5-μm, pure-aluminum launch layer using thin-film epoxy. The top right picture shows a flyer similarly attached to a composite launch layer consisting of 0.25-μm of aluminum and 4.75-μm of Al_2O_3. The bottom left picture shows a flyer attached directly to the fused silica substrate (no launch layer) using thin-film epoxy, and the bottom right picture shows a flyer diffusion bonded to a 5-μm, pure-aluminum launch layer.

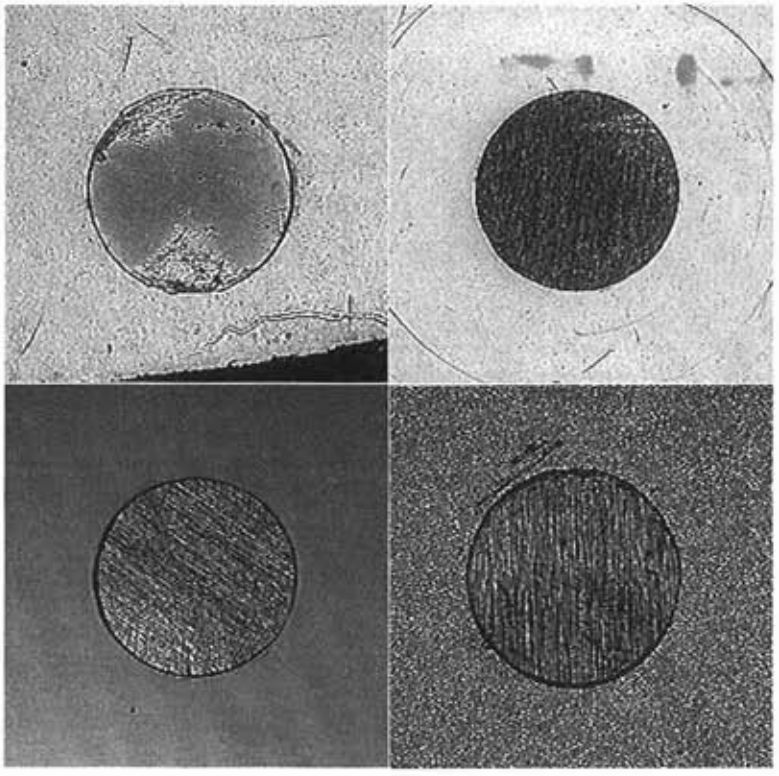

Fig. 9. Different launch assembly configurations for 800-μm diameter, 6061-T6 aluminum flyers.

These four launch assembly configurations were used in experiments with the Quantel laser system to examine resulting differences in the plasma formation and lateral expansion. Figure 10 shows flyer and plasma motion recorded with the IMACON 790 camera for the four launch assembly configurations using an incident laser fluence of 17.9 ± 0.6 J/cm^2. The laser energy reaching the substrate launch layer is calculated from the reference energy measured before the fiber injection lens (Fig. 5) and the measured transmission of 84.4% from this point to the launch layer. The incident laser fluence is based on the beam profile at the launch layer shown in Fig. 6b, and corresponds to the average value within the center 90% of the flyer's 800-μm diameter.

a) launch layer: none (bare substrate); bonding: thin-film epoxy

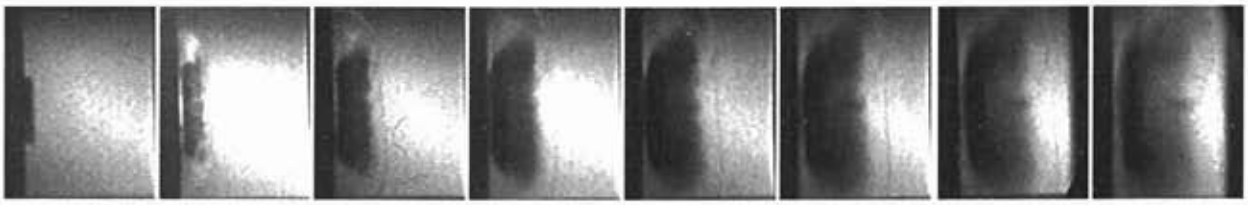

b) launch layer: 5 μm of aluminum; bonding: thin-film epoxy

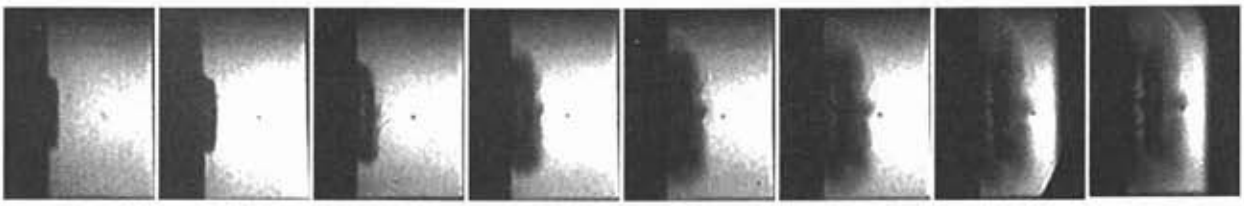

c) launch layer: 0.25 μm of aluminum and 4.75 μm of Al_2O_3; bonding: thin-film epoxy

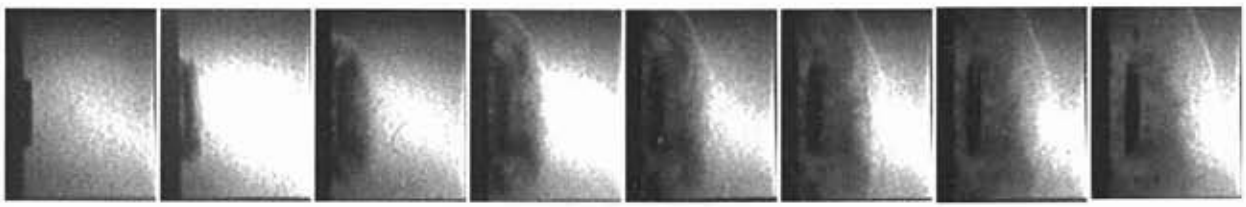

d) launch layer: 5 μm of aluminum; bonding: diffusion bond

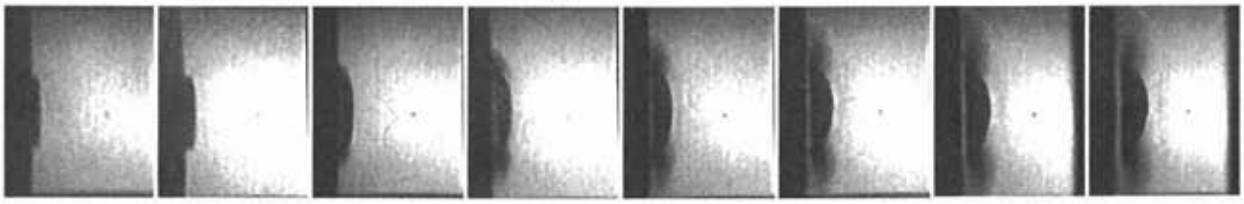

Fig. 10. Flyers launched at ~18 J/cm^2 from four different launch assemblies.

The film prints were converted into a digital image by scanning, then commercial software (Adobe Photoshop) was used to select and rearrange the individual images into the figure format. The qualitative features shown for each launch assembly case are quite different. Figure 11 shows a similar comparison using an incident laser fluence of 28.1 ± 0.3 J/cm^2. Although greater plasma formation and spreading are apparent as expected, the qualitative features for each launch assembly case closely match those seen in Fig. 10. Clearly, the launch layer composition and the method of flyer bonding make a substantial difference in the flyer acceleration features that can be observed in this manner. The exact position of the flyer in each

a) launch layer: none (bare substrate); bonding: thin-film epoxy

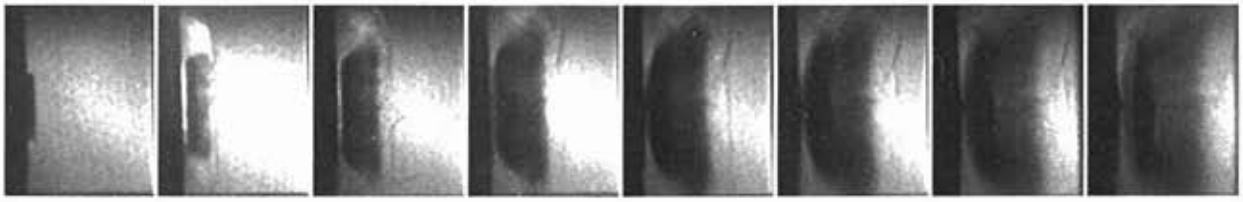

b) launch layer: 5 μm of aluminum; bonding: thin-film epoxy

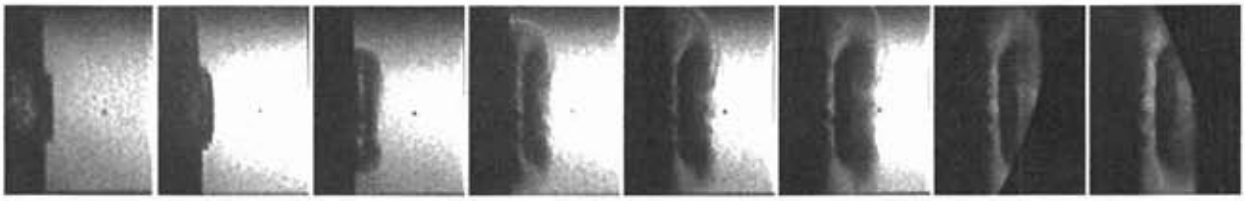

c) launch layer: 0.25 μm of aluminum and 4.75 μm of Al_2O_3; bonding: thin-film epoxy

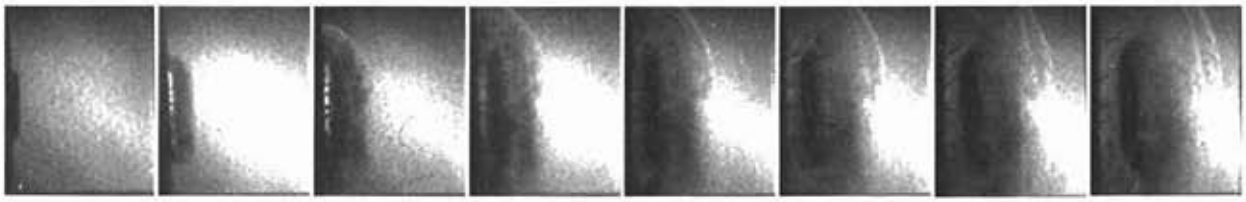

d) launch layer: 5 μm of aluminum; bonding: diffusion bond

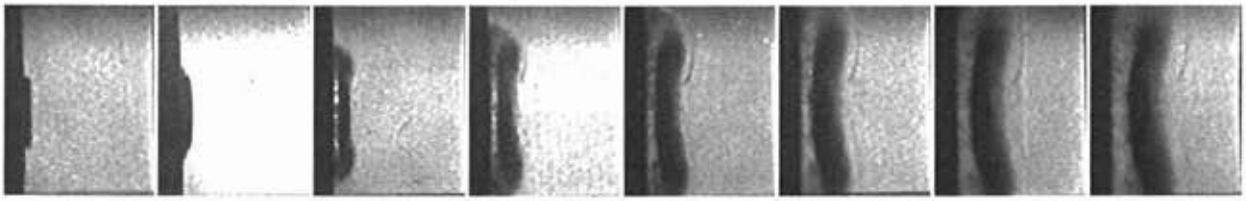

Fig. 11. Flyers launched at ~28 J/cm^2 from four different launch assemblies.

shadowgraph image is generally difficult to determine. Plasma flows both laterally along the substrate surface and perpendicular to the substrate behind the flyer back surface and around the flyer perimeter. Because plasma velocities greatly exceed flyer velocities, an axisymmetric, conical flow can be seen moving ahead of the flyer by the second or third image in a given sequence. Surprisingly little emission from the plasma is recorded in the early frames, possibly because the plasma cools rapidly to a vapor phase compared to the relatively slow sampling by the camera (Fig. 7b). The flow appears dark or even opaque in the shadowgraph images, typically masking the flyer location. Late in time the cloud thins and becomes more transparent. In all of the cases, air shocks appear in front of the expanding cloud. Air shocks and extended regions of plasma absorption were observed in earlier high-resolution shadowgraphs of the launch of much thinner flyers [19].

Disturbances ahead of the flyer appear to be consistently greater for flyers bonded using thin-film epoxy, rather than diffusion bonded. The case having no launch layer showed the largest formation of dark and opaque regions, indicating a significant contribution of the epoxy to this feature. The case using a composite launch layer (0.25 μm of aluminum followed by 4.75 μm of Al_2O_3) showed the smallest very dark or opaque regions. The plasma flow with diffusion-bonded flyers was predominantly lateral, but the opaque region appeared to have more curvature than the other cases. As noted previously, both some distortion in the flyer shape and a change in the texture of the launch layer were apparent after bonding for this case (Fig. 9).

From these qualitative comparisons, a composite launch layer and an absolute minimum of adhesive appear to be advantageous. Diffusion bonding obviously eliminates the adhesive, but may introduce additional concerns when aluminum surfaces must be joined. Figure 12 shows the results from launching diffusion-bonded aluminum flyers at incident laser fluences ranging from 17 to 50 J/cm^2. Significant curvature in the dark features is apparent in the lower fluence cases, but the entire disc/cloud structure becomes flatter as the incident fluence is raised. To achieve the 50 J/cm^2 condition (Fig. 12e), a pulse energy of 272 mJ was injected into the 800-μm diameter fiber, with 230 mJ reaching the launch layer. At this level, the launch process results in severe damage to the substrate. Figure 13 shows photographs of post-launch sites from the diffusion-bonded launch assembly. These pictures were taken with backlighting so that the post-launch transparency of the substrate could be observed. At the lowest fluence the substrate appears to be undamaged, with some aluminum re-deposited on the surface. As the incident

fluence is increased, mechanical damage to the substrate becomes apparent over a region extending several millimeters. At the highest fluences the substrate is extensively shattered and

a) incident laser fluence 17.3 J/cm^2

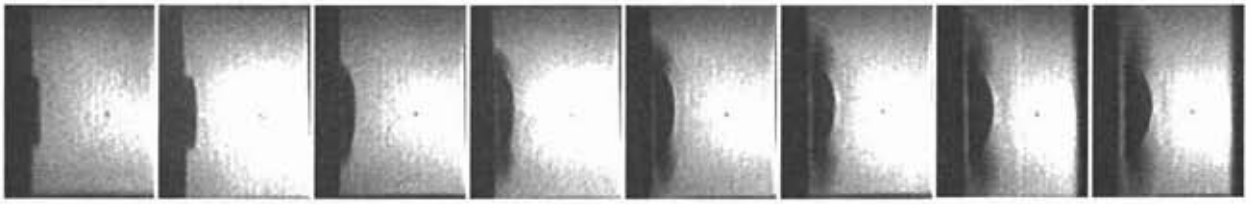

b) incident laser fluence 22.3 J/cm^2

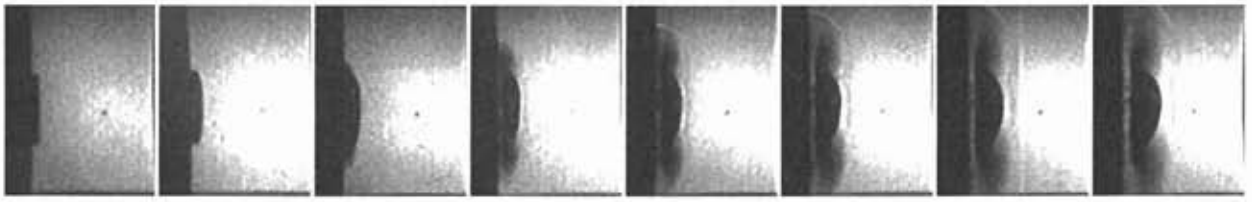

c) incident laser fluence 28.4 J/cm^2

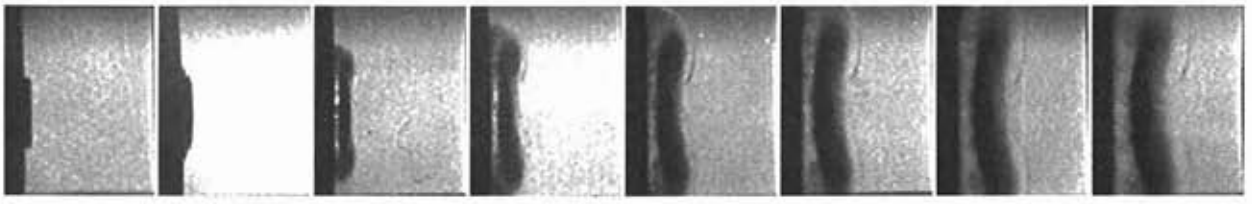

d) incident laser fluence 38.6 J/cm^2

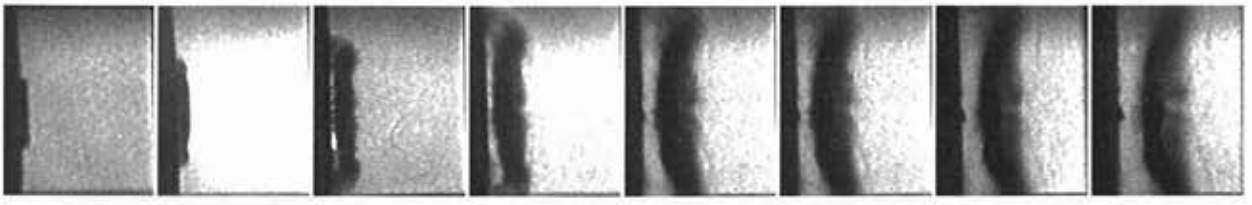

e) incident laser fluence 50.3 J/cm^2

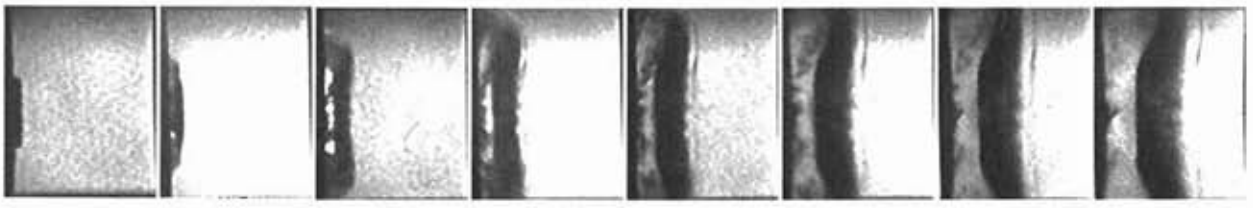

Fig. 12. Acceleration of flyers diffusion-bonded to a 5-μm aluminum launch layer.

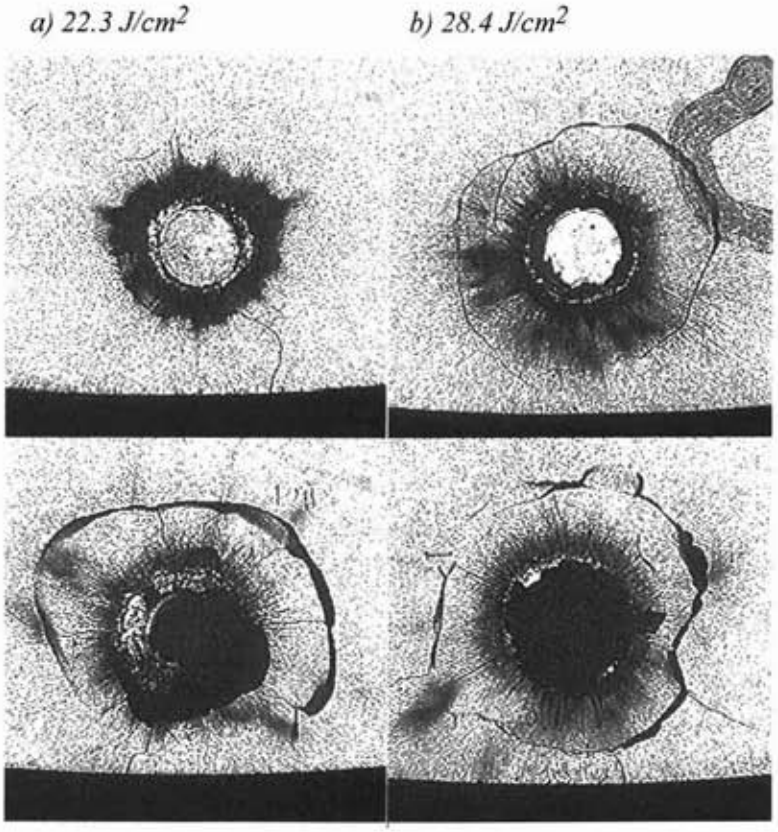

Fig. 13. Photographs of post-launch sites for the diffusion-bonded launch assembly.

has no residual transmission. The violence of this event was sufficient to dislodge adjacent flyers in diffusion-bonded assemblies (Fig. 8), but not in assemblies that used thin-film epoxy.

As mentioned previously, a second 250 mJ system was assembled with the Lasermetrics Nd:glass laser and ORVIS instrumentation. In this system, the lenses used to image the fiber exit face onto the launch layer were adjusted to slightly overfill the 800-μm flyer diameter. Figure 14 shows velocity histories recorded with this system for the case of 87-μm-thick aluminum flyers attached to a 5-μm aluminum launch layer using an adhesive. The ORVIS records in these experiments were rather noisy due to limited light reflected from the flyer back surfaces (ORVIS instrumentation will be discussed in more detail in the next section). Most of the flyer acceleration occurs within 100 ns after the start of back surface motion, and the total time shown is much smaller than the time spanned by the framing camera images. The final velocities shown in Fig. 14 agree reasonably well with velocities predicted by the one-dimensional, time-independent model discussed previously.

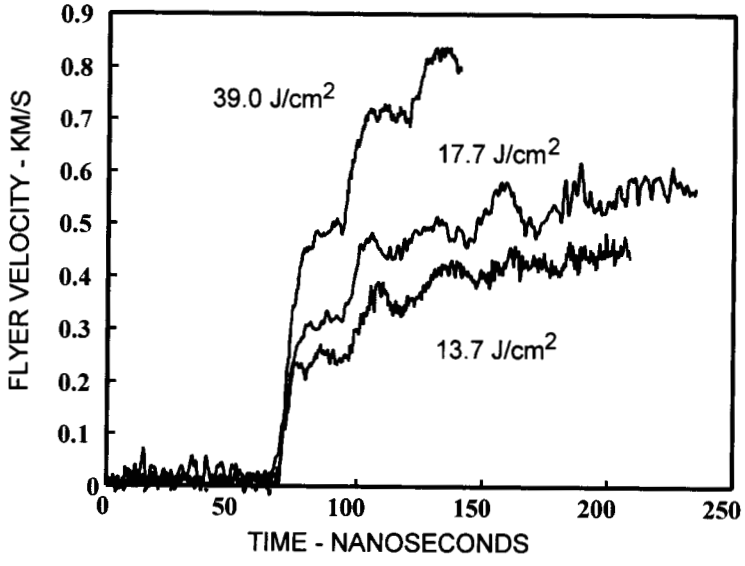

Fig. 14. Velocity histories of 87-μm-thick aluminum flyers attached to a 5-μm aluminum launch layer using an adhesive.

6. 2 J Photonic Driving System

A subsequent goal for the present study was to develop a photonic driving system that could operate at laser pulse energies up to 2 J. For this energy to result in driving fluences of 25, 50, 75, or 100 J/cm^2, flyer diameters would need to be 3.2, 2.3, 1.8, or 1.6 mm, respectively. Laser-induced damage considerations led to the choice of using nominal flyer diameters of 2.0-2.5 mm with the 2 J system. The basic scaling relations (Fig. 1) are independent of flyer area, and a flyer thickness $\leq$ 0.10 mm is still necessary in order to achieve velocities approaching 1.0 km/s. The higher laser energy does not provide longer test times, but does enable the use of flyers with a larger diameter-to-thickness aspect ratio resulting in less impact tilt over larger areas, and also makes fabrication and handling of launch assembly components more convenient.

Achieving a reasonably uniform laser intensity over the flyer area was again an essential requirement. In the 250 mJ system, this was achieved using an 800-μm-diameter optical fiber transmitting an average fluence as high as 55 J/cm^2. To transmit a 2 J pulse at this average fluence level would require an optical fiber having a core diameter of nearly 2.2 mm. The transmission of Q-switched laser pulses at this wavelength requires step-index fiber with a fused-silica core and doped fused-silica cladding [30], and standard commercial fiber with these characteristics is generally not available at diameters above 1.0 mm. Custom fiber having a diameter of 1.5 mm is available but very expensive. Thus, despite having multimode lasers with very non-Gaussian profiles, the only recourse was to pursue beam-shaping optics.

Prior work at Sandia National Laboratories on custom optics to facilitate the injection of lower-energy, Q-switched laser pulses into optical fibers had led to two basic designs [31]. One design, called a "beam scrambler," consists of many small diffractive elements arranged in a number of concentric rings. The total area covered by these elements is larger than the incident laser beam. The portion of the laser beam incident on a particular element is diffracted into several angles, resulting in several discrete spots in the focal plane of a primary focusing lens. Each element results in spots at different positions within the focal plane. The net result is a fairly uniform re-distribution of the laser near-field profile within a much smaller region in the focal plane of a lens. The second design, called a "beam integrator," consists of an array of small, hexagonal, refractive lenlets covering an area larger than the laser beam. The lenslet array spatially divides an incident laser beam into a number of separate beamlets. Upon passing through a large primary focusing lens (as in the first design), each beamlet is focused to the same

area within the focal plane of this lens. The net result is a superposition of all the separate beamlets within a small region in the focal plane. Interference effects can result from this superposition, producing local intensity variations whose amplitudes depend on the coherence properties of the laser.

The first design had been developed and fabricated at Sandia National Laboratories, and an effort was made to modify this design to accommodate the larger Nd:glass laser beams used in the present study. Despite the investment of significant time and resources, the net result was a fabricated optic that failed to perform as intended, and the pursuit of this design was discontinued. The second design had been developed at Sandia but fabricated by a commercial vendor, and a subsequent effort was made to modify this design for the Lasermetrics laser to be used in the 2 J photonic driving system. This laser has a "filled doughnut" near-field profile much like the Quantel laser (Fig. 6a), except that the center intensity is not nearly as low, and the beam diameter is nearly 20 mm. A design for a 30-mm-diameter optic containing an array of 2.5-mm hexagonal lenslets was developed, and the same commercial vendor (MEMS Optical, Inc., Huntsville, AL) was asked to fabricate the optic. The new design called for refractive (rather than diffractive) lenslets as in the original design, but after a considerable delay the vendor stated that they could only provide diffractive lenslets without substantial (and unacceptable) increases in both cost and delivery time. When the diffractive device was finally received, fabrication errors had resulted in an incorrect focal length for the lenslets and a significant percentage of undiffracted laser light. This latter problem resulted in a very large intensity spike in the focal plane of the primary lens, making the device useless for accelerating planar flyers. The vendor made a second effort at fabrication, and this time a device was received that performed as intended except for a smaller spike in the focal plane resulting from ~2% of undiffracted beam energy. By moving away from the focal plane, however, this spike could be suppressed at the expense of having the incident laser spread over a larger area with less edge definition. This performance was similar to what had been achieved with a binary diffractive optic that had been temporarily borrowed from Los Alamos National Laboratory. A decision was made to proceed with the "beam integrator" optic in the 2 J system, with flyer diameters now fixed at 2.5 mm. Much more detail on the design and evaluation of this optic can be found in Appendix C.

The 2 J photonic driving system was able to benefit from a significant improvement that had been made to the ORVIS instrumentation within the lab. Earlier versions of this laser interferometry system determined the average velocity within a 50-100 μm spot centered on the flyer surface. Modifications to the optics now produced intense illumination along a line segment at the flyer back surface, with Doppler-shifted reflected light from this line mapped into an interference pattern appearing at the entrance slit of a streak camera. Recorded displacements of the local fringe field are directly proportional to local changes in the surface velocity along the illuminated line, resulting in a capability for spatially resolved surface velocity measurements [35,36]. The "line-imaging ORVIS" instrumentation is particularly useful for examining two-dimensional effects in flyer acceleration. Figure 15 shows line-imaging ORVIS data recorded during a low-fluence (13.7 J/cm^2) launch of an 800-μm-diameter, 87-μm-thick aluminum flyer.

a) Line-imaging ORVIS streak record

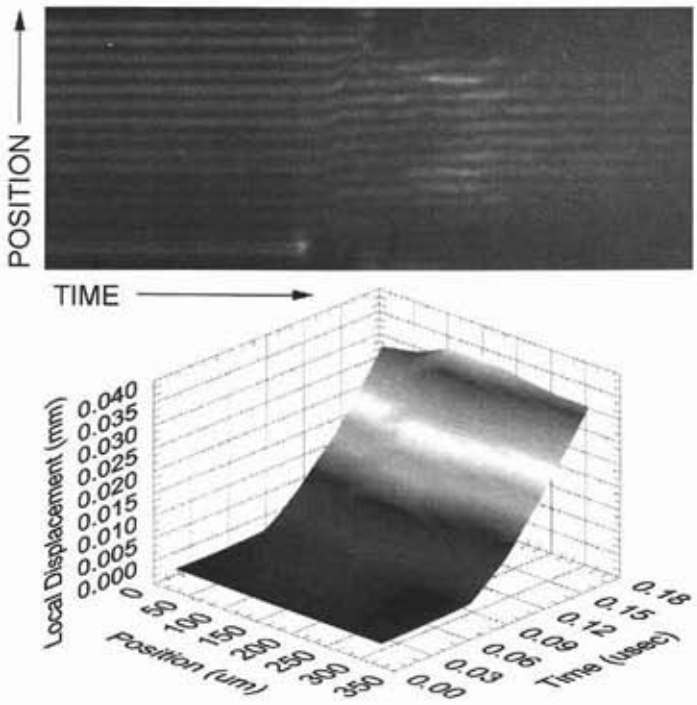

b) Flyer surface displacement history determined from the streak record.

Fig. 15. ORVIS streak record and reduced displacement data for a low-fluence flyer launch.

The velocity information that directly results from the streak record has been integrated in time to show the corresponding surface displacement history. The displacement data show the motion

along a 300-μm line centered on the flyer back surface. This dimension is typical for the present study, but can be adjusted over a fairly broad range [35]. Distinct "bowing" of the flyer surface is clearly occurring as the flyer is accelerated. This is consistent with the curvature seen in the shadowgraph images for low-fluence launch cases (Fig. 12). More details of the 2 J photonic driving system and the ORVIS instrumentation can be found in Appendix D.

7. Shock Hugoniot Experiments

The 2 J photonic driving system described in the previous section has been used to conduct demonstration shock physics experiments. The goal of these experiments is to show that photonic driving techniques will provide accurate measurements of shock properties for materials whose properties have been well-established using conventional techniques. This goal was the reason for developing methods to fabricate launch assemblies using 6061-T6 aluminum. The same techniques described previously for fabricating 800-μm-diameter, 100-μm-thick discs of this alloy were used to fabricate discs having the same thickness but 2.5 mm in diameter. To facilitate alignment of the incident laser beam with the flyer, launch layers consisted of discrete 5-μm-thick "spots" of aluminum vapor-deposited on fused silica substrates over an area slightly larger than the flyer area. Diffusion bonding of the flyers onto these areas was performed under the same conditions as were used for the smaller flyers, resulting in assemblies whose planarity, thickness, and diameter were carefully recorded using optical profilometry.

The launch assemblies were used in "reverse-impact" experiments to determine shock Hugoniot states for test materials. In this type of experiment, a material of interest is accelerated and impacted into a "witness plate" window material whose shock properties are well known. ORVIS measurements of the impact velocity and the subsequent velocity of the impact interface, together with the shock properties of the window material, are used to calculate a shock Hugoniot state for the material of interest. Figure 16 shows a general configuration for such experiments using a photonic driving system.

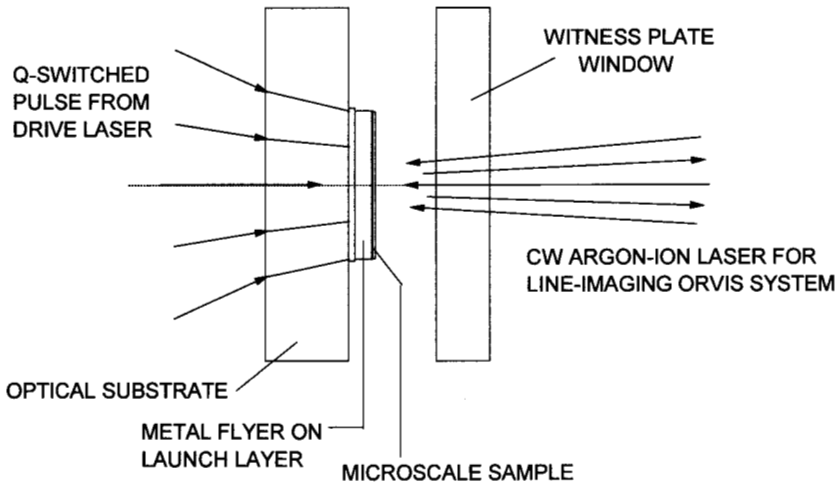

Fig. 16. General configuration for reverse-impact experiments.

Figure 16 shows an additional layer on the back surface of the flyer, which will be discussed shortly. This layer was absent in initial experiments for which the test material was simply the 6061-T6 aluminum flyer. By varying the incident laser fluence, flyers were accelerated and impacted into a fused silica window over a range of impact velocities. Figure 17 shows typical ORVIS data for these experiments. The streak record shows a very flat impact over the flyer area examined by the ORVIS system. The velocity history represents an average over this area.

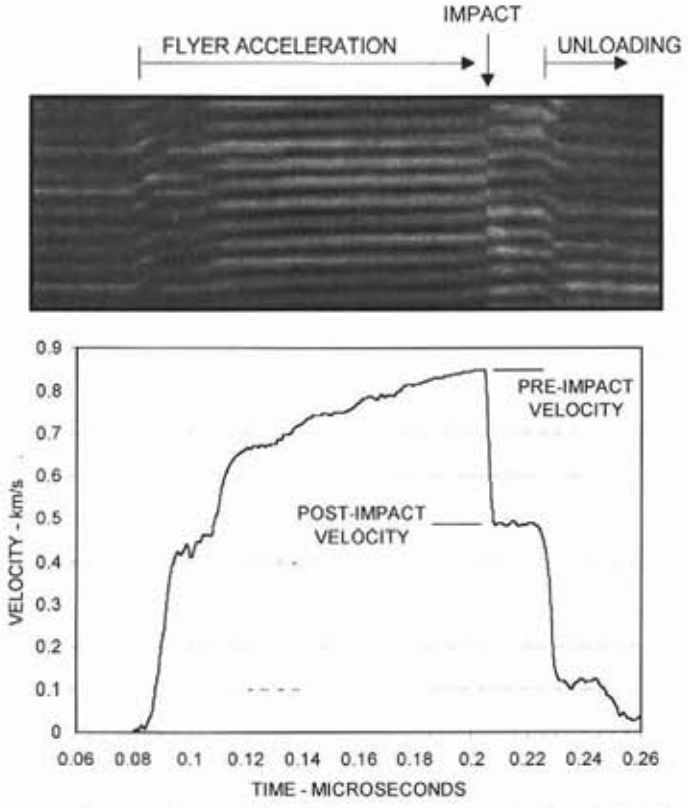

Fig. 17. Typical ORVIS streak record and reduced flyer velocity for 6061-T6 aluminum flyer impact into a fused silica window.

Figure 18 shows the shock Hugoniot states determined for the 6061-T6 aluminum flyers, together with previous measurements for this material obtained with conventional shock-loading techniques [34,37]. The measured impact velocities have been corrected for refractive index effects in the fused silica window [38]. The data represent states of shock pressure (in GPa) and particle velocity (in km/s) that can be achieved in this material through compression by a steady shock wave. The current results range from 1.9 to 8.7 GPa, and the good agreement indicates that the impact state of much of the flyer is at or near ambient conditions. This is consistent with the results of numerical simulations (Fig. 4). Higher shock Hugoniot states cannot be achieved

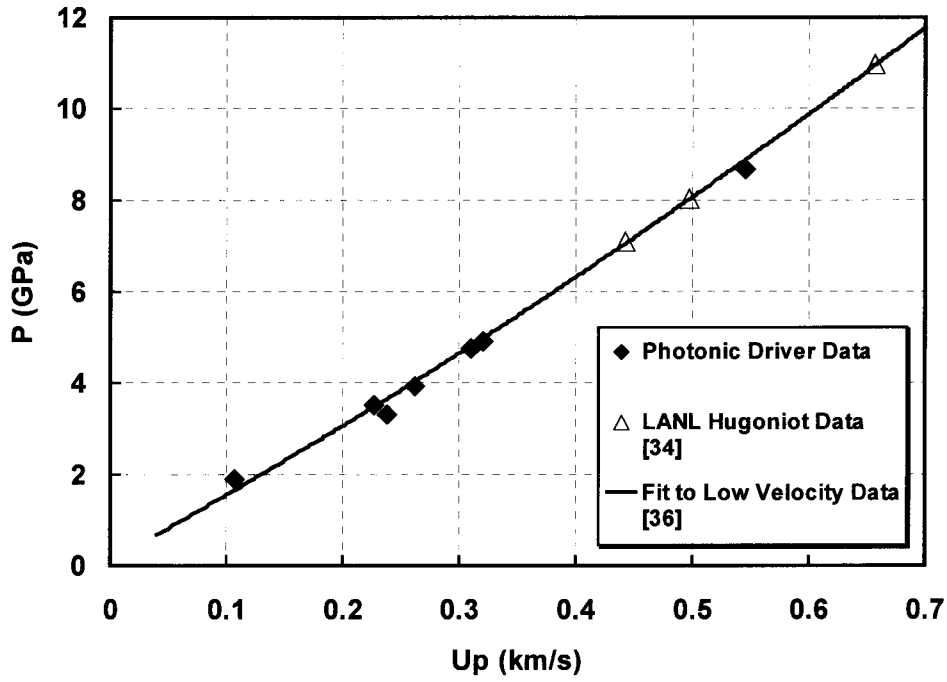

Fig. 18. Shock Hugoniot states for 6061-T6 aluminum.

with fused silica windows, as fused silica undergoes a phase transition above 9.0 GPa. To extend the data, higher-impedance sapphire can be used for the window.

An essential goal for the present study was to develop the capability for measuring shock properties in materials that can only be obtained or fabricated in dimensions that are too small for conventional techniques. To demonstrate such a capability with the 2 J photonic driving system, thin films of polyimide were chosen as test materials. Polyimide film, typically Kapton® from DuPont, is made in thicknesses from 7.5 to 125 μm and has been well-characterized for its shock properties [34] because of its extensive use in detonators. As indicated in Fig. 16, a "microscale sample" can be the test material in a reverse-impact experiment. The sample is simply carried by the metal flyer, much like a test sample can be carried at the front of a projectile in a conventional gas gun experiment. Important issues include the time resolution necessary to measure an impact interface velocity that will persist for a very short time, whether or not the initial sample state will be altered by thermal transport through the flyer, and how the test material is processed and attached to the flyer surface.

Polyimide film having a thickness of 12.7 μm will result in a shock sustained for approximately 9 ns at the impact interface, and this thickness was chosen for reverse-impact experiments. Both test data and numerical simulations indicated that thermal transport through a

100-μm-thick flyer of 6061-T6 aluminum was minimal, so the remaining question was how to bond the polyimide film to the aluminum flyer. Adhesives were considered, but a better method was developed using diffusion bonding. Approximately 1000 angstroms of gold was vapor deposited on both the polyimide film and the back surfaces of a number of aluminum flyers previously attached to a substrate. Polyimide discs 2.5-mm in diameter were punched from the film, and the gold coating was diffusion bonded to the flyer coating by heating at 200 C for 30 minutes in a vacuum oven with an applied weight. Polyimide is unaffected by this temperature, and excellent bonds were obtained. Figure 19 shows an ORVIS streak record from one of the reverse-impact experiments in which a flyer/film assembly was impacted into a fused silica

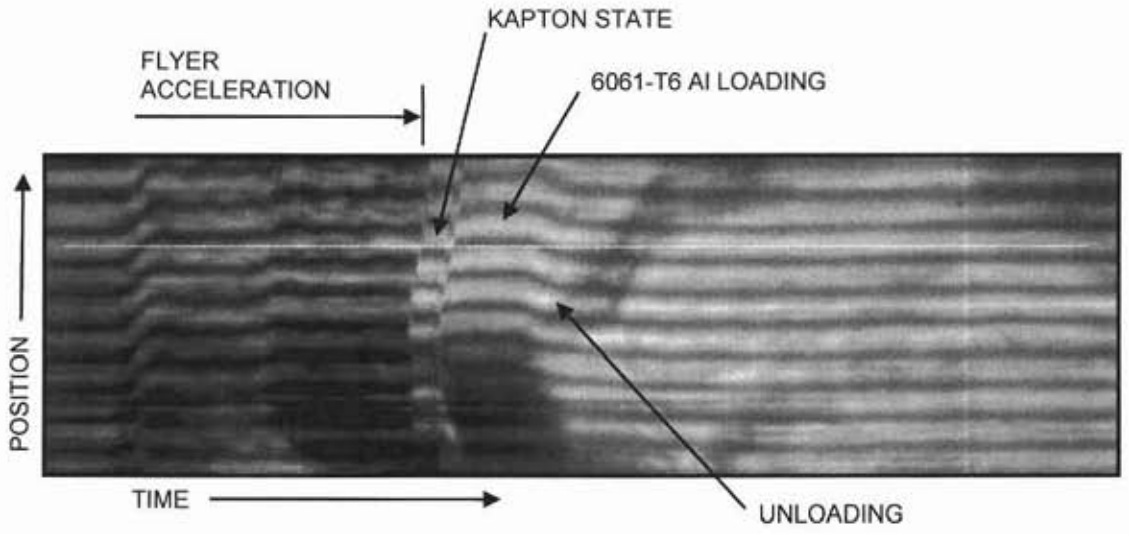

Fig. 19. ORVIS streak record for a flyer/film assembly impacting a fused silica window.

window. Some curvature in this flyer is apparent, but a well-resolved state following polyimide impact is clearly shown. Figure 20 shows polyimide shock Hugoniot states determined from the photonic driving experiments, together with conventional measurements made previously for this material [34]. The data points labeled "best" are from initial experiments that produced very clear streak records. The data points labeled "marginal" are from later experiments using flyers attached to the same substrate, but the corresponding streak records were more difficult to analyze. Inspection of the multiple-flyer launch assembly indicated that the violent substrate damage during a given experiment (Fig. 13) was probably affecting the integrity of adjacent flyer structures. Building multiple-flyer launch assemblies reduces the time and cost of each experiment, but adequate spacing obviously needs to be provided between the flyers. Despite

these limitations, the experiments with polyimide film confirmed that valid data could be readily obtained from relatively thin samples.

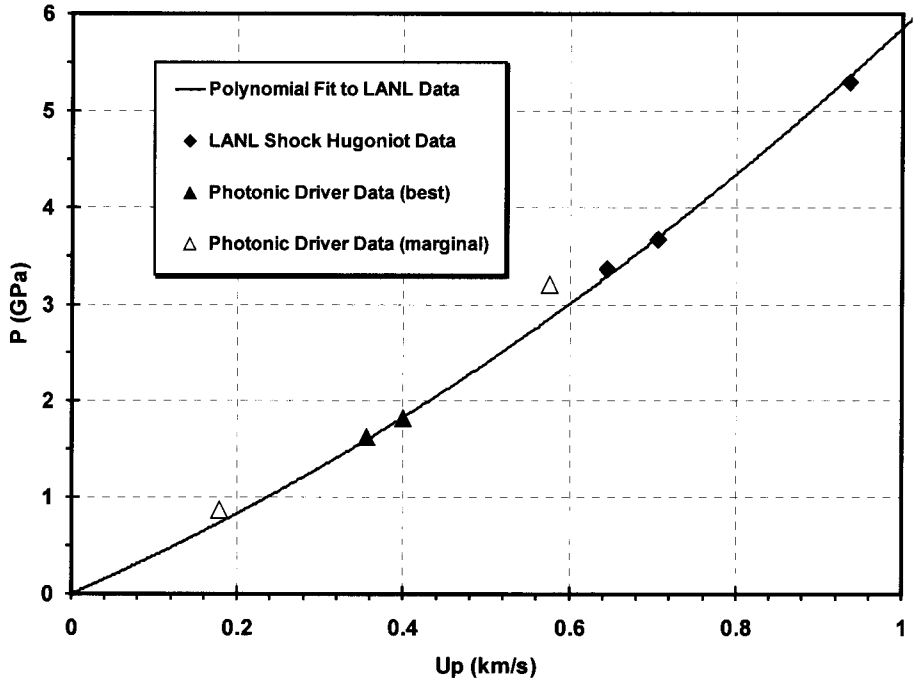

Fig. 20. Shock Hugoniot states for polyimide.

A final goal for the present study was to determine previously unknown shock properties for a microscale material of interest. The material chosen was polycrystalline silicon, which is the basic structural material in surface micromachines. Chemical vapor deposition and an elevated annealing temperature are typically used to produce a thin film a few microns in thickness. Using standardized deposition facilities and procedures for flyer assemblies was not feasible, so alternate methods were pursued. Past studies indicated that e-beam evaporation was a possible method, and an effort was undertaken to examine silicon films produced using different deposition parameters and annealing conditions. Conventional films of polycrystalline silicon were obtained and examined by X-ray diffraction to guide the e-beam deposition studies. A film with a suitable structure was achieved by deposition on a 300 C substrate without additional annealing steps.

Incorporation of such a film on a launch assembly was the next step. Chemical compatibility issues led to the identification of molybdenum as a good choice for a metal flyer upon which polycrystalline silicon could be deposited. Because of its higher density compared to aluminum,

a flyer thickness of 30 μm was chosen in order to achieve impact velocities up to 1 km/s. Sputtering of molybdenum to this thickness was feasible, although optimum deposition conditions for optical substrates needed to be determined. Mismatches in coefficients of thermal expansion caused significant film cracking and ruled out fused silica substrates, but either sapphire or BK-7 glass were found to be acceptable. Because sapphire is difficult to polish to the surface finish necessary for adequate resistance to laser-induced damage, the baseline substrate became BK-7 glass. Figure 21 shows a SEM photograph of a prototype launch assembly structure consisting of a substrate, a 30-μm layer of molybdenum, and a 3.5-μm layer of polycrystalline silicon. The bar at the top left of the picture is 20 μm long.

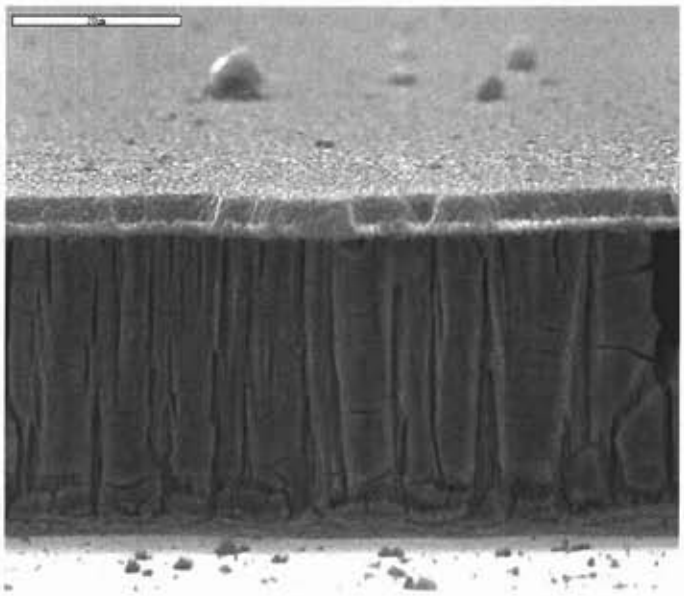

Fig. 21. Prototype launch assembly structure for experiments on polycrystalline silicon.

Because the thickness of polycrystalline silicon films was limited to a few microns, an additional modification to the line-imaging ORVIS instrumentation was made. Measuring a shock Hugoniot state in a reverse-impact experiment with a very thin film requires the recording of the entire flyer acceleration history as well as the very short-lived state at impact. The disparate time scales for these requirements prompted the addition of a second streak camera to the ORVIS system. The second camera is swept at a much faster rate in order to resolve the impact event. Additional details on the "dual time base, line-imaging ORVIS" system can be found in Appendix D.

Attempts to measure polycrystalline silicon Hugoniot states using 2.5-mm diameter assemblies with the structure shown in Fig. 21 have not been successful. Impact of this launch assembly should result in a discernable velocity state lasting ~1 ns. However, the streak records have failed to clearly depict a state at impact that could be identified with the polycrystalline silicon. Numerical simulations of these experiments were performed with the CTH hydrodynamics code, assuming approximate shock properties for the polycrystalline silicon. The simulations indicated that rapid thermal transport through the 30-μm layer of molybdenum was occurring during flyer acceleration, and the test film was experiencing severe heating. Improving the launch assembly structure is clearly necessary in order to achieve this challenging measurement, but this task remains for future studies.

8. Summary

A need still exists at Sandia National Laboratories and elsewhere for characterizing the dynamic properties of many materials, including materials having dimensions too small for conventional testing techniques. A multiyear effort has been made to develop a new capability for determining material shock properties. By utilizing a significant reduction in experimental length and time scales, this new capability addresses both the high per-experiment costs of conventional techniques and the need to characterize materials with very small dimensions. Based on earlier work to develop laser-based techniques for detonating explosives, the present study examined the laser acceleration, or *photonic* driving, of small metal flyers for generation of shock waves by planar impact.

Photonic driving systems were developed and evaluated at two driving levels. The first level, corresponding to laser pulse energies up to 250 mJ, was roughly an order of magnitude higher than levels used during the earlier studies. Limitations due to laser-induced damage in optical substrates resulted in bounds on possible flyer diameters, and existing scaling laws and a simple analytical model defined the relationships between flyer material, flyer thickness, and achievable impact velocities. A flyer diameter of 0.8 mm was chosen, and large-core optical fiber was used to achieve a uniform laser intensity incident over the flyer area. Numerical simulations using a modified version of the CTH hydrodynamics code were used to examine design options for launch assemblies consisting of an optical substrate, a launch layer consisting of one or more vapor-deposited materials, and the flyer. To assess these issues and to examine different methods for flyer attachment, experiments were conducted using fast-framing photography in one of two 250-mJ photonic driving systems assembled. Spatially resolved laser interferometry (line-imaging ORVIS) was used with the second 250-mJ system to examine flyer acceleration and planarity as functions of launch conditions.

A 2 J system was subsequently developed and used for demonstration shock physics experiments. The use of an optical fiber to achieve a uniform incident intensity was no longer feasible, and various diffractive beam-shaping optics were designed and fabricated specifically for the system laser. These efforts were time consuming, expensive, and largely unsuccessful. A Sandia-designed, commercially fabricated optic was eventually obtained whose performance was adequate for launching flyers 2.5 mm in diameter. Flyers made from bulk-processed, 6061-T6 aluminum sheet were used in reverse-impact experiments to demonstrate that accurate shock

Hugoniot states could be obtained using photonic driving techniques. To demonstrate that accurate measurements could be made on much thinner samples, 12.7-μm-thick samples of polyimide (DuPont Kapton®) film were mounted on aluminum flyers and used as test materials in reverse-impact experiments. In both of these demonstrations, the most challenging aspect of the experiments was the fabrication of the launch assembles. This aspect proved too challenging in a long effort to obtain shock properties of polycrystalline silicon. Deposition of films with an appropriate polycrystalline character, chemical and thermal-expansion compatibility throughout the launch assembly, thermal transport through the flyer during acceleration, and temporal resolution requirements for the ORVIS instrumentation were significant issues confronted during this effort.

The primary conclusion that can be drawn from the present study is that photonic driving techniques are viable additions to the conventional methods presently used to obtain dynamic material properties. Improvements in launch conditions and in diagnostic instrumentation are certainly achievable. A new laser selected for optimum beam characteristics would mitigate the difficulties experienced in this study in obtaining useful beam-shaping optics. Refinements to the current image recording, processing and analysis capabilities for ORVIS streak records would improve accuracy and temporal resolution. With careful substrate selection and processing, average incident laser fluences of 100 J/cm^2 or more should permit the launch of thicker flyer assemblies to higher velocities. The main challenge for future applications, as in the present study, will be the successful design and fabrication of launch assemblies for materials of interest.

References

1. J. F. Ready, Effects of High-Power Laser Radiation, Academic Press, Orlando, 1971.

2. L. C. Yang, J. Appl. Phys. 45, 2601 (1974).

3. L. C. Yang and V. J. Menichelli, in Proceedings of the Sixth Symposium (International) on Detonation, Office of Naval Research, ACR-221, Arlington, VA, 1976, p. 612. Also: references therein.

4. D. L. Paisley, in Proceedings of the Ninth Symposium (International) on Detonation, Office of the Chief of Naval Research, OCNR 113291-7, Arlington, VA, 1991, p. 1110.

5. A. M. Renlund, P. L. Stanton, and W. M. Trott, in Proceedings of the Ninth Symposium (International) on Detonation, Office of the Chief of Naval Research, OCNR 113291-7, Arlington, VA, 1991, p. 1118.

6. S. A. Sheffield and G. A. Fisk, in Shock Waves in Condensed Matter – 1983, edited by J. R. Asay et al., Elsevier, New York, 1984, p. 243.

7. S. A. Sheffield, J. W. Rogers, Jr., and J. N. Castaneda, in Shock Waves in Condensed Matter, edited by Y. M. Gupta, Plenum Press, New York, 1986, p. 541.

8. D. D. Bloomquist and S. A. Sheffield, J. Appl. Phys. 54, 1717 (1983).

9. D. L. Paisley, in Shock Compression of Condensed Matter – 1989, edited by S. C. Schmidt et al., Elsevier, New York, 1990, p. 773.

10. W. M. Trott and K. D. Meeks, in Shock Compression of Condensed Matter – 1989, edited by S. C. Schmidt et al., Elsevier, New York, 1990, p. 997.

11. W. M. Trott and K. D. Meeks, J. Appl. Phys. 67, 3297 (1990).

12. W. M. Trott, in Shock Compression of Condensed Matter – 1991, edited by S. C. Schmidt et al., Elsevier, New York, 1992, p. 829.

13. D. L. Paisley, R. H. Warnes, and R. A. Kopp, in Shock Compression of Condensed Matter – 1991, edited by S. C. Schmidt et al., Elsevier, New York, 1992, p. 825.

14. A. V. Farnsworth, Jr. and R. J. Lawrence, in Shock Compression of Condensed Matter – 1991, edited by S. C. Schmidt et al., Elsevier, New York, 1992, p. 821.

15. R. J. Lawrence and W. M. Trott, Int. J. Impact Engineering 14, 439 (1993).

16. A. V. Farnsworth, Jr., in Shock Compression of Condensed Matter – 1995, edited by S. C.

Schmidt and W. C. Tao, AIP Conference Proceedings 370, Part 2, Woodbury, NY, 1996, p. 1225.

17. D. L. Paisley, N. I. Montoya, D. B. Stahl, and I. A. Garcia, in 19th International Congress on High Speed Photography and Photonics, edited by P. W. Fuller, Proceedings of SPIE 1358, Bellingham, WA, 1991, p. 760.

18. W. M. Trott, in High-Pressure Science and Technology – 1993, edited by S. C. Schmidt et al., AIP Conference Proceedings 309, Part 2, Woodbury, NY, 1994, p. 1655.

19. A. M. Frank and W. M. Trott, in Ultrahigh- and High-Speed Photography, Videography, and Photonics '94, edited by G. A. Kyrala and D. R. Snyder, Proceedings of SPIE 2273, Bellingham, WA, 1994, p. 196.

20. A. M. Frank and W. M. Trott, in Shock Compression of Condensed Matter – 1995, edited by S. C. Schmidt and W. C. Tao, AIP Conference Proceedings 370, Part 2, Woodbury, NY, 1996, p. 1209.

21. W. M. Trott, in Shock Compression of Condensed Matter – 1995, edited by S. C. Schmidt and W. C. Tao, AIP Conference Proceedings 370, Part 2, Woodbury, NY, 1996, p. 921.

22. B. Cazalis, C. Boissiere, and G. Sibille, in Shock Compression of Condensed Matter – 1995, edited by S. C. Schmidt and W. C. Tao, AIP Conference Proceedings 370, Part 2, Woodbury, NY, 1996, p. 1217.

23. D. J. Hatt and J. A. Waschl, in Shock Compression of Condensed Matter – 1995, edited by S. C. Schmidt and W. C. Tao, AIP Conference Proceedings 370, Part 2, Woodbury, NY, 1996, p. 1221.

24. J-L Labaste, D. Brisset, and M. Doucet, in Shock Compression of Condensed Matter – 1999, edited by M. D. Furnish et al., AIP Conference Proceedings 505, Part 2, Woodbury, NY, 2000, p. 1189.

25. R. H. Warnes, D. L. Paisley, and D. L. Tonks, in Shock Compression of Condensed Matter – 1995, edited by S. C. Schmidt and W. C. Tao, AIP Conference Proceedings 370, Part 1, Woodbury, NY, 1996, p. 495.

26. D. B. Stahl, R. J. Gehr, R. W. Harper, T. D. Rupp, S. A. Sheffield, and D. L. Robbins, in Shock Compression of Condensed Matter – 1999, edited by M. D. Furnish et al., AIP Conference Proceedings 505, Part 2, Woodbury, NY, 2000, p. 1087.

27. D. L. Robbins, R. J. Gehr, R. W. Harper, T. D. Rupp, S. A. Sheffield, and D. B. Stahl, in Shock Compression of Condensed Matter – 1999, edited by M. D. Furnish et al., AIP Conference Proceedings 505, Part 2, Woodbury, NY, 2000, p. 1199.

28. J. E. Kennedy, "Gurney Energy of Explosives: Estimation of the Velocity and Impulse Imparted to Driven Metal," Sandia National Laboratories Report SC-RR-70-790 (1970).

29. R. M. Wood, Laser Damage in Optical Materials, Adam Hilger, Bristol, UK, 1986.

30. R. E. Setchell, in Laser-Induced Damage in Optical Materials: 1996, edited by H. E. Bennett, et al., Proceedings of SPIE 2966, Bellingham, WA, 1997, p. 608.

31. R. E. Setchell, in Laser Beam Shaping, edited by F. M. Dickey and S. C. Holswade, Proceedings of SPIE 4095, 2000, p. 74.

32. For example, see: F. Ranier, L. J. Atherton, J. H. Campbell, F. P. DeMarco, M. R. Kozlowski, A. J. Morgan, and M. C. Staggs, in Laser-Induced Damage in Optical Materials: 1991, Proceedings of SPIE 1624, 1992, p. 116.

33. R. E. Setchell, in Laser-Induced Damage in Optical Materials: 1992, edited by H. E. Bennett, et al., Proceedings of SPIE 1848, 1993, p. 15.

34. S. P. Marsh, ed., LASL Shock Hugoniot Data, U. Calif. Press, Berkeley, CA, 1980.

35. W. M. Trott and J. R. Asay, in Shock Compression of Condensed Matter – 1997, edited by S. C. Schmidt et al., AIP Conference Proceedings 429, Woodbury, NY, 1998, p. 837.

36. W. M. Trott, M. D. Knudson, L. C. Chhabildas, and J. R. Asay, in Shock Compression of Condensed Matter – 1999, edited by M. D. Furnish et al., AIP Conference Proceedings 505, Part 2, Woodbury, NY, 2000, p. 993.

37. D. R. Christman, W. M. Isbell, S. G. Babcock, A. R. McMillan, and S. J. Green, "Measurements of Dynamic Properties of Materials – Vol. III: 6061-T6 Aluminum," General Motors Corporation, MSL-70-23, Vol. III, November, 1971.

38. R. E. Setchell, J. Appl. Phys. 50, 8186 (1980).

APPENDICES

A. W. M. Trott, R. E. Setchell, and A. V. Farnsworth, Jr., *Investigation of the effects of target material strength on the efficiency of acceleration of thick laser-driven flyers*

presented at: 1999 Conference of the American Physical Society Topical Group on Shock Compression of Condensed Matter, Snowbird, Utah, June 27-July 2, 1999.

published in: Shock Compression of Condensed Matter – 1999, edited by M. D. Furnish et al., AIP Conference Proceedings 505, Part 2, Woodbury, NY, 2000, p. 1203.

B. A. Farnsworth, W. Trott, and R. Setchell, *A computational study of laser driven flyer plates*

presented at: 2001 Conference of the American Physical Society Topical Group on Shock Compression of Condensed Matter, Atlanta, GA, June 26-29, 2001.

published in: Shock Compression of Condensed Matter – 2001, edited by M. D. Furnish, AIP Conference Proceedings (in press).

C. W. M. Trott, R. E. Setchell, J. N. Castenada, and D. M. Berry, *Evaluation of a diffractive, microlens-array beam shaper for use in acceleration of laser-driven flyers*

presented at: SPIE's 46th Annual Meeting, The International Symposium on Optical Science and Technology, San Diego, CA, July 29-August 3, 2001.

published in: Laser Beam Shaping II, edited by F. M. Dickey, et al., Proceedings of SPIE 4443, Bellingham, WA, 2001, p. 166.

D. W. M. Trott, R. E. Setchell, and A. V. Farnsworth, Jr., *Development of laser-driven flyer techniques for equation-of-state studies of microscale materials*

presented at: 2001 Conference of the American Physical Society Topical Group on Shock Compression of Condensed Matter, Atlanta, GA, June 26-29, 2001.

published in: Shock Compression of Condensed Matter – 2001, edited by M. D. Furnish, AIP Conference Proceedings (in press).

Appendix A

INVESTIGATION OF THE EFFECTS OF TARGET MATERIAL STRENGTH ON THE EFFICIENCY OF ACCELERATION OF THICK LASER-DRIVEN FLYERS*

Wayne M. Trott, Robert E. Setchell, and Archie V. Farnsworth, Jr.

Sandia National Laboratories, Albuquerque, NM 87185-0834

Abstract. Experimental techniques for laser-driven flyer generation offer considerable promise as a compact, repeatable, and relatively inexpensive driver for fundamental shock compression studies. Acceleration of microgram samples of thin metal films to high velocities (>3 km-s^{-1}) using Q-switched, solid-state lasers has become well established. Scaling of these methods to provide well-conditioned shock loading with considerably larger sample dimensions and mass would greatly enhance the utility of this driver. As flyer target thickness and mass increase, however, the dynamic shear strength and yielding behavior of the material become important factors in limiting performance. Experiments exploring methods for optimizing the bounding material at the driving laser spot perimeter are described. Results are being incorporated in a 2-D hydrocode model of flyer generation to aid in optimization of target designs.

INTRODUCTION

Techniques for pulsed laser-driven flyer generation provide a promising approach to the development of a compact, relatively inexpensive capability for quantitative studies of material response to shock loading. Upward scaling of intensively investigated methods (1-5) for acceleration of thin (<10 μm) metal films to achieve precise, sustained, one-dimensional loading by substantially thicker flyers is critically needed for this application. Fundamental research areas of interest include measurements of Hugoniot states and spall strength (6, 7) as well as shock-induced phase transitions and chemistry (8).

The dynamic phenomena in laser-acceleration of flyers are extremely complex and present significant challenges to the realization of a robust, well-characterized driver. Critical issues identified in thin-flyer studies include the uniformity of drive intensity, excessive thermal transport within the flyer structures, and rapid development of drive instabilities (9, 10). With substantial increases in the flyer target thickness and mass, the dynamic yield strength and yielding behavior of the material also become important considerations. In a typical configuration the beam from a Q-switched laser is focused onto a circular area within a larger spatial extent of a flyer target film that has been deposited on a transparent substrate. As the irradiated region begins to move, the film material around the perimeter of this area undergoes dynamic shearing and yielding. Given sufficient drive intensity, this material ultimately ruptures. The required mechanical work prior to rupture represents a loss mechanism in the flyer acceleration process. Indeed, at lower incident intensities the plasma pressure generated by laser absorption can be insufficient to overcome the material shear strength. However, the perimeter material does prevent free lateral expansion of the plasma and subsequent loss of accelerating pressure prior to rupture. These nominally two-dimensional (2-D) effects suggest that carefully tailored target materials and geometry may be required to optimize the efficiency of thick-flyer acceleration. Design of optimal targets will depend on different (application specific) loading conditions and would benefit from a validated computational model that captures the relevant physics.

In this paper we describe experiments to explore effects of the flyer bounding material. One series of

* Sandia is a multiprogram laboratory operated by Sandia Corporation, a Lockheed Martin Company, for the United States Department of Energy under Contract DE-AC04-94AL85000.

tests investigated the response of thick (11-35 μm) films to a range of incident laser fluence. These films covered an extended spatial area compared to the laser beam. A second series of experiments compared the acceleration of individual islands of film material to extended films of identical thickness. Salient features of a complementary 2-D analytical tool are also briefly described, and a preliminary computation that illustrates some of the 2-D effects in flyer acceleration is presented.

EXPERIMENTAL

Modifications to the previously described (1, 3) experimental design for laser-driven flyer generation were made to deliver a relatively uniform laser intensity distribution to variable-diameter flyer targets deposited on fused silica substrates. Laser energy exiting a 0.4-mm-diameter optical fiber was collected and roughly collimated by a fast (*f*1.6), short-focal-length (40 mm) lens. A second lens of the same type was used to refocus the light to the flyer target plane. With this arrangement we achieved drive conditions approximating a "top hat" intensity distribution. Typical profiles along two orthogonal axes are shown in Fig. 1. The diameter of the uniform intensity region could be varied by translating the two lenses along the beam axis.

Other diagnostics included: [1] an energy meter for determination of energy incident on the flyer targets, [2] a velocity interferometer (ORVIS) for flyer velocity measurements (11), and [3] a noncontact optical profilometer for pretest characterization of target geometry and uniformity as well as posttest measurements of the remaining bounding material, substrate ablation, etc. Flyer targets were prepared by physical vapor deposition on 1.59-mm-thick fused silica discs. The composite samples consisted of a 0.25-μm-thick layer of aluminum in contact with the substrate followed by an insulating 0.25-μm-thick layer of Al_2O_3 and variable thicknesses of aluminum. Available masks were used to generate full film coverage on half of the surface and numerous small-diameter circular islands on the other half. This arrangement allowed rapid "turnaround" in set up between the extended samples and island targets. Optical profilometer measurements showed negligible variation (<0.5%) in target thickness for the different geometries.

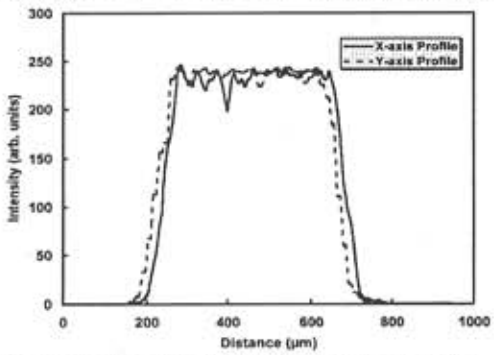

FIGURE 1. Spatial profile of drive laser beam in flyer tests.

COMPUTATIONAL TOOL

The CTH hydrocode used in 2-D simulations is an Eulerian code with a fixed grid that is distorted during a Lagrangian step and then remapped back to the original grid for each hydrodynamic cycle. It contains numerous models for handling material properties and strength, and it accesses a large material property database. The code allows energy transport by thermal diffusion. Also included is a grid-following laser transport package that allows materials to be either transparent or absorbing. Energy deposition routines are appropriate to metallic absorption in cool materials or plasma absorption when materials become sufficiently hot. Details regarding the implementation of these routines and the treatment of ionization properties of metals, as well as results of 1-D computations, have been described elsewhere (9). Recently this computational package has been configured to take advantage of parallel processing.

RESULTS AND DISCUSSION

The response of an extended 23-μm-thick film was observed for incident energies ranging from 5 to 20 mJ (corresponding to fluences ~5-20 J-cm^{-2}). A photograph illustrating the observed behavior is shown in Fig. 2. Near the threshold for material motion (~ 7 mJ), the material shear strength easily resists rupture; only a cone-like structure is raised above the substrate surface. This type of response pertains until the incident energy exceeds 11 mJ. Above this value material rupture occurs during the acceleration process.

Surface profiling provides a more quantitative picture of this yielding behavior, as illustrated in Fig. 3. The sharp threshold for material motion is demonstrated by the threefold increase in surface elevation when the incident energy is raised from 7.3

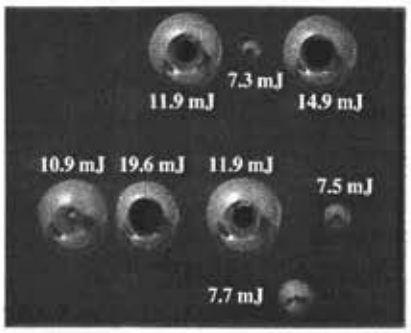

FIGURE 2. Photograph of material remaining after irradiation of 23-μm composite film at different energies.

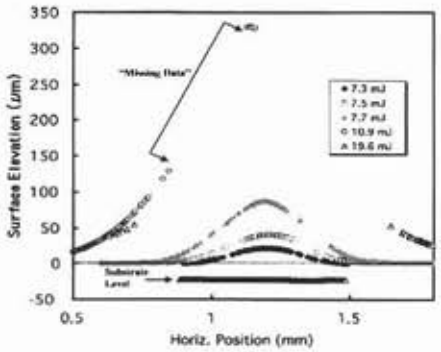

FIGURE 3. Surface profiles of flyer targets (post-test).

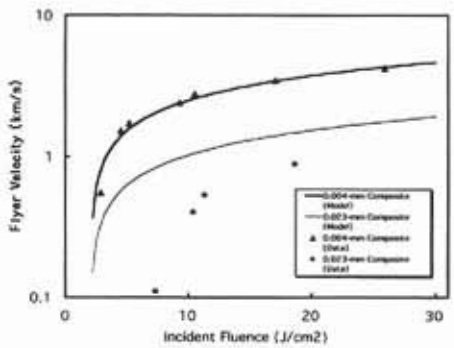

FIGURE 4. Comparison of data to analytical model for two different flyer thicknesses.

to 7.7 mJ. At the larger drive level, evidence of significant work performed by plasma expansion on material outside the perimeter of the laser spot begins to be seen. The posttest profile of the sample irradiated by 10.9 mJ clearly demonstrates the impressive ductility of the predominantly aluminum target. In this case the material stretched without rupture to an elevation exceeding 0.3 mm (the relatively steep slope in the surface elevation results in "missing data" in the interferometer scan). Moreover, the extent of mechanical work expended laterally was substantial; significant surface elevation can be observed to a radius approaching 1 mm (only half of the symmetric profile for this sample is plotted in Fig. 3). It is interesting that the surface elevation slope of material remaining after flyer launch at 19.6 mJ is somewhat lower. This result points to rupture relatively early in the plasma expansion and suggests that the yield strength is strongly dependent on the rate of flyer acceleration.

The cost in mechanical work needed to overcome thick target material strength is reflected in the corresponding flyer velocities, as indicated in Fig. 4. As reported previously (3), ORVIS terminal velocity data for thin (4 μm) composite flyers closely track the fluence dependence predicted by a 1-D, time-independent analytical model (12). In this model, ablation of the composite material is assumed to be confined to the thin Al layer initially in contact with the substrate. The calculated coupling efficiency (flyer kinetic energy divided by incident energy) approaches 40 percent at high fluence. In the absence of 2-D loss processes, essentially identical behavior should be seen in the 23-μm flyer case (with velocities scaling inversely with the square root of target mass). Measured velocities, however, fall far below the predicted curve, especially at low fluence. This trend is more pronounced as flyer target thickness increases.

In view of the substantial effect of the material strength of extended thick flyer targets on coupling efficiency, it is interesting to compare results obtained on "island" targets under similar drive conditions. In these tests the spot size was adjusted to be significantly larger than the target diameter so that the sample experienced essentially uniform irradiance. Some preliminary results are summarized in Table I. Over the limited data range examined here, it is apparent that losses arising from free lateral expansion of the accelerating plasma are generally comparable to those seen in overcoming yield strength in extended targets. The island target configuration (no confining material at the perimeter

TABLE I. Comparison of Peak Flyer Velocities (km-s^{-1}) for Extended vs. Island Targets

Target Thickness	Incident Energy	Velocity (Full)	Velocity (Island)
0.011-mm	11.5 mJ	1.40	1.40
0.023-mm	11.5 mJ	0.55	0.60
0.035-mm	11.5 mJ	0.38	0.45
0.023-mm	7.5 mJ	0.10	0.15

of the laser spot) appears to become somewhat more favorable as target thickness increases and at lower incident energies. The optimal confinement (comprising thickness, geometry, and bounding material composition) is likely to depend on the flyer specifications required by different applications.

Optimization of the flyer target bounding material is an issue that can be efficiently addressed by a validated 2-D numerical tool. Dynamic 2-D effects in flyer acceleration are evident in the simulation results for a thin aluminum flyer case displayed in Fig. 5. The plots track calculated material interface boundaries (independent of material density) as a function of time after laser arrival. Heat transport from plasma to flyer material is reflected in the significant longitudinal expansion of the flyer layer; this effect arises from melting and vaporization (decreased density) of a substantial fraction of the aluminum. Forward expansion of the glass material boundary is indicative of the important role of the substrate material as a component of the driving plasma, as described previously (9). The ductility of the aluminum is evident in the observed degree of stretching at the perimeter of the irradiation region.

In the near future 2-D CTH hydrocode calculations of thick flyer targets will be performed and compared to an expanded database of experimental flyer velocities and surface profiles. The combined experimental and analytical approach will be used to evaluate and optimize target materials and confinement conditions for specific applications in fundamental shock compression studies.

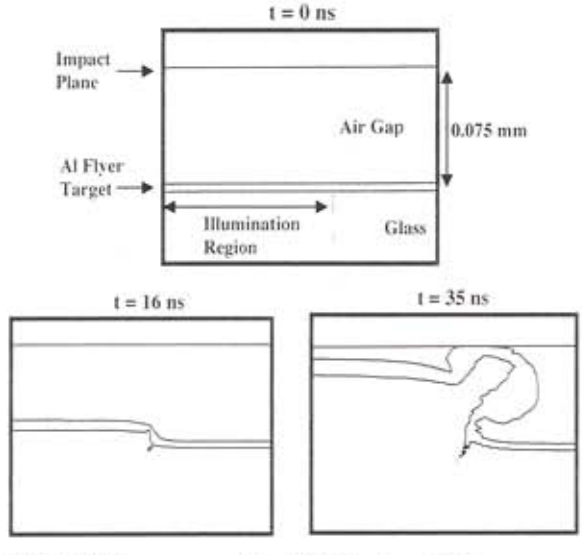

FIGURE 5. Time sequence of material interfaces in 2-D simulation of thin flyer launch.

ACKNOWLEDGEMENTS

The excellent technical assistance of Jaime Castaneda and Dante Berry is gratefully acknowledged. Catharine Sifford and Juan Romero skillfully prepared the flyer target films.

REFERENCES

1. Trott, W. M., and Meeks, K. D., "Acceleration of Thin Foil Targets Using Fiber-Coupled Optical Pulses," in *Shock Compression of Condensed Matter—1989*, edited by S. C. Schmidt, et al. New York, Elsevier, 1990, pp. 997-1000.
2. Paisley, D. L., "Laser-Driven Miniature Flyer Plates for Shock Initiation of Secondary Explosives," in *Shock Compression of Condensed Matter—1989*, edited by S. C. Schmidt, et al. New York, Elsevier, 1990, pp. 733-736.
3. Trott, W. M., "Investigation of the Dynamic Behavior of Laser-Driven Flyers," in *High-Pressure Science and Technology--1993*, edited by S. C. Schmidt et al. New York, AIP Press, 1994, pp. 1655-1658.
4. Labaste J. L., Doucet, M., and Joubert, P., "Shocks Induced by Laser Driven Flyer Plates: I—Experiments," in *Shock Compression of Condensed Matter—1995*, edited by S. C. Schmidt and W. C. Tao, Woodbury, NY, AIP Press, 1996, pp. 1213-1215.
5. Hatt, D. J., and Waschl, J. A., "A Study of Laser-Driven Flyer Plates," in *Shock Compression of Condensed Matter—1995*, edited by S. C. Schmidt and W. C. Tao, Woodbury, NY, AIP Press, 1996, pp. 1221-1224.
6. Warnes, R. H., Paisley, D. L., and Tonks, D. L., "Hugoniot and Spall Data from the Laser-Driven Miniflyer," in *Shock Compression of Condensed Matter—1995*, edited by S. C. Schmidt and W. C. Tao, Woodbury, NY, AIP Press, 1996, pp. 495-498.
7. Robbins, D. L., Stahl, D. B., and Sheffield, S. A., "Laser-Driven Miniflyer Induced Gold Spall," (this volume).
8. Dlott, D. D., Hambir, S., and Franken, J., *J. Phys. Chem. B*, **102**, 2121-2130 (1998).
9. Farnsworth, A. V., Jr., "Laser Acceleration of Thin Flyers," in *Shock Compression of Condensed Matter—1995*, edited by S. C. Schmidt and W. C. Tao, Woodbury, NY, AIP Press, 1996, pp. 1225-1228.
10. Frank, A. M., and Trott, W. M., "Investigation of Thin Laser-Driven Flyer Plates Using Streak Imaging and Stop-Motion Microphotography," in *Shock Compression of Condensed Matter—1995*, edited by S. C. Schmidt and W. C. Tao, Woodbury, NY, AIP Press, 1996, pp. 1209-1212.
11. Bloomquist, D. D., and Sheffield, S. A., *J. Appl. Phys.* **54**, 1717-1722 (1983).
12. Lawrence, R. J., and Trott, W. M., *Int. J. Impact Engineering*, **14**, 439-449 (1993).

Appendix B

A COMPUTATIONAL STUDY OF LASER DRIVEN FLYER PLATES

Archie Farnsworth, Wayne Trott, and Robert Setchell

Sandia National Laboratories; Albuquerque, NM 87185

Abstract— The existence of both short pulse, high power lasers that can be used drive material flyers to high velocities, and excellent laser diagnostics for determining flyer velocities as a function of time has made the use of such tools an attractive alternative to conventional means for measuring the high pressure properties of materials under shock loading. It provides an especially attractive means for the study of thin materials such as the poly-silicon layers used in the surface micromachine fabrication process. In the current study, our previously developed laser deposition physics addition to the Sandia CTH hydrocode is being used to explore the parameter space of material layering and laser pulse characteristics to develop promising experimental configurations for material property studies. For ordinary materials, thicker foils for acceleration are wanted to provide longer dwell time of the shocked state in a target material. Thermal insulation of the body of the foil from the laser heated accelerating plasma is another desired characteristic for these experiments.

We have performed 1-D studies of material layering with varying thicknesses of the first heated material, Aluminum, and insulating material, Alumina, to find desirable combinations. Other candidate materials exist, of course, and some are currently being considered. Two dimensional studies of flyer acceleration have been performed to guide the selection of laser spacial profiles that may be helpful in providing uniform acceleration across the foil, aiming to provide the maximum attainable flat surface following acceleration.

INTRODUCTION

It has been possible for some time to drive thin flyer plates to km/s velocities using short pulse, high intensity lasers. Likewise, laser velocimeters of various types have been developed, that allow the precision measurement of flyer velocity. These developments invite the investigation of small samples of various materials to determine the high pressure properties of such materials under shock loading, by driving the flyers into target materials of known shock induced behavior. The technique is especially attractive for materials that are inherently thin, that is, materials that are purposely created in very thin layers, for particular applications. The materials used in the development of the micro-machines currently being constructed[1] at Sandia National Laboratories fit in this category. It is known that many materials display different properties when formed in thin layers than are displayed in bulk quantities, so investigation of thin layers for these materials is required.

We are using capabilities previously developed at Sandia, to develop and improve techniques for equation of state (EOS) investigations using laser driven flyers. Coordinated experimental and computational studies are underway, with computations guiding some of the setup parameters for experiments, and experiments both validating the computations and providing areas of increased interest for greater study. The CTH hydrocode as modified by the first author[2] is being used for the computations, and the ORVIS[3] device for experiments. We present here some findings of the computational studies to date.

DISCUSSION

The launching of a laser driven foil is typically done by bringing the laser light through a transparent substrate material onto an absorbing material. The flyer may be of the same material as the first absorbing material, or otherwise. In the case of EOS studies, it is frequently desired to launch a foil that is near room temperature, unheated by the high temperature plasma associated with the launch process. In many of our investigations, we use a thermally insulating material between the launch material and the foil of

interest, as is shown in Figure 1. The launch layer material (frequently aluminum in these studies) is followed by a layer of Alumina (or other material) for insulating purposes, and then the foil of interest.

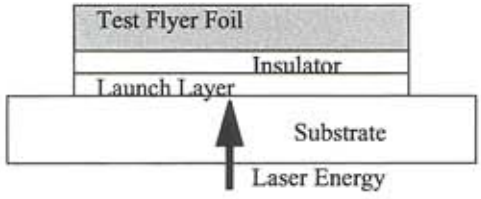

FIGURE 1. Typical layers for EOS experiment.

As we have discussed in a previous presentation[2], the driving plasma is mostly composed of the substrate material, after the initial heating of the launch layer. It is therefore not necessary for the launch layer to be very substantial. Our first optimization study of this arrangement showed one quarter micron of aluminum quite sufficient for the purpose.

The second, insulating layer, however, if it is to prevent heating of the test material flyer, must be considerably thicker. A layer of about 10 microns of alumina seems to be required for the laser pulses studied here. Protecting the foil material is particularly important when studies of very thin materials (a few microns thick, say) are to be performed. The computations show about 3-5 microns of alumina is vaporized by the higher energy pulses studied, while 10 microns prevents significant heating of the flyer. The choice of a thin layer of aluminum backed by an insulator like alumina is also beneficial for maximizing flyer velocity[2], as is seen in Figure2.

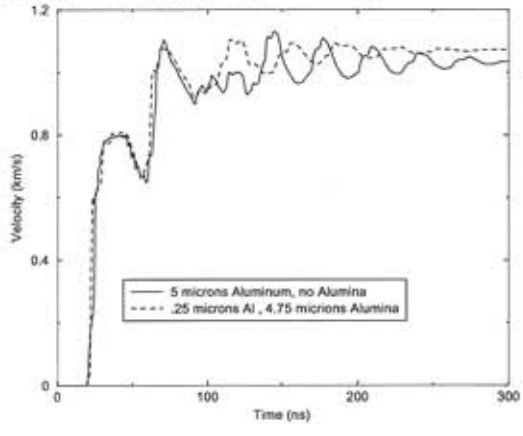

FIGURE 2. Velocity vs. time for acceleration of 100 micron aluminum flyer with and without an insulating layer of alumina.

For EOS studies, the observed data is the velocity of the foil surface before and during impact with the transparent target material. This is represented in the computations by placing a Lagrangian (material following) tracer point very near the foil surface. When impact occurs, the velocity of the combined materials is a function of the shock properties of the interacting materials. Direct comparison of the computed velocity and the experimental velocity can be made. The experiments are arranged so that the multi-dimensional effects are minimized, so comparison with 1-D computational results is reasonable, but not perfect, since it is not possible to eliminate all multi-dimensional effects in the experiments.

Efforts to compare detailed experimental results with computation are underway. In a recent test for which extensive experimental details were provided, a 1-D computational was performed and the velocity vs. time result is shown and compared with the experimental result in Figure 3. For this experiment, the substrate and target material is fused silica. The accelerated foil material is 92 microns of 6061 T-6 Aluminum, and the launch layer consisted of 5 microns of pure aluminum, vapor deposited on the substrate material. There was no insulating layer in this case, and the foil was heated most of the way through the foil thickness. The driving laser pulse consisted of a 1.6J, 20 ns full width at half maximum pulse of 1.06 micron light.

As illustrated in Figure 3, the magnitudes of the peaks are reasonably well simulated, as is the pulse width. Exact comparisons with timing were not possible since the experiment here lacked detailed correlation between driving laser pulse and the observed

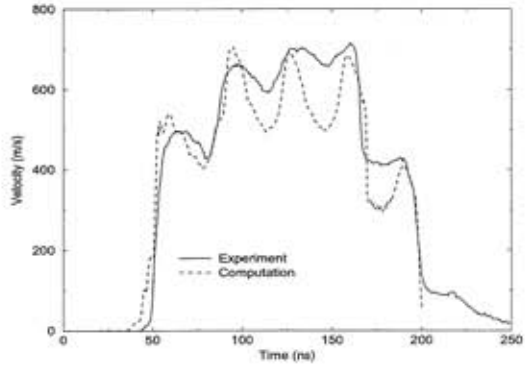

FIGURE 3. Comparison of computed vs. experimentally determined velocity for typical flyer plate experiment. At about 165 ns, impact of the flyer with the target occurs.

signal. The deep valleys between peaks in the computational result are compared with the shallow ones in the experiment. This difference may be the result of two dimensional effects in the experiment, where the spot size observed is about 100 microns in diameter.

We are considering the issues associated with studying the thin layers of silicon frequently used for micro-machine fabrication. One configuration tested computationally consisted of 0.25 microns of Aluminum followed by 0.25 microns of Alumina and a 30 micron layer of molybdenum. The molybdenum has been found experimentally to provide a good support layer for silicon, as deposited in the normal process, consequently it was used here for a supporting material, even though it does not qualify as a good thermal insulator for protecting the silicon foil. The results of an initial computation is seen in Figure 4.

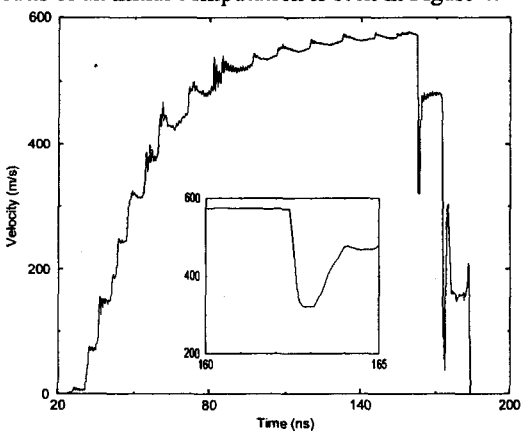

FIGURE 4. Computed velocity vs. time for a silicon flyer on Molybdenum plate. The inset plot shows a magnified time interval containing the silicon impact signal.

The 30 microns of Moly fails to thermally insulate the silicon in this computation, which is that of a first cut experimental arrangement. However, we infer from these results that a discernible silicon signal may be obtained from the brief dwell time of the silicon impact on a fused silica target. That very brief time interval before the properties of the molybdenum begin to dominate the signal is sufficiently small however, (less than one-half nanosecond) that a significant experimental challenge is indicated in making the measurement. The silicon EOS used for this computation is that of the bulk material, so it is to be expected that the experimental result, when obtained, may differ. Finding that difference is a critical component of this work.

We have performed some 2-D computations, to assess the effects of non-uniformity of the laser profile. It is known that in experiments of this kind, the center of the foil moves slightly ahead of the outer edge. This is in part a result of pressure relief from the foil edge, which then propagates toward the center. We had thought that an extra push at the outer edge, by purposely arranging higher laser intensity there, might be desirable, and is not difficult to obtain from our laser. Two 2-D computations were performed, one with a flat topped profile with a Gaussian decrease of laser intensity near the target edge, and the other with a laser intensity that was volcano like in appearance, flat in the center, but significantly higher at the outer edge. The same energy was delivered by each pulse. The comparison is not an ideal one, since more of the energy fell past the edge of the flyer in the case of the curve peaked at the edge. The results of these computations, with respect to foil flatness, is seen in Figure 6. Surprisingly little effect is seen from the added intensity at the edge, but the effect of the greater intensity at the foil edge is clear in the size of the plasma plume seen there.

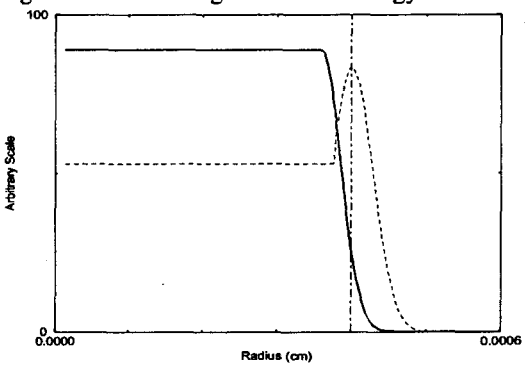

FIGURE 5. Intensity vs. radius for two computations.

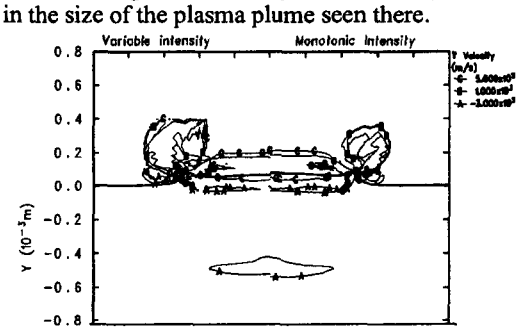

FIGURE 6. Contours of vertical velocity for two computations. The variable intensity on the left (see dashed line of Figure 5), and the monotonic intensity on right side.

FUTURE DIRECTIONS

The tools of this study are being found profitable for exploring the intended parameters. We expect to continue utilizing them to further define materials and layering that will produce favorable experimental results. In particular, we will continue to seek arrangements that will allow good experimental results for very thin materials, and their associated brief signal times.

As more detailed experimental and computational studies are performed, we expect to continue to gain insights into the fundamental processes associated with laser acceleration of thin flyer plates, and therefore be able to better define parameters profitable for equation of state studies.

SUMMARY

The computational and experimental exploration of the parameter space of thin flyers launched by powerful lasers is underway at Sandia National Laboratories. We find that a very thin launch layer is sufficient, since the accelerating plasma consists mostly of substrate material in any case. The presence of a thermally insulating layer seems necessary if thin foils are to be kept near their original state throughout the acceleration process. This layer may be significantly larger than the material being tested. Inherently thin layers may be tested in this way, provided that experimental resolution can be pushed into the sub nanosecond regime, as we expect it can. We also find a rather low sensitivity of the flyer shape at impact time to the details of the laser profile in space, at least near the foil edge.

ACKNOWLEDGMENTS

Sandia is a multiprogram laboratory operated by Sandia Corporation, a Lockheed Martin Company, for the United States Department of Energy under Contract DE-AC04-94AL85000.

REFERENCES

1. E. J. Garcia and J. J. Sniegowski, "Surface Micro-machined Micro Engine", *J. Sensors and Actuators, A*, vol. 48, 203-214, 1995.
2. A. V. Farnsworth, Jr., "Laser Acceleration of Thin Foil", in Shock *Compression of Condensed Matter*, 1991, pp. 1225-1228.
3. D. D. Bloomquist and S. A. Sheffield, *J. Applied Phys.*, Vol 54, 1717-1722, 1983.

Appendix C

Evaluation of a diffractive, microlens-array beam shaper for use in acceleration of laser-driven flyers

Wayne M. Trott, Robert E. Setchell, Jaime N. Castañeda, and Dante M. Berry

Sandia National Laboratories, Albuquerque, New Mexico 87185-0834

ABSTRACT

A promising new tool in shock wave physics is the generation of shock waves in test materials through the impact of small, laser-accelerated discs ("flyers"). In order to achieve the necessary one-dimensional condition of uniaxial strain in the shock-loaded material, it is vital that flyers maintain a nearly planar geometry during the acceleration and impact processes. The geometry of the flyer is significantly influenced by the spatial intensity profile of the driving laser beam. With the goal of achieving a nearly uniform drive intensity for this application, we have evaluated a diffractive, microlens-array beam shaper for use with a high-energy, Nd:Glass laser driver. Based on the near-field spatial profile of this multimode laser, a 30-mm-diameter array containing multiple hexagonal diffractive lenslets was designed and fabricated. In combination with a primary integrator lens of 76.2-mm focal length, this optical element was intended to produce a uniform intensity distribution over a 2-mm-diameter spot at the focal plane of the primary lens. Beam profiling studies were performed to determine the performance of this optical assembly. At the focal plane of the primary lens, the beam shaping optics generated a reasonably uniform profile over a large portion of the focused beam area. However, a small amount of undiffracted light resulted in a high-intensity, on-axis spike. A beam profile approaching the desired "top hat" geometry could be obtained by moving the flyer launch plane a few mm inside or outside of the focal plane. The planarity of flyers generated using this optical assembly was evaluated using a line-imaging, optically recording velocity interferometer system (ORVIS). Results of these measurements demonstrate the deleterious effect of the on-axis spike on flyer planarity. Acceptable conditions for useful flyer impact experiments can be obtained by operating at a position that provides a near-top-hat profile.

Keywords: beam-shaping optics, laser-driven flyers, Nd:Glass laser

1. INTRODUCTION

Successful refinement of techniques for pulsed-laser acceleration of small metal discs ("flyers") could result in important new methods for quantitative studies of material response under shock wave loading. Methods for acceleration of thin (< 10-μm-thick) metal films have been extensively investigated.[1-5] However, significant upward scaling of these methods to achieve precise, sustained, one-dimensional loading by substantially thicker flyers is critically needed. Fundamental research areas of interest include measurements of Hugoniot states and spall strength[6,7] as well as shock-induced phase transitions and chemistry.[8] Shock compression using laser-driven flyers is particularly suited to investigation of materials that cannot be obtained with sufficient dimensions for use in conventional gas gun tests. An important example is the basic structural material used in the fabrication of surface micromachines, polycrystalline silicon.[9] This material is generally prepared in characteristic layer thicknesses of 2-6μm. Coupled with high-speed diagnostics (e.g., velocity interferometry), the low temporal jitter available with laser-driven flyer techniques facilitates well-controlled production and measurement of short-duration (few ns) compression states in such microscale materials. A typical experimental configuration for studies of this type is illustrated schematically in Fig. 1. In this approach, a pulsed laser beam impinges on a metal disc affixed to an optically transparent substrate. Laser absorption occurs in a thin layer of the disc at this interface, rapidly driving the material (and substrate material near the interface as well) to vaporization and plasma formation. The plasma efficiently absorbs the remainder of the laser pulse, resulting in a highly localized source of stored energy. Plasma expansion then accelerates the disc (flyer) off the substrate to a high velocity. In the configuration shown in Fig. 1, the flyer carries the sample of interest across a small gap to impact a well-characterized witness plate material. This "reverse impact" configuration can provide a direct measurement of a shocked state ("Hugoniot" state) for a sample impacting a window with well-established Hugoniot properties (e.g., fused silica), as a result of the boundary condition that axial stress and material velocity must be continuous across the interface.

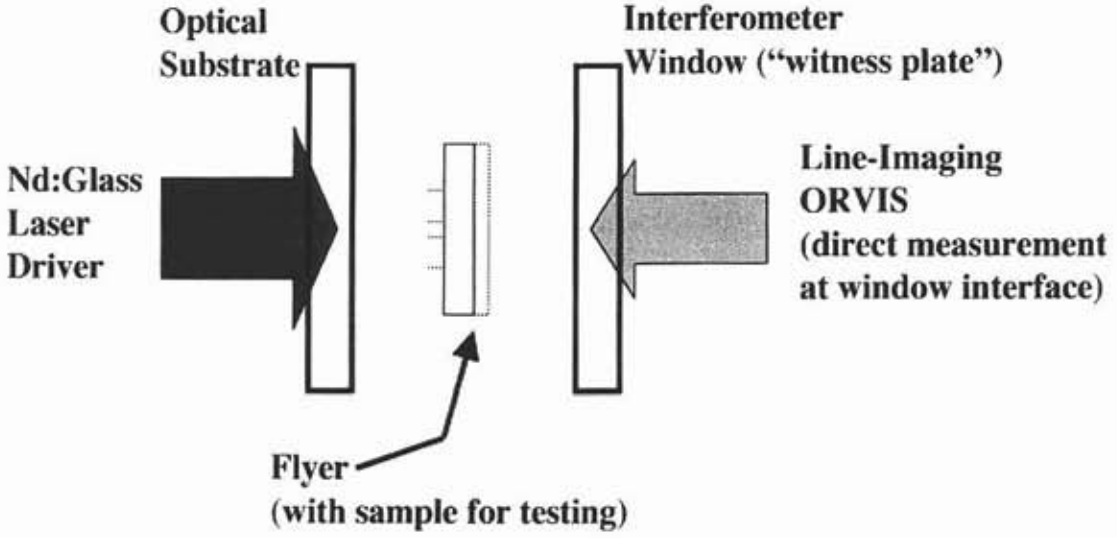

Figure 1. Schematic diagram of reverse impact experiment utilizing a laser-driven flyer/impactor.

Although the design for impact experiments using laser-driven flyers is conceptually simple, the dynamic phenomena in laser-acceleration of metal discs are extremely complex and present significant challenges to the realization of robust, well-characterized acceleration and impact techniques. Critical issues include the development of methods for consistent fabrication of metal discs and samples, management of thermal transport (diffusing from the high-temperature driving plasma) within the flyer/sample structures, mitigation of drive instabilities (a characteristic problem associated with a relatively low density plasma pushing the higher density flyer), and optimization of the laser intensity profile driving the flyer. Strategies for addressing the last issue include: (1) "homogenizing" the laser beam spatial profile by transmitting the light through a sufficient length of optical fiber and re-imaging the fiber output to the substrate/flyer interface, and (2) directly tailoring the laser profile by means of a beam shaping optical assembly. The former approach can provide a very uniform ("top hat") profile at the desired location; however, the available energy on target is constrained by optical damage limits in the conditioning fiber.[10] For applications requiring flyer diameters > 1 mm, this method becomes impractical as a result of the expense and limited availability of corresponding large-diameter optical fibers. The recent development of beam shaping optics utilizing microlens arrays for conditioning high power, multimode laser profiles is a promising approach for the second strategy.[11]

In an effort to tailor the laser spatial profile to optimize impact planarity for tests involving large-diameter (up to 2.5 mm) flyers, we have evaluated a diffractive, microlens array beam shaper for use with a high-energy Nd:Glass laser. Results of this evaluation, including preliminary flyer acceleration tests and impact studies, are reported in this paper. Section 2 provides important laser characteristics and the essential design parameters for the beam shaping optics. Results illustrating the performance of the microlens array are reported in Section 3. A brief description of the velocity interferometer system used to analyze flyer acceleration and impact, and results of flyer experiments conducted using the beam shaping optical assembly are presented in Section 4. Finally, a brief summary is given in Section 5.

2. BEAM SHAPER DESIGN

2.1 Nd:Glass Drive Laser Characteristics

The driving laser used in this work is a Q-switched Nd:Glass system (Lasermetrics Model 9380). The laser output (λ=1.054 μm) is horizontally polarized and multimode. This system can be operated in either an oscillator-only or oscillator/amplifier configuration. Maximum output energies in these operational modes are 4.5 J and 20 J, respectively. The typical laser pulse duration is ~20 ns (FWHM). Coarse spectral analysis has shown that the output is relatively broadband (~1.3 nm, FWHM).

Typical beam divergence in the oscillator-only configuration is 3 mrad. Examples of typical near-field spatial intensity distributions generated in separate shots by the Nd:Glass oscillator are shown in Fig. 2. The profiles are slightly elliptical with isolated "hot spots." With very careful alignment of the laser cavity, these "hot spots" can be distributed into a fairly even annular pattern. Under normal operating conditions, however, the isolated regions of high intensity tend to drift in location from shot to shot. These output properties were used to develop the beam shaper design described below. For comparison, plots of horizontal and vertical line scans (corresponding to the profile in Fig. 2b) are displayed in Fig. 3.

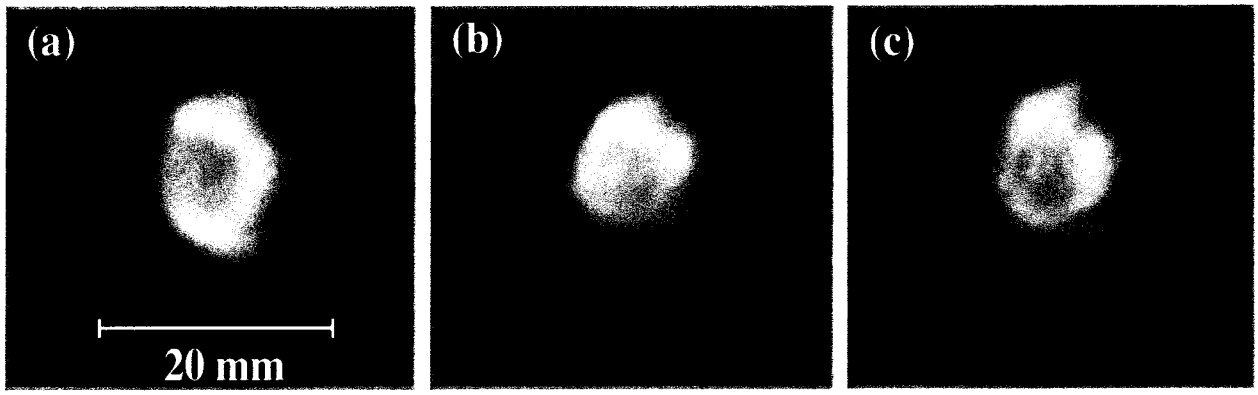

Figure 2. Near-field spatial profiles of Nd:Glass drive laser; image magnification at CCD camera = 0.1745.

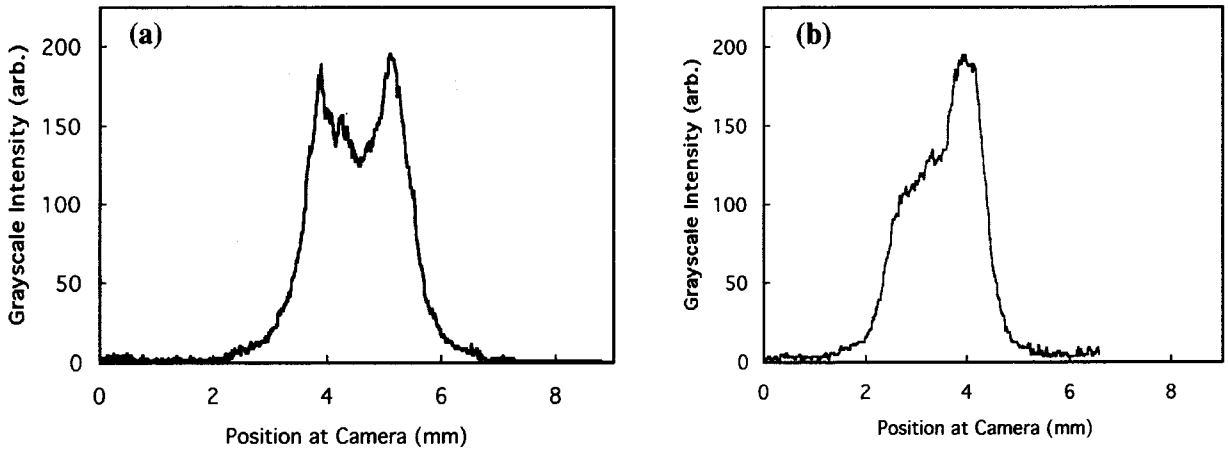

Figure 3. Line scans of Nd:Glass laser intensity for record displayed in Fig. 2b: (a) horizontal line scan; (b) vertical line scan; image magnification at CCD camera = 0.1745.

2.2 Beam Shaper Specifications

Given the output characteristics of the Nd:Glass laser, a beam shaper was designed with the goal of "homogenizing" the intensity profile over a ~2-mm-diameter spot. The basic optical architecture is illustrated in Fig. 4. The system includes a multi-aperture, diffractive lenslet array element (LL2) and a primary injection lens (L_1) that overlaps the beamlets from each subaperture at the lens focal plane.[11] The specified diameter (D_{LL2}) of the lenslet array was 30 mm, easily accommodating the ~18 mm input beam diameter (D). The thickness (t) of the lenslet array was 1.0 mm. Specifications for the hexagonal lenslets included a diameter of 2.5 mm (measured flat to flat) with a focal length of 95.2 mm and a fill factor >98%. The full optical prescription for the array was prepared by MEMS Optical. Four of the array elements were fabricated by MEMS Optical for our evaluation. The beam shaper design called for a user-supplied plano/convex primary injection lens with a focal length (f_1) of 76.2 mm. The spot diameter (D_{spot}) for the integrated intensity profile was specified to be 2.0 mm.

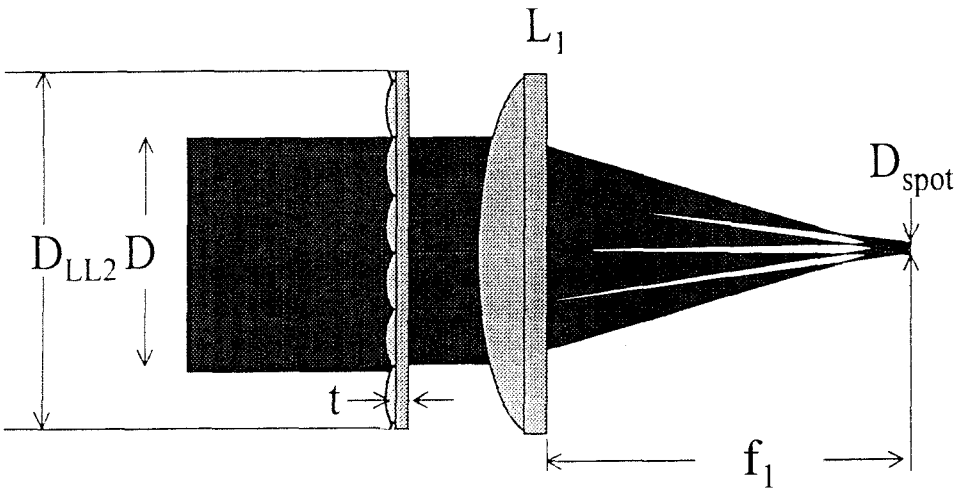

Figure 4. Schematic diagram of optical architecture for the diffractive beam shaper described in the text.

3. BEAM SHAPER PERFORMANCE

Qualitative inspection of the beam shaper geometry and surface roughness was performed using a Numarski microscope equipped with a digital camera for recording images. Detailed profiles of the near-field intensity distribution of the Nd:Glass driver laser (Fig. 2) as well as beam shaper output were recorded using a variety of CCD cameras including:

(1) Cohu Model 4800--240 x 240 pixels, 23 μm wide by 27 μm high, 8-bit energy resolution
(2) Cohu Model 4810--780 x 244 pixels, 11.5 μm high by 27 μm high, 8-bit energy resolution
(3) Silicon Mountain Design Model SMD-1M15--900 x 1024 pixels, 14 μm square, 12-bit energy resolution.

Beam-profiling software was used to display and analyze the acquired intensity distributions. In analyzing the beam shaper output, we utilized two figures of merit. The effective "spot size" was evaluated by defining (in the software) a circular aperture (typically 2-2.5 mm diameter for our applications) centered on the beam profile, and then determining the fraction of energy within this aperture. The uniformity of the intensity distribution, on the other hand, was addressed by determining the ratio of peak (P) to average (A) fluences as follows:

$$P/A = \frac{\text{peak local fluence}}{(\text{total energy incident on aperture})/(\text{aperture area})}$$

A perfect "top hat" fluence distribution extending over the entire aperture area would achieve a value of unity for this ratio. In practice, as described below, we observed values for this ratio ranging from 1.6 to greater than 10 for various positions relative to the focal plane of the primary lens.

The output characteristics of the Nd:Glass laser for which the beam shaper was designed were described in the previous section. We also examined beam shaper output using an oscillator-only, multimode Nd:YAG laser (Laser Photonics Model YQL-102). This device was operated at the fundamental wavelength (λ=1.064 μm) in a Q-switched, single-shot mode. Average pulse width for this laser is 9.4 ns (FWHM). Additional characteristics of this laser system have been described in detail elsewhere.[12]

As indicated above, initial evaluation of the diffractive beam shaper included visual inspection under the Numarski microscope. Photographs at two different magnifications are shown in Fig. 5 and Fig. 6, respectively. The essential geometry of the individual lenslets (described in previous section) is illustrated in the low-magnification view given in Fig. 5. The high-magnification view in Fig. 6 indicates a relatively smooth surface profile for the individual elevations of each lenslet. Relatively low surface roughness is critical factor in applications requiring efficient transmission of high-energy laser pulses with a correspondingly high energy threshold for optical damage.

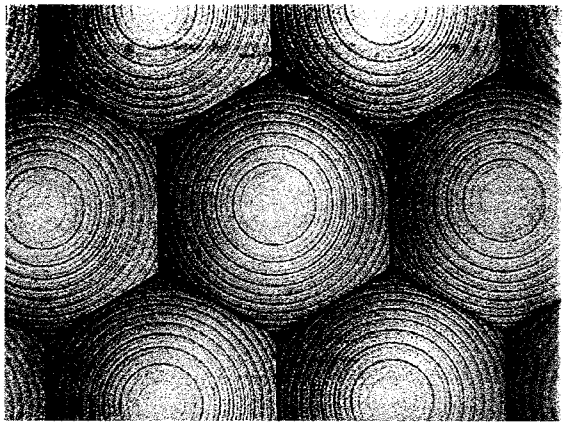

Figure 5. Hexagonal lenslet array in the beam integrator element; area shown is 6.1 mm wide by 4.5 mm high.

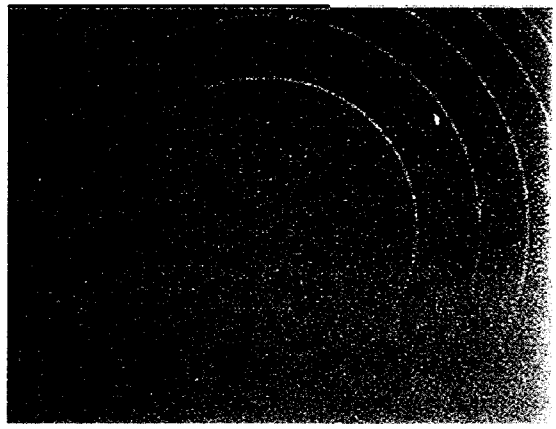

Figure 6. View of the center of an individual lenslet; area shown is 240 μm wide by 180 μm high.

The first series of beam profile measurements were performed with the Q-switched Nd:YAG laser source and utilized the diffractive lenslet array in combination with a primary integrator lens of 77.4-mm focal length (slightly larger than the specified value). In these tests, we were able to exploit the high spatial resolution and 12-bit energy resolution capability of the Silicon Mountain Design Model SMD-1M15 CCD camera. As described elsewhere, the near-field profile of this Nd:YAG laser typically exhibits a semi-Gaussian shape with some elongation along one axis and minor "hot spots."[12] Representative profiles obtained with the beam shaper are shown in Fig. 7. Figure 7a displays the intensity distribution obtained at the focal plane of the primary lens. Corresponding horizontal and vertical line scans of the light intensity are plotted along the bottom and left edge, respectively, of the image record. Several important features are evident in this profile. The intensity pattern at the focal plane reflects the hexagonal geometry of the individual lenslets; however, we consistently observed a significant intensity asymmetry associated with one vertex of the hexagonal pattern. For the most part, the intensity is homogenized reasonably well across the field. Unfortunately, the pattern also displays a small amount of undiffracted light (zero order) that is focused to a sharp intensity "spike" by the primary lens. The fraction of undiffracted light is this experimental configuration is estimated to be 1.9%. Applying the figures of merit described above, we determined that 86.6% of the laser energy is contained within a 2-mm-diameter circular aperture with P/A = 5.58.

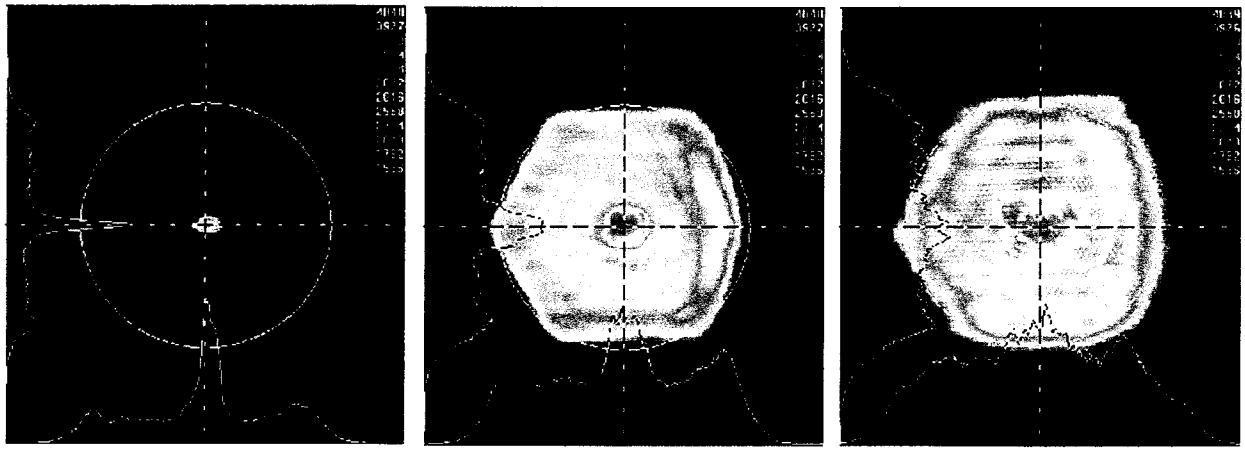

(a) (b) (c)

Figure 7. Beam profiles for Q-switched Nd:YAG laser transmitted through the beam shaper: (a) profile acquired at the focal plane of the primary integrator lens; (b) profile at location 5.0 mm downstream from focal plane; (c) profile at location 10.0 mm downstream from focal plane.

Although the fraction of undiffracted light is small, the resulting spike in the intensity distribution could present serious difficulties in conditioning a high-energy drive laser for flyer acceleration. One consideration is that an intensity spike may lead to entry damage in a thin optical substrate and promote self-focusing within the substrate material. As shown in Section 4, a feature of this type is also likely to result in very uneven flyer acceleration. Figure 7 displays two other profiles that illustrate the evolution of the intensity distribution at locations 5.0 mm and 10.0 mm beyond the focal plane of the integrator lens (Fig. 7b and Fig. 7c, respectively). Substantial broadening of the high intensity spike can be achieved in this manner but only at the cost of a corresponding smearing out of the hexagonal pattern. This effect is directly reflected in the figures of merit for P/A and percent energy transmission. P/A falls to 2.11 and 1.63 for the measurements at +5.0 mm and +10.0 mm, respectively; however, the energy contained in the 2-mm-diameter aperture drops to 79.7% in the former case and to 73.3% at the +10.0 mm test plane. Similar focusing characteristics were observed with all of the beam shaping elements fabricated for this study.

Very similar results were obtained with the pulsed Nd:Glass laser for which the beam shaper was designed. For this series of experiments, we used a primary integrator lens of 75-mm focal length (slightly smaller than the specified value). Beam profiles were acquired and analyzed for a series of locations ranging from 7.0 mm before (-) to 5.0 mm beyond (+) the focal plane of the integrator lens. A typical profile acquired at the focal plane is displayed in Fig. 8. In all respects, the essential features of the observed intensity distribution are similar to those described above. Figure 9 shows that broadening of the intensity spike and overall hexagonal pattern occurs inside of the focal plane as well as outside. Our results are summarized in Table I. In terms of our two figures of merit, the observed intensity distribution varies nearly symmetrically on both sides of the focal plane. For a given measurement location, shot-to-shot variations in beam profiles were observed to be negligible, indicating that the beam shaper design successfully accommodates the drift in "hot spot" location characteristic of the Nd:Glass laser system.

TABLE I. Variations in Intensity Distribution Using Beam Shaper as a Function of Position Relative to the Focal Plane of the Primary Integrator Lens (75-mm Focal Length)

Position Relative to Primary Integrator Lens Focal Plane (mm)	*Percent Energy Contained Within 2-mm-Diameter Aperture*	*P/A*
+5.0	84.7	1.96
+4.0	86.7	1.75
+3.0	89.2	2.29
+2.0	91.8	2.99
+1.5	92.5	3.42
+1.0	93.4	5.49
+0.5	94.1	6.79
0	94.6	9.46
-0.5	94.9	6.31
-1.0	93.9	3.88
-2.0	91.5	2.65
-3.0	88.1	1.94
-4.0	85.1	1.70
-5.0	82.2	1.73
-6.0	79.3	1.95
-7.0	75.9	1.97

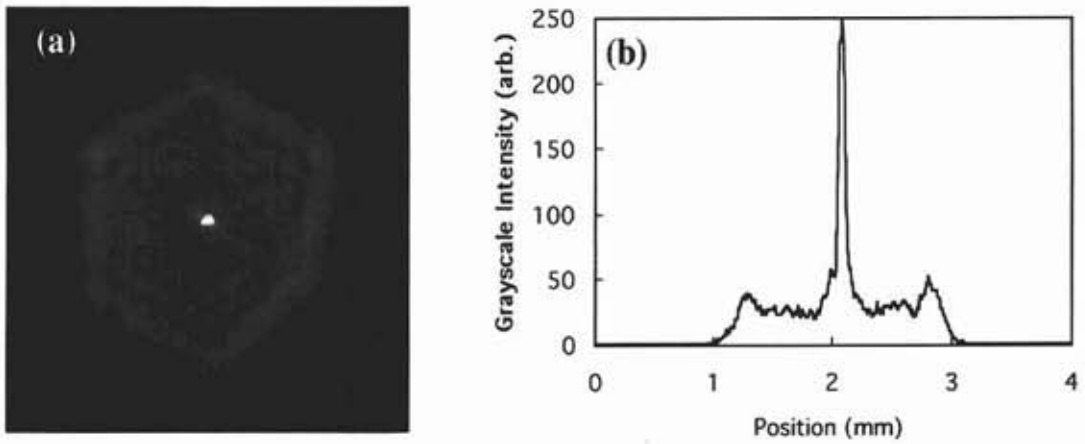

Figure 8. Beam profile for Q-switched Nd:Glass laser transmitted through the beam shaper: (a) image record acquired at the focal plane of the primary integrator lens; (b) horizontal line scan of laser intensity.

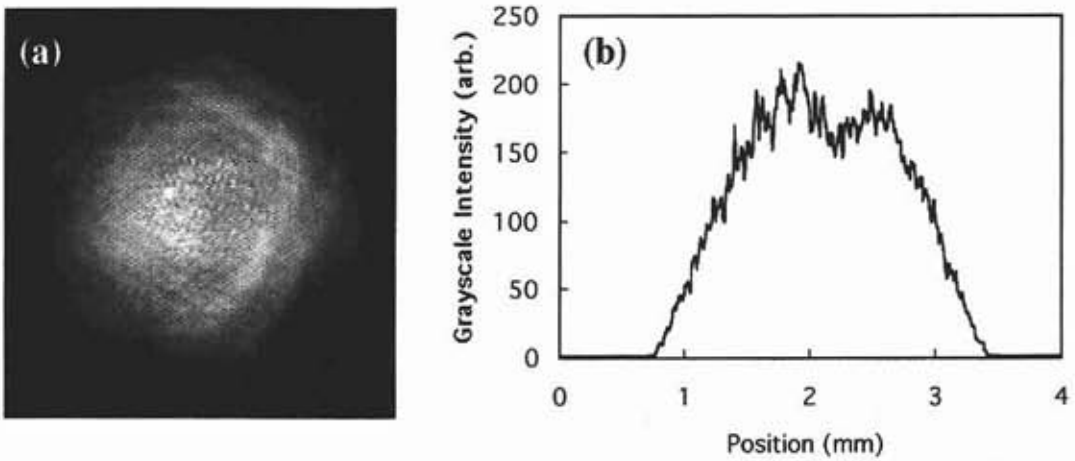

Figure 9. Beam profile for Q-switched Nd:Glass laser transmitted through the beam shaper: (a) image record acquired at a location 5.0 mm upstream of the focal plane of the primary integrator lens; (b) horizontal line scan of laser intensity.

4. FLYER ACCELERATION AND IMPACT EXPERIMENTS

4.1 Velocity Interferometer for Characterization of Flyer Performance

Dynamic flyer performance and impact planarity were evaluated using a line-imaging optically recording velocity interferometer system (ORVIS). The essential elements of the optical design for this instrument are displayed schematically in Fig. 10. Coherent light from a continuous-wave laser source (2W argon ion laser, λ=514.5 nm) is directed through a set of spherical and cylindrical lenses that produce intense illumination along a line segment at the target (cf. Fig. 1). Diffusely reflected light from the target is collected and roughly collimated by a lens. The resulting beam is reduced in size by down-collimating telescope optics (L1, L2 in Fig. 10) and directed into the interferometer cavity. The beam is separated by the 50/50 beamsplitter into two equal-intensity components, one of which serves as a reference leg. The second leg passes through a variable-length fused silica cylinder. This optical component imparts a time delay (proportional to cylinder length) in the second beam. The beams are then recombined at the beamsplitter, producing two redundant legs of equal intensity. In the same manner as conventional, single-point ORVIS,[13] the orientation and position of mirrors M1 and M2 can be adjusted

to provide a high-contrast, nearly "straight line" interference fringe pattern. With proper adjustment of the relay optics (collection lens, L1, L2 in Fig. 10), this pattern can be superimposed onto a magnified image of the target. Observed displacement of the interference fringes is directly proportional to velocity; hence, local variations in target surface velocity are reflected in corresponding local translations of the fringe field. This motion of the fringe field along the magnified image of the illuminated line segment can be recorded by a high-speed streak camera. If needed, a second streak camera can be utilized for data recording on a different time base. A more detailed discussion of the line-imaging ORVIS, and methods for image data reduction to generate spatially resolved velocity-time profiles, are given elsewhere.[14]

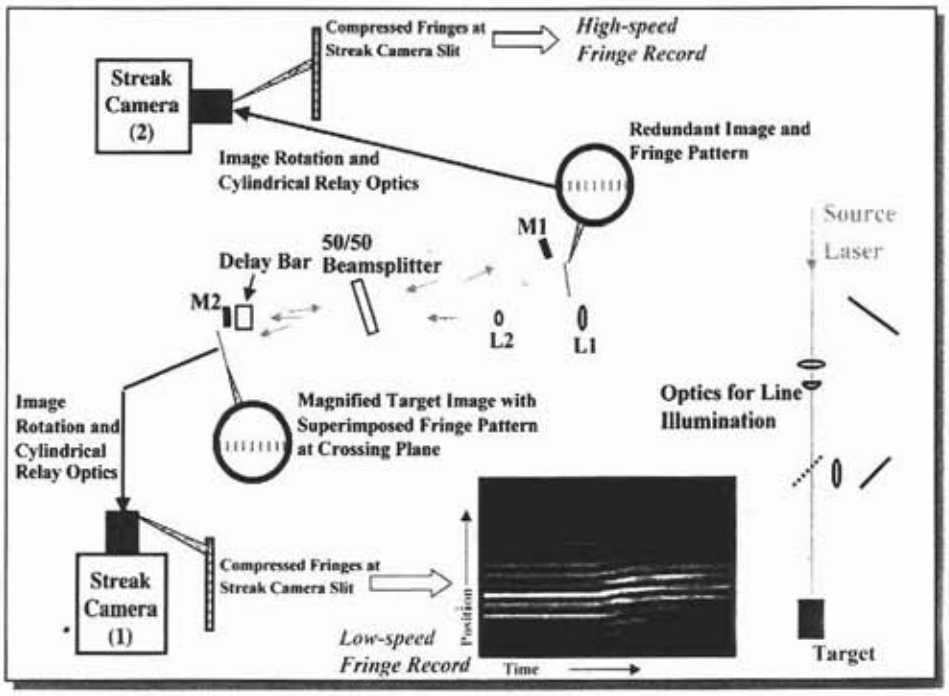

Figure 10. Schematic diagram of line-imaging ORVIS design; two streak cameras can be used for dual time base recording.

In this study, we employed line-imaging ORVIS to examine flyers launched using different drive profiles generated by the beam shaper. For these measurements, the interferometer viewed the free surface of the flyer directly. To evaluate the performance of the beam shaper in generating flat impacts, we also performed witness plate experiments in the basic configuration shown in Fig. 1. With careful masking of specular reflections from the witness plate window, it is possible to record both the flyer acceleration and the post-impact interface velocity on the same image (see below). This technique can be used to determine Hugoniot properties either for the flyer material itself or for samples carried to impact by the flyer.[15]

4.2 Beam Shaper Evaluation Tests with 6061-T6 Aluminum Flyers

Conditioning the Nd:Glass laser output with the beam shaper produces clearly discernable differences in the shape of laser-accelerated flyers. For these tests, we generated and analyzed spatially resolved velocity-time plots over a ~0.5-mm-long line segment centered on laser-driven, 100-μm-thick 6061-T6 aluminum flyers. Flyer diameter was 2.5 mm, rather than the 2.0-mm value in Table 1. Methods for preparing the 6061-T6 test samples on fused silica substrates have been described elsewhere.[15] We evaluated the effect of beam shaper driving profiles for two cases: (1) with the flyer/substrate interface positioned at the focal plane of the primary integrator lens and (2) with the flyer/substrate interface positioned 4.0 mm inside of this focal plane. Efficient energy coupling was available in both configurations; beam profile measurements demonstrated that >98% of the incident energy is confined within the area defined by the 2.5-mm-diameter flyer. Since the intensity of the conditioned beam drops off to a low value at the outer regions of the 2.5-mm diameter, the corresponding P/A ratios are larger than those listed in Table I. For the flyer/substrate interface located at the focal plane, P/A = 13.56. Positioning the interface 4.0 mm inside the focal plane results in P/A value of 2.31.

Figure 11a displays an interferometer fringe record for a flyer driven with the intensity distribution available at the integrator lens focal plane (cf. Fig. 8). As indicated previously, the line segment at the flyer free surface was viewed directly; i.e., without an interferometer window in the optical path. Laser energy incident on the flyer was approximately 0.55 J. The optical delay in the interferometer cavity was set to produce a displacement of one fringe for a velocity of 0.52 km-s^{-1}. Onset of flyer motion occurs nearly simultaneously across the line segment probed by the velocity interferometer; however, uneven acceleration is manifested in the dark zone which appears in a localized area of the fringe record shortly after the onset of motion and rapidly propagates outward. A systematic loss in reflected light intensity of this type often indicates significant surface curvature. The spatially resolved velocity-time plot determined from the fringe record provides a more quantitative picture of the uneven acceleration. This plot is shown in Fig. 11b. A definite peak in flyer velocity is clearly evident near the center of the line segment. The extent of flyer curvature can be evaluated by integration of the velocity record to generate a plot of displacement vs. time. The displacement history over the line segment is displayed in Fig. 11c. These results show that large variations in the spatial intensity distribution of the drive laser can have a deleterious effect on the planarity of the driven plate, even for relatively thick flyers. The highly localized flyer curvature seen in this case is consistent with the small-diameter, high-intensity spike generated at the focal plane of the integrator lens.

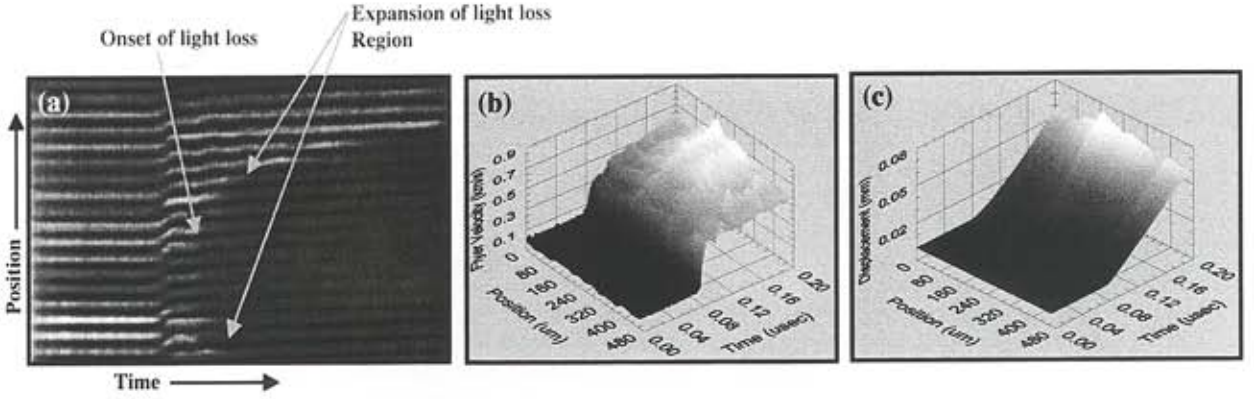

Figure 11. Line-imaging ORVIS record of 6061-T6 aluminum flyer launched using the spatial profile generated at the focal plane of the primary integrator lens: (a) interferometer fringe record; (b) spatially resolved velocity-time plot; (c) spatially resolved displacement-time plot.

Flyers exhibiting considerably less curvature were obtained when the flyer/substrate interface was positioned 4.0 mm inside of the focal plane. The drive laser profile available at this location is very similar to that shown in Fig. 9; i.e., the central spike is distributed over much of the hexagonal profile (which also exhibits significant broadening at the edges). Data obtained in this configuration are shown in Fig. 12. The sample geometry, incident laser energy, and optical delay in the interferometer cavity were essentially identical to the conditions for the test illustrated in Fig. 11. The reduced velocity-time record (Fig. 12b) is somewhat "noisier" than that shown in Fig. 11b, primarily as a result of the low intensity of light reflected from the flyer surface (corresponding to a significantly more diffuse surface finish) in this case. Nevertheless, the velocity is substantially more uniform across the line segment. A reduced surface curvature is indicated by the relatively constant fringe contrast vs. time in the interferometer image data (Fig. 12a) and is clearly evident in the displacement-time profile (Fig. 12c). The uniform drive conditions obtained in this configuration are sufficient for quantitative impact experiments of the type shown schematically in Fig. 1.

Successful reverse impact experiments have been performed using the beam shaper to condition the drive pulse. In these tests, 6061-T6 aluminum flyers (2.5-mm-diameter, 100-μm-thick) were launched and allowed to impact a fused silica "witness plate" window. The Hugoniot properties of both the flyer and window material have been well-characterized.[16,17] Hence, the accuracy of our flyer impact experiments can be evaluated directly. Based on the flyer acceleration results described above, we utilized the broadened spatial intensity distribution available with the flyer/substrate interface positioned 4.0 mm inside the focal plane of the primary integrator lens. A line-imaging ORVIS record showing the full flyer acceleration history as well as interface velocities both at impact and during the subsequent shock unloading is displayed in Fig. 13a. In

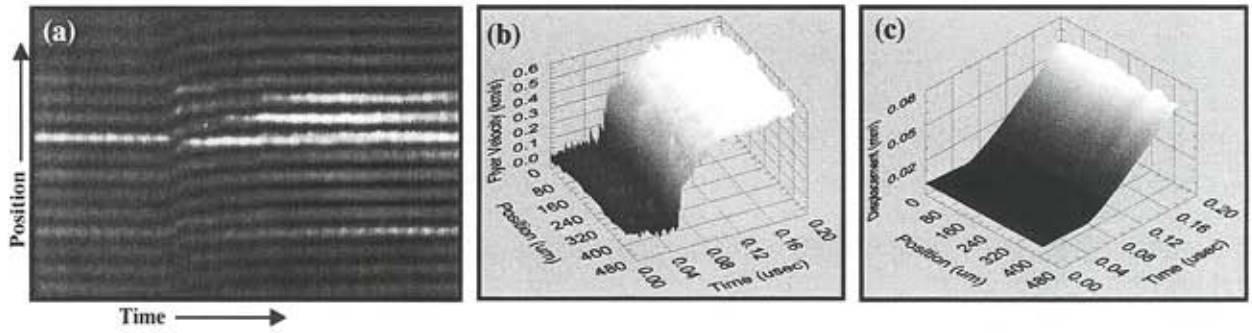

Figure 12. Line-imaging ORVIS record of 6061-T6 aluminum flyer launched using the spatial profile generated at 4.0 mm inside of the focal plane of the primary integrator lens: (a) image data; (b) spatially resolved velocity-time plot; (c) spatially resolved displacement-time plot.

this case, laser energy incident on the flyer was approximately 1.45 J. The flyer surface curvature under these conditions is small enough to produce nearly simultaneous impact over much of the line segment. A plot of the relevant velocities (spatially averaged over regions of flat impact) is shown in Fig. 13b. Both the flyer velocity at impact and the post-impact interface velocity (with appropriate refractive index corrections for the fused silica interferometer window)[18] can be derived from this velocity-time curve. The known Hugoniot properties for 6061-T6 aluminum and fused silica indicate that an impact at 0.87 km-s^{-1} should produce a post-impact interface velocity near 0.5 km-s^{-1}. Our results in Fig. 13 are consistent with this expected behavior. A more detailed discussion of our methods for using flyer impact experiments for Hugoniot property measurements is available elsewhere.[15]

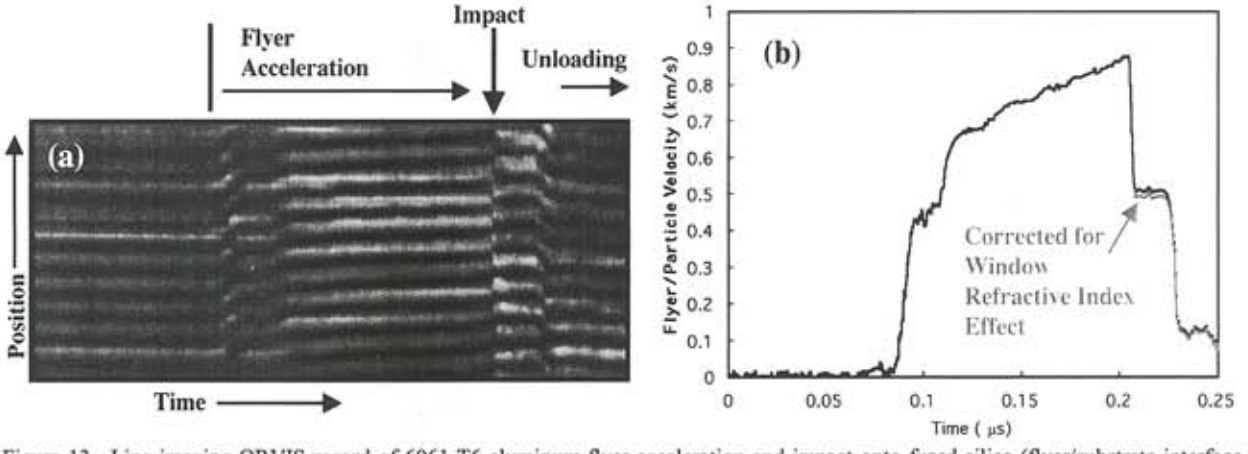

Figure 13. Line-imaging ORVIS record of 6061-T6 aluminum flyer acceleration and impact onto fused silica (flyer/substrate interface located 4.0 mm inside of the focal plane of the primary integrator lens): (a) image data; (b) velocity-time plot spatially averaged over flat impact region. The required small correction for refractive index effects in the fused silica window is illustrated in the velocity-time plot.

5. SUMMARY

Diffractive microlens array beam shapers provide a useful tool to condition high-energy laser beams for applications requiring uniform illumination. One application of interest to shock physics research is the tailoring of a drive laser spatial intensity distribution for uniform acceleration of flyer plates. Laser-accelerated flyers with minimal surface curvature can be utilized in a variety of high-velocity impact experiments for dynamic material studies. In this paper, we have examined a beam shaper designed to homogenize the output of a Nd:Glass laser for this type of work. The beam shaper successfully distributed nearly all of the Nd:Glass output into a fairly uniform-intensity hexagonal profile that confined about 95% of the

energy within the area defined by a 2-mm-diameter circular aperture. The roving "hot spots" characteristic of the Nd:Glass laser system were also effectively distributed by the beam shaping optics. Unfortunately, the intensity profile at the focal plane of the primary integrator lens exhibited a small fraction (~2%) of undiffracted light that was focused to a sharp intensity spike. The effect of this spike was clearly evident in flyer acceleration experiments. With the flyer/substrate interface initially positioned at the focal plane, laser-accelerated flyers with significant surface curvature were produced. Much improved flyer planarity can be achieved, however, with the flyer/substrate interface located a few mm on either side of the integrator lens focal plane. We have shown that this configuration can be used with the Nd:Glass laser oscillator to accelerate flyers to velocities approaching 1 $km\text{-}s^{-1}$. With this approach, we have obtained flyer impact at geometries affording nearly one-dimensional shock loading conditions and we have demonstrated that this system can be used to acquire Hugoniot measurements in good agreement with published values. Refinement of the beam shaper design and fabrication to eliminate the undiffracted light would represent a very useful enhancement to this system.

ACKNOWLEDGMENTS

Sandia is a multiprogram laboratory operated by Sandia Corporation, a Lockheed Martin Company, for the United States Department of Energy under Contract DE-AC04-94AL85000. The authors would like to thank Juan Romero and Cathy Sifford of Sandia National Laboratories for their talented assistance in preparation of flyer/substrate fixtures. Funding for this work was provided by the Laboratory Directed Research and Development program at Sandia.

REFERENCES

1. W. M. Trott and K. D. Meeks, "Acceleration of Thin Foil Targets Using Fiber-Coupled Optical Pulses," in Shock Compression of Condensed Matter—1989, Elsevier, New York, 1990, pp. 997-1000.

2. D. L. Paisley, "Laser-Driven Miniature Flyer Plates for Shock Initiation of Secondary Explosives," in Shock Compression of Condensed Matter—1989, Elsevier, New York, 1990, pp. 733-736.

3. W. M. Trott, "Investigation of the Dynamic Behavior of Laser-Driven Flyers," in High-Pressure Science and Technology—1993, AIP Press, New York, 1994, pp. 1655-1658.

4. J. L. Labaste, M. Doucet, and P. Joubert, "Shocks Induced by Laser Driven Flyer Plates:1—Experiments," in Shock Compression of Condensed Matter—1995, AIP Press, Woodbury, NY, 1996, pp. 1213-1215.

5. D. J. Hatt and J. A. Waschl, "A Study of Laser-Driven Flyer Plates," in Shock Compression of Condensed Matter—1995, AIP Press, Woodbury, NY, 1996, pp. 1221-1224.

6. R. H. Warnes, D. L. Paisley, and D. L. Tonks, "Hugoniot and Spall Data from the Laser-Driven Miniflyer," in Shock Compression of Condensed Matter—1995, AIP Press, Woodbury, NY, 1996, pp. 495-498.

7. D. L. Robbins, D. B. Stahl, and S. A. Sheffield, "Laser-Driven Miniflyer Induced Gold Spall," in Shock Compression of Condensed Matter—1999, AIP Proceedings 505, 1199 (2000).

8. D. D. Dlott, S. Hambir, and J. Franken, "The New Wave in Shock Waves," J. Phys. Chem. B 102, 2121 (1998).

9. E. J. Garcia and J. J. Sniegowski, "Surface Micromachined Microengine," Sensors and Actuators A 48, 203 (1995).

10. R. E. Setchell, "Laser-Induced Damage in Step-Index, Multimode Fibers," Proc. SPIE 1848, 15 (1993).

11. L. S. Weichman, F. M. Dickey, and R. N. Shagam, "Beam Shaping Element for Compact Fiber Injection Systems," Proc. SPIE 3929, 176 (2000).

12. R. E. Setchell, "Laser Injection Optics for High-Intensity Transmission in Multimode Fibers," Proc. SPIE, 3929 74 (2000).

13. D. D. Bloomquist and S. A. Sheffield, "Optically Recording Interferometer for Velocity Measurements with Subnanosecond Resolution," J. Appl. Phys. 54, 1717 (1983).

14. W. M. Trott, J. N. Castañeda, J. J. O'Hare, M. R. Baer, L. C. Chhabildas, M. D. Knudson, J. Davis, and J. R. Asay, "Dispersive Velocity Measurements in Heterogeneous Materials," Sandia National Laboratories Report SAND 2000-3082, December 2000.

15. W. M. Trott, R. E. Setchell, and A. V. Farnsworth, Jr., "Development of Laser-Driven Flyer Techniques for Equation-of-State Studies of Microscale Materials," in Shock Compression of Condensed Matter - 2001, edited by M. D. Furnish, AIP Conference Proceedings (in press).

16. D. R. Christman, W. M. Isbell, S. G. Babcock, A. R. McMillan, and S. J. Green, "Final Report Measurements of Dynamic Properties of Materials—Volume III: 6061-T6 Aluminum," General Motors Corporation MSL-70-23, Vol. III, November 1971.

17. S. P. Marsh, ed., LASL Shock Hugoniot Data, U. Calif. Press, Berkeley, CA, 1980.

18. R. E. Setchell, "Index of Refraction of Shock-Compressed Fused Silica and Sapphire," J. Appl. Phys. 50, 8186 (1979).

Appendix D

DEVELOPMENT OF LASER-DRIVEN FLYER TECHNIQUES FOR EQUATION-OF-STATE STUDIES OF MICROSCALE MATERIALS*

Wayne M. Trott, Robert E. Setchell, and Archie V. Farnsworth, Jr.

Sandia National Laboratories, Albuquerque, NM 87185-0834

Abstract. Experimental methods utilizing laser-acceleration of flyer plates and high-speed velocity interferometry are being developed for investigation of the dynamic material properties of microscale materials (e.g., polycrystalline silicon). Hugoniot measurements are performed using reverse impact of the laser-driven flyer onto a known witness plate material (e.g., fused silica). A line-imaging optically recording velocity interferometer system (ORVIS) can be used to record both pre-impact flyer velocity and post-impact interface velocity as well as to determine the geometry (along a line segment) of the flyer at impact, providing a viable approach for direct state measurements. Results for 6061-T6 aluminum flyers are consistent with the well-established Hugoniot properties of this material. Methods for fabricating flyers containing thin layers of polycrystalline silicon and for measuring the short duration shock state in this material at impact are discussed.

INTRODUCTION

Methods for pulsed-laser-acceleration of miniature flyer plates provide a promising approach to quantitative studies of material response under shock wave loading (1,2). These methods are particularly suited to investigation of materials that cannot be obtained with sufficient dimensions for use in conventional gas gun tests. An important example is the basic structural material used in surface micromachines, polycrystalline silicon (3). This material is generally prepared in characteristic layer thicknesses of ~2-6μm. Coupled with high-speed, optically recording velocity interferometry, the low temporal jitter available with laser-driven flyer techniques is suited to well-controlled production and measurement of short-duration (few ns) compression states in such microscale materials.

In this paper, we discuss an experimental approach for equation-of-state studies of materials such as polycrystalline silicon. The experimental design utilizes reverse impact of laser-driven flyers onto a well-characterized witness plate material (e.g., fused silica). This configuration can provide a direct state measurement for a sample impacting a window with a well-established Hugoniot, as a result of the boundary condition that axial stress and particle velocity must be continuous across the interface. Important aspects of our efforts include [1] tailoring of the drive laser spatial profile to optimize flyer/impactor planarity, [2] development of methods for consistent, well-characterized flyer fabrication, and [3] execution and interpretation of high-speed witness plate experiments using velocity interferometry. Significant insight into these issues can be obtained from complementary 1-D and 2-D hydrocode simulations of flyer acceleration (4). Results of "baseline" Hugoniot measurements of 6061-T6 aluminum flyers are presented. For this application, we demonstrate a flyer/window and interferometer configuration that allows direct measurement of the flyer impact velocity and post-impact interface velocity on a single record. Initial efforts to obtain Hugoniot measurements from a 3.5-μm layer of polycrystalline silicon coupled to a 30-μm-thick molybdenum flyer are also discussed.

* Sandia is a multiprogram laboratory operated by Sandia Corporation, a Lockheed Martin Company, for the United States Department of Energy under Contract DE-AC04-94AL85000.

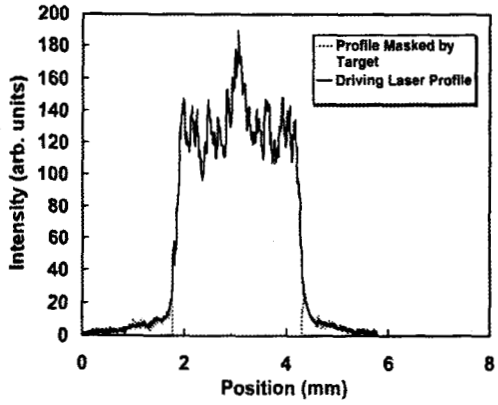

FIGURE 1. Typical spatial profile of drive laser beam used in flyer experiments.

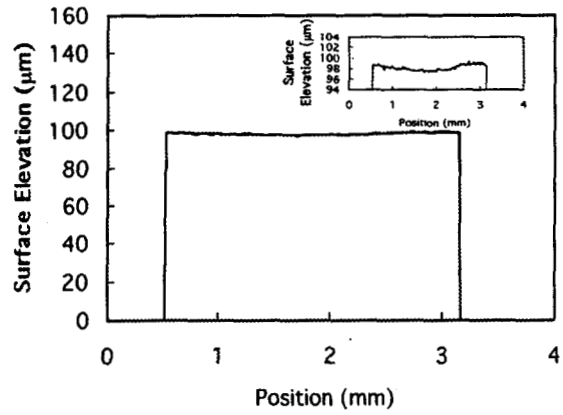

FIGURE 2. Typical surface profile (along one axis) of 6061-T6 Al flyer target prepared by diffusion bonding. Inset: Profile at expanded vertical scale.

LASER-DRIVEN FLYER METHODS

The driving laser used in this work was a Q-switched Nd:Glass oscillator (Lasermetrics Model 9380). The laser output (λ =1.054μm) was horizontally polarized and multimode. The spatial intensity distribution of the laser beam at the flyer plane was routinely monitored using a beam profiling system. In an attempt to optimize flyer planarity, we evaluated several optical designs (e.g., microlens arrays, diffractive elements) for beam conditioning in order to achieve a uniform intensity distribution over a flyer diameter of 2.5mm at incident fluences up to 50 J-cm^{-2}. None of these designs provided a true "top hat" distribution for the multimode beam. A typical drive profile is illustrated in Fig. 1. The intensity distribution exhibited an on-axis region of higher intensity but it was free of severe "hot spots." We tailored the beam area to overfill slightly the flyer diameter (Fig. 1). This drive profile provided satisfactory flyer performance. Results of 2-D numerical simulations have shown that the flyer planarity is in fact surprisingly insensitive to the intensity profile and is more dependent on the hydrodynamics associated with expansion of the driving plasma (4).

FLYER TARGET FABRICATION

For initial evaluation of our test methods, flyers of 6061-T6 aluminum were prepared for use in reverse impact studies. For this purpose, 2.5-mm-diameter discs were carefully punched out of a 0.1-mm-thick sheet of this material. We tried several flyer assembly processes utilizing a variety of thin adhesives to bond the discs to fused silica substrates (transparent substrates are used to provide confinement for the driving plasma, thereby increasing the flyer acceleration efficiency). These processes did not provide consistent results in terms of bond strength or target geometry. Our best results were achieved with an adhesive-less process that included the following steps: [1] careful hand-polishing of the 6061-T6 Al discs to a tolerance of a few μm, [2] preparation of slightly oversized 5-μm-thick pads of aluminum on fused silica via physical vapor deposition (PVD), and [3] diffusion bonding of the discs and pads at a temperature of 480°C. This process produced very uniform flyer targets, as illustrated by the typical optical profilometer record shown in Fig. 2.

PVD has also been used to fabricate multiple 30-μm-thick molybdenum flyers intended to carry thin layers (~3.5μm) of polycrystalline silicon to impact onto a witness plate. The polycrystalline silicon layers were prepared via deposition with the substrate temperature held at 300°C. Molybdenum provides a useful base layer for the polycrystalline silicon as a result of its chemical compatibility under high-temperature processing. The thermal expansion characteristics of fused silica preclude its use as a substrate in this process. Satisfactory results were obtained with sapphire and BK-7 glass, however.

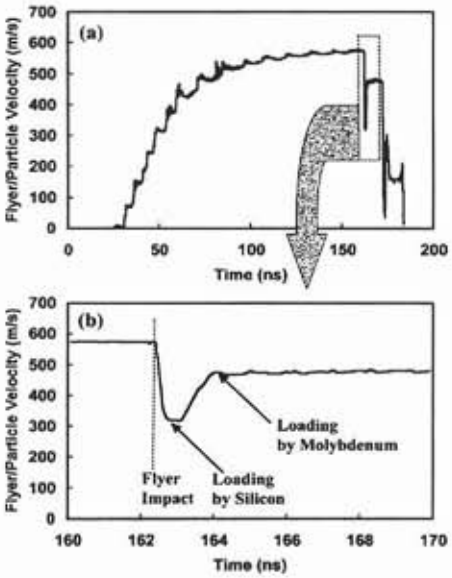

FIGURE 3. 1-D hydrocode calculation of composite flyer (30-μm-thick Mo/3-μm-thick Si) impacting fused silica: (a) curve showing flyer acceleration and impact; (b) expanded view showing short duration state induced by thin Si layer.

DUAL TIME BASE LINE-IMAGING VELOCITY INTERFEROMETRY

Witness plate measurements have been made using a line-imaging optically recording velocity interferometer system (ORVIS). The essential elements of the optical design for this system and methods for image data reduction are described elsewhere (5). Successful measurement of shock states produced by microscale materials in a reverse impact flyer experiment requires an accurate recording of both the flyer impact velocity and the short-duration interface velocity induced by the thin material on impact. Figure 3 displays results of a 1-D hydrocode calculation (4) for acceleration of a composite flyer (consisting of 3-μm-thick silicon coupled to 30-μm-thick molybdenum) and the velocity states produced by this flyer on impact with fused silica. Figure 3b, in particular, illustrates the demanding nature of this application. The time duration of the state induced by the thin silicon is ~1 ns or less. The time required for the flyer acceleration process, on the other hand, is typically much longer (~100 ns).

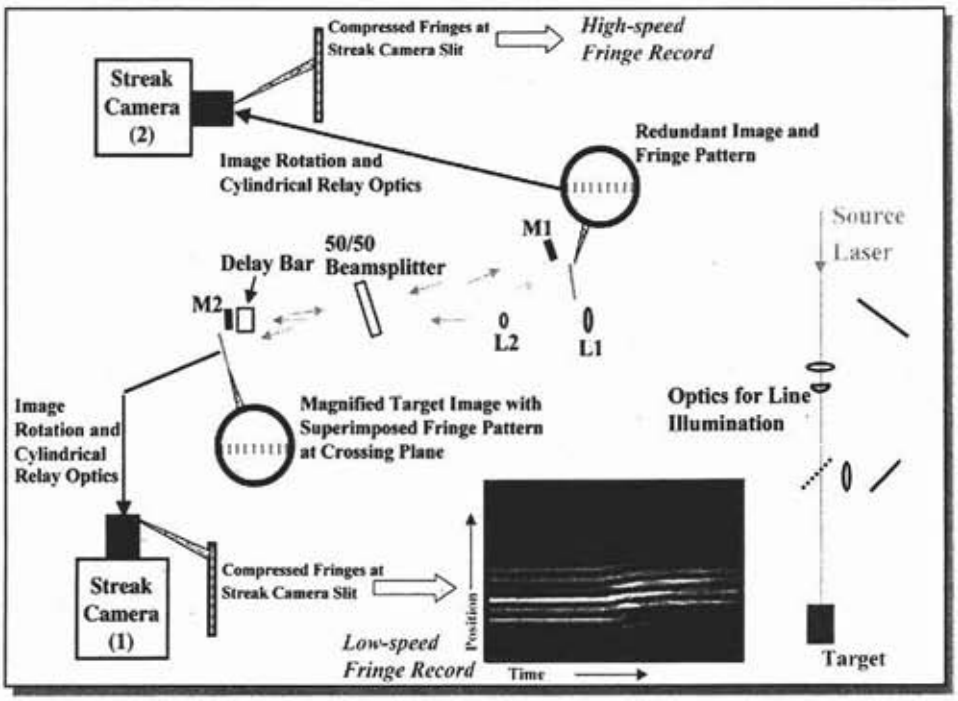

FIGURE 4. Schematic diagram of line-imaging ORVIS with two streak cameras for dual time base recording.

To capture these events, we have employed the system shown in Fig. 4. Fortunately, the ORVIS set-up provides redundant beam recombination legs that carry both magnified image and fringe displacement information. With careful masking of specular reflections from the witness plate window, it is possible to record the flyer acceleration and the post-impact interface velocity on the same image (see below). The streak camera viewing the fringe record on one leg is swept at a relatively slow rate to obtain the full flyer acceleration history, providing an accurate measurement of the impact velocity. The second streak camera is swept at a fast rate to view the impact event at high temporal resolution in order to capture the short-duration particle velocity measurement.

HUGONIOT MEASUREMENTS

The diagnostic system described above was successfully utilized in the 6061-T6 Al flyer reverse impact experiments. An image record showing the full flyer acceleration history as well as impact and unloading events is shown in Fig. 5. The usual image reduction methods (5) were used to evaluate the flyer velocity at impact as well as the interface velocity (with appropriate refractive index corrections for the interferometer window). The line-imaging ORVIS is very useful for revealing flyer tilt and other 2-D effects. We utilized only "flat" impact regions in determining points for the 6061-T6 Al Hugoniot. The flyer reverse impact results are in excellent agreement with published Hugoniot data (6,7), as shown in Fig. 6. Hydrocode computations indicate that 6061-T6 Al material in the vicinity of the impact surface is only modestly affected by the acceleration process; e.g., this region experiences negligible heating (~8 °C).

Our initial efforts at measuring the short duration shock states for 3.5-μm-thick layers of polycrystalline silicon coupled to 30-μm-thick molybdenum have produced only marginal results thus far; i.e., the transient state was poorly resolved. The hydrocode computations point to one important shortcoming in our target design in that substantial heating of the polysilicon layer likely occurs during acceleration. In future tests, we intend to improve our design by incorporating a thermally insulating layer such as amorphous alumina in the target.

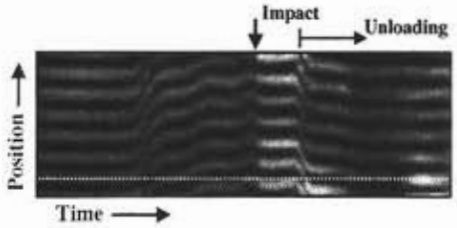

FIGURE 5. ORVIS image record of reverse impact experiment: 6061-T6 Al flyer impacting fused silica.

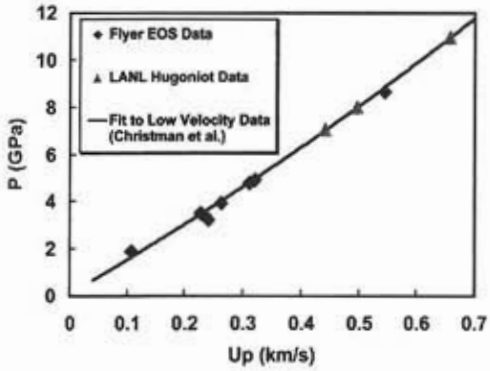

FIGURE 6. Comparison of 6061-T6 Al Hugoniot data obtained in flyer tests with previously reported data.

REFERENCES

1. Robbins, D. L., Gehr, R. J., Harper, R. W., Rupp, T. D., Sheffield, S. A., and Stahl, D. B., "Laser-Driven Miniflyer Induced Gold Spall," in *Shock Compression of Condensed Matter--1999*, edited by M. D. Furnish, et al., AIP Conference Proceedings 505, Melville, NY, 2000, pp. 1199-1202.
2. Trott, W. M., Setchell, R. E., and Farnsworth, Jr., A. V., "Investigation of the Effects of Target Material Strength on the Efficiency of Acceleration of Thick Laser-Driven Flyers," in *Shock Compression of Condensed Matter--1999*, edited by M. D. Furnish, et al., AIP Conference Proceedings 505, Melville, NY, 2000, pp. 1203-1206.
3. Garcia, E. J., and Sniegowski, J. J., "Surface Micromachined Microengine," *Sensors and Actuators A* 48, 203-214 (1995).
4. Farnsworth, Jr., A. V., Setchell, R. E., and Trott, W. M., "A Computational Study of Laser Driven Flyer Plates" (this volume).
5. Trott, W. M., et al., "Dispersive Velocity Measurements in Heterogeneous Materials," Sandia National Laboratories Report, SAND2000-3082, December 2000.
6. Christman, D. R., Isbell, W. M., Babcock, S. G., McMillan, A. R., and Green, S. J., "Final Report Measurements of Dynamic Properties of Materials--Volume III: 6061-T6 Aluminum," General Motors Corporation, MSL-70-23, Vol. III, November 1971.
7. Marsh, S. P., ed., *LASL Shock Hugoniot Data*, U. Calif. Press, Berkeley, CA, 1980, pp. 182-183.

Distribution

1	MS-0188	LDRD Office, 1030
1	MS-0328	J. A. Wilder, Jr., 2612
1	MS-0328	D. M. Berry, 2612
1	MS-0328	F. M. Dickey, 2612
1	MS-0328	S. R. Vigil, 2612
1	MS-0328	L. S. Weichman, 2612
1	MS-0482	K. D. Meeks, 2131
1	MS-0482	S. C. Holswade, 2131
1	MS-0820	P. F. Chavez, 9232
2	MS-0820	A. V. Farnsworth, Jr., 9232
1	MS-0824	A. C. Ratzel, 9110
1	MS-0834	M. R. Prairie, 9112
1	MS-0834	J. N. Castaneda, 9112
5	MS-0834	W. M. Trott, 9112
1	MS-0885	D. B. Dimos, 1802
1	MS-1415	W. B. Gauster, 1110
1	MS-1421	G. A. Samara, 1120
1	MS-1421	M. U. Anderson, 1122
10	MS-1421	R. E. Setchell, 1122
1	MS-1427	J. M. Phillips, 1100
1	MS-9018	Central Technical Files, 8945-1
2	MS-0899	Technical Library, 9616
1	MS-0612	Review & Approval Desk, 9612 for DOE/OSTI